Final Scientific/Technical Report

Project Title: Biomass Gas Cleanup Using a Therminator

Award Number: DE-FG36-04GO14312

Recipient: RTI International

Project Location: Research Triangle Park, NC 27709

Project Director/Principal Investigator: David C. Dayton

Team Members: Clemson University, Cratech, Biofuels Center of North Carolina, Süd Chemie

Executive Summary

The growing gap between petroleum production and demand, mounting environmental concerns, and increasing fuel prices have stimulated intense interest in research and development (R&D) of alternative fuels, both synthetic and bio-derived. Currently, the most technically defined thermochemical route for producing alternative fuels from lignocellulosic biomass involves gasification/reforming of biomass to produce syngas (carbon monoxide [CO] + hydrogen [H_2]), followed by syngas cleaning, Fischer-Tropsch synthesis (FTS) or mixed alcohol synthesis, and some product upgrading via hydroprocessing or separation. A detailed techno-economic analysis of this type of process has recently been published [1] and it highlights the need for technical breakthroughs and technology demonstration for gas cleanup and fuel synthesis. The latter two technical barrier areas contribute 40% of the total thermochemical ethanol cost and 70% of the production cost, if feedstock costs are factored out. Developing and validating technologies that reduce the capital and operating costs of these unit operations will greatly reduce the risk for commercializing integrated biomass gasification/fuel synthesis processes for biofuel production.

Project Description

The objective of the project was to develop and implement a two-stage process for deep cleaning of raw biomass gasifier syngas using a dual fluidized bed reactor system called "Therminator" operating at 600-700ºC (1112-1292ºF) in the first stage. A novel attrition-resistant triple function catalyst system used in the Therminator simultaneously reforms, cracks, or removes tar, ammonia (NH_3) and hydrogen sulfide (H_2S) from the raw biomass-derived syngas. The catalyst is circulated between the coupled fluidized-bed reactors (absorber and regenerator). The gas leaving the Therminator will be cooled and filtered using a candle filter system at 200 to 300ºC (392-576ºF). The filtered gas can be further cleaned in a second (polishing) stage consisting of a fixed-bed of a mixed-metal oxide sorbent-catalyst to reduce the tar, ammonia, and H_2S so that the syngas can be directly used in a downstream process for synthesis of liquid fuels and chemicals.

The proposed Therminator technology is designed to be a low cost (capital and operating) option for removing tars, ammonia, and sulfur from biomass-derived syngas for use in a mixed alcohol catalytic synthesis process to produce cost-competitive biofuels. The project goals were to develop 1) a tri-functional catalyst system for cracking or reforming tars, dissociating ammonia, and removing sulfur to specified target levels, 2) a circulating, continuously regenerating reactor design to maximize catalyst performance and lifetime, and 3) test the skid-mounted Therminator with inert flows and biomass-derived syngas. The revised work plan will be carried out in four tasks.

The Project was divided up into four main technical tasks as described in the following:

Task 1. Laboratory Testing and Catalyst Scale-up

Laboratory-scale catalyst testing at Clemson University was completed in FY08. Mixed metal oxide catalyst performance will be validated in a laboratory-scale fluidized bed reactor system at RTI with model tar compounds in simulated syngas mixtures.

Task 2. Bench-Scale Therminator Testing

A skid-mounted bench-scale fluidized-bed Therminator capable of operation up to 700ºC (1306ºF) at 150 psia that can accommodate the equivalent of 20 kg/hr of biomass derived syngas was designed, fabricated and integrated with a pilot-scale indirectly heated biomass gasifier.

Task 3. Technology Implementation

The skid-mounted Therminator unit was fabricated and installed at the University of Utah in their biomass gasification facility.

Task 4. Engineering Evaluation and Commercial Assessment

The NREL Mixed Alcohol Design Report was used as the basis of determining the techno-economic performance of the Therminator. The ASPEN Plus process models that were used in the NREL report will be downloaded and modified by RTI to input the design and performance specification as the Therminator as the primary gas cleanup unit operation with a downstream polishing stage. Mass and energy balances will be calculated around the gas cleanup steps and for the whole, integrated biomass gasification/gas cleanup/fuel synthesis process. An economic analysis that includes the overall capital cost estimates for the integrated biomass gasification process including the Therminator technology was performed and compared to other gas cleanup options.

Publications:

Pansare, S. S.; Goodwin, J. G., Ammonia decomposition on tungsten-based catalysts in the absence and presence of syngas. Industrial & Engineering Chemistry Research 2008, 47, (12), 4063-4070.

Pansare, S. S.; Goodwin, J. G.; Gangwal, S., Simultaneous Ammonia and Toluene Decomposition on Tungsten-Based Catalysts for Hot Gas Cleanup. Industrial & Engineering Chemistry Research 2008, 47, (22), 8602-8611.

Pansare, S. S.; Goodwin, J. G.; Gangwal, S., Toluene decomposition in the presence of hydrogen on tungsten-based catalysts. Industrial & Engineering Chemistry Research 2008, 47, (12), 4077-4085.

Pansare, S. S.; Torres, W.; Goodwin, J. G., Ammonia decomposition on tungsten carbide. Catalysis Communications 2007, 8, (4), 649-654.

Pansare, S. S.; Torres, W.; Goodwin, J. G.; Gangwal, S. K. In WC catalyzed NH3 decomposition for clean production of H2 from biomass gasification, 2006; 2006; pp 47-PETR.

Torres, W.; Pansare, S. S.; Goodwin, J. G., Hot gas removal of tars, ammonia, and hydrogen sulfide from Biomass gasification gas. Catalysis Reviews-Science and Engineering 2007, 49, (4), 407-456.

Presentations:

Dayton, D.C.; Kataria, A.; Yellin, W.; Turk, B.; and Gupta, R."Biomass Gasification Tar Cracking Technology Development", presented at Biomass '10 in Grand Forks, ND July 20-21, 2010

Technologies/Techniques:

None

Table of Contents

Introduction

The President's Advanced Energy Initiative (2006) calls for a change in the way Americans fuel their vehicles to promote improved energy security. Increasing biofuels production from domestic lignocellulosic resources requires advanced technology development to achieve the aggressive targets set forth recently to reduce motor gasoline consumption by 20% by 2017. A large fraction of the targeted 35 billion gallons of alternative fuels must come from sustainable biomass resources to minimize environmental impact and help to decelerate the impact of fossil fuels on global climate change. The U.S. Department of Energy (USDOE) Office of the Biomass Program (OBP) is actively funding research and development in both biochemical and thermochemical conversion technologies to accelerate the deployment of biofuels technologies in the near future to meet the goals of the Advanced Energy Initiative.

Thermochemical conversion technology options include both gasification and pyrolysis to enable the developing lignocellulosic biorefineries and maximize the biomass resource utilization for production of biofuels. Moving forward, the role of thermochemical conversion is to provide a technology option for improving the economic viability of the developing bioenergy industry by converting the faction of the biomass resources that are not amenable to biochemical conversion technologies into liquid transportation fuels.

Gasification is the most flexible technology for biomass utilization. Syngas from gasification can be used to produce electric power, hydrogen, steam and/or a wide variety of fuels/chemicals depending on site requirements. Fluidized-bed biomass gasifiers have the best potential for becoming a large-scale operation and are the gasifiers of choice. The problem, however, is that the syngas produced by these gasifiers contains tar, ammonia (NH_3), hydrogen sulfide (H_2S) and particles that must be removed before it can be used in an engine, turbine or fuel cell for producing power or in a catalytic reactor for producing liquid fuels and chemicals.

Biomass gasification integrated with gas cleanup and fuel synthesis has emerged as the nearer term technology option for thermochemical biofuels production primarily because ethanol can be produced via mixed alcohol synthesis. The acceptance of non-ethanol biofuels is increasing as accelerated biofuels production is sought for increasing energy security and mitigating climate change and compatibility with the existing fuel distribution and infrastructure is becoming more of a technical challenge as the volume of biofuels production increases. Given the sheer magnitude of the challenge of reducing gasoline consumption by 20% in 10 years (35 billion gallons of renewable and alternative fuels plus 5% increase in vehicle efficiency), alternative transportation fuels such as coal to liquids (CTL) is also being considered but the environmental concerns have quelled interest compared to biofuels even though economies of scale and CO_2 sequestration can improve the image of CTL.

Given the large volume targets established for biofuels production, mixed alcohol production from syngas (~90 gal/ton – comparable with fermentation) has received more interest than FT diesel (~50 gal/ton) for largely political reasons – ethanol is an accepted gasoline additive that gets the tax credit and the passenger car fleet predominantly uses gasoline, not diesel. These arguments do not hold for overseas possibilities for biofuels where FT diesel has a much stronger position to help meet EU biofuels goals. Other options like dimethyl ether (DME) that can be produced in high yields from syngas - via methanol conversion and dehydration – are also being considered as a diesel substitute and LPG alternative.

The production of mixed alcohols from syngas has been known since the beginning of the last century; however, the commercial success of mixed alcohol synthesis has been limited by poor selectivity and low product yields. Single pass yields are on the order of 10% syngas conversion to alcohols with methanol typically being the most abundant alcohol produced [2, 3]. Methanol can be recycled to produce higher alcohols or removed and sold separately. One of the major hurdles to overcome before HAS becomes an economic commercial process is improved catalysts that increase the productivity and

selectivity to higher alcohols [4]. To date modified methanol and modified FT catalysts have been more effective in the production of mixed alcohols; the sulfide-based catalysts tend to be less active than the oxide-based catalysts [2, 3].

The objective of the project is to develop and demonstrate a novel fluidized-bed process module called a "Therminator" to simultaneously destroy and/or remove tar, NH_3 and H_2S from raw syngas produced by a fluidized-bed biomass gasifier. The raw syngas contains as much as 10 g/m^3 of tar, 4,000 ppmv of NH_3 and 100 ppmv of H_2S. The goal of the Therminator module would be to use promising regenerable catalysts developed for removing tar, ammonia, and H_2S down to low levels (around 10 ppm). A second polishing step can then be added to further reduce the tar, ammonia, H_2S and heavy metals to less than 100 parts-per-billion (ppb) so it can be directly used in a downstream process for synthesis of liquid fuels and chemicals. Since the Therminator will be able to accept a particle-laden syngas, particles in the gas can be removed in a downstream filter. The key to the development of the Therminator is the development of an attrition resistant and active triple-function catalyst system to remove tar, ammonia and sulfur.

Tars are cracked to a non-condensable gas and coke that would deposit on the acid catalyst. We will deposit coke, much like a fluid catalytic cracker (FCC) in a petroleum refinery. The deposited coke fouls the catalyst, much like FCC, but the coke would be burned off in the regenerator and the regenerated catalyst would be returned to the cracker. The rapid circulation between the cracker and regenerator would ensure the availability of the required amount of regenerated catalyst to accomplish our goal. Also, by removing sulfur down to less than 10 ppmv, NH_3 decomposition would also be possible in the cracker at 600-700°C.

In the cracker, tar decomposes and lays down coke on the acid sites of the catalyst, NH_3 is decomposed using a small amount of metal (e.g., nickel or iron) catalyst incorporated into the catalyst matrix, and H_2S is removed by a small amount of a metal oxide (e.g. zinc oxide or zinc titanate) by the H_2S-metal oxide reaction to form metal sulfide. After a tolerable decline in activity for these reactions, the catalyst particles (and additives) are transported to the regenerator where they are exposed to air to remove the coke and to regenerate the metal sulfide back to metal oxide. Sulfate formation is avoided by running the regeneration with slightly sub-stoichiometric quantity of oxygen. Following regeneration, the catalyst is transported back to the cracker and the cycling continues. Analogous to an FCC reactor system, rapid cycling will allow the use of very active cracking catalysts that lose activity due to coking within the order of several seconds.

The regeneration tail gas consisting of CO_2 and trace levels of SO_2 can be disposed in an environmentally acceptable manner depending on requirements. Regeneration provides the heat necessary to maintain the solid temperatures above the gasifier exit temperature so no added heat is necessary. In fact, the tail gas can provide surplus heat for drying the biomass.

Particles in the syngas do not get captured in the Therminator; they simply pass through. In a potential commercial embodiment, a particle control device (some combination of a cyclone and a filtering device) will be installed downstream of the Therminator. For a more stringent cleanup requirement, such as for fuel cell or fuel cell/turbine hybrid power devices, a polishing step (e.g. a zinc oxide guard bed for H_2S and wet scrubber for residual ammonia and particulates) could also be added. A modular approach allows the development of the Therminator independently of the development of the upstream and downstream equipment.

Candidate Catalysts

The objective was to develop a tri-functional catalyst system comprised of two or three separate materials whose particle sizes are comparable for fluidization, or a composite catalyst with three active components incorporated in each attrition resistant particle. These 3 active components or 2 or 3 separate catalysts would be an acid catalyst for tar cracking, an ammonia decomposition catalyst, and a

catalyst/material to remove H_2S. Each of these components has to function in a gas containing H_2, H_2O, CO, CO_2, tars, ammonia, and H_2S.

The high concentrations of H_2 and CO in biomass-derived syngas can reduce metallic components (metal oxide, carbide, nitride, etc.) in the catalyst even in the presence of significant amounts of H_2O. Water vapor at high temperatures can cause or increase catalyst sintering and loss of surface area, dealumination of zeolitic materials, metal oxide formation, and compound formation between base metals and alumina/silica. CO_2 and NH_3 can compete for adsorption on acid sites and poison or block them for acidic reactions. CO and H_2S can compete for adsorption and poison sites for NH_3 decomposition. Coke formation from tar cracking can block nonacidic sites active for ammonia decomposition. Of course, by its nature, tar cracking necessitates oxidative regeneration to remove surface coke. Coke oxidation can provide the latent heat for the endothermic tar cracking reactions.

Acid catalysts investigated for tar cracking included ultra stable rare earth Y (REY) zeolite, silica-alumina, and tungstated zirconia (WZ). Sulfated zirconia (SZ) is a strong acid catalyst and is as active as REY zeolite (typically used commercially for catalytic cracking of hydrocarbons). WZ is less acidic than SZ, but acidic enough for tar cracking reaction conditions. However, the particular catalytic properties of an element are heavily affected by its valence state and compound formed during pretreatment/regeneration and during exposure to the biomass-derived syngas.

NH_3 decomposition catalysts in the presence of syngas with and without H_2S have been extensively studied by RTI. In the presence of low levels of H_2S (< 10 ppmv), NH_3 can be effectively decomposed at 650-700ºC using commercially available nickel-based catalysts such as HTSR-1 from Haldor-Topsoe and G-65 from Süd Chemie. In addition to these primary candidates, other candidates based on W, Mo, Zr, Mn and Fe will also be investigated. Zinc titanate would be the primary candidate for H_2S removal because of its ability to resist reduction at high temperature. RTI has commercialized an attrition-resistant fluidizable zinc titanate H_2S sorbent known as EX-SO3 for coal-derived syngas desulfurization.

The emphasis of the catalyst development was on acidic catalysts capable of tar cracking. Of particular interest were those elements which may be able to serve multiple functions – although not necessarily in the same state. For example, in WZ, tungsten is supported on zirconia in quantities on the order of 2-10 wt%; however, there is an optimum amount that seems to form the interaction with zirconia producing strong acid sites. Some tungsten exists as free tungsten oxide. Thus, it may be the case that the tungsten strongly interacting with the zirconia would provide the cracking component while free tungsten oxide may provide active sites for ammonia decomposition. As a potential tri-functional catalyst, iron (Fe) and manganese (Mn) could be added to WZ to form Fe/WZ, Mn/WZ, or FeMn/WZ. Use of Fe and Mn has been shown to produce more active SZ catalysts so the this should apply for WZ as well. Both Fe and Mn can function as NH_3 decomposition catalysts and as H_2S getters.

Project History

This project was originally awarded on September 15, 2004 with a period of performance that extended through the end of 2007. The proposed project was structured with RTI as the prime awardee and Clemson University, Cratech, and Sud Chemie as sub-awardees. The required cost share for the project was to be provided by our industrial partners Cratech and Sud Chemie.

The objective of the proposed project was to develop and demonstrate a novel process module called a Therminator to simultaneously destroy and/or remove tar, ammonia (NH_3) and hydrogen sulfide (H_2S) from raw syngas produced by a fluidized-bed biomass gasifier. This raw syngas contains as much as 10 g/m^3 of tar, 4,000 ppmv of NH_3 and 100 ppmv of H_2S. The goal of the Therminator module would be to reduce tar to <0.1 g/m^3, reduce H_2S to <10 ppm and decompose >90% of the NH_3 to N_2 and H_2. The Therminator was designed as two coupled bubbling fluidized-bed or transport reactors to operate at a

temperature of 600-700ºC (1112-1292ºF). The approach is similar to a fluid catalytic cracking (FCC) unit in a petroleum refinery.

The original concept was to couple the Therminator module with a pressurized air-blown biomass gasifier being developed by Cratech, a small business established in 1990 to design and develop a new generation of biomass power plants. The goal was to use Cratech's pressurized fluidized-bed biomass gasifier for demonstrating the Therminator technology by cleaning and conditioning a slip stream from their 1,000 lb/h of biomass gasification system at pressures ranging from 20 to 165 psia.

The project consisted of development and scale-up of the triple function catalyst; design, construction and commissioning of a skid-mounted bench-scale Therminator; transport to and installation of the Therminator at an operating pressurized fluidized-bed biomass gasification pilot-plant; and slip-stream demonstration of the Therminator over long-term tests using actual biomass gasification syngas. The catalyst effectiveness was to be fine tuned in lab scale studies prior to these bench scale activities. Engineering evaluation and commercial assessment of the Therminator technology would proceed in parallel to its development.

Several major project management challenges were encountered during this project that led to project scope changes and a no-cost extension of the period of performance. After the project was awarded, the goals of the Thermochemical Conversion Platform in the Office of Biomass Program changed in FY05 to focus gas cleanup and conditioning to achieve syngas quality targets for fuel synthesis instead of power production. Consequently, the goals and objectives of this project were modified to align with the Office of Biomass Program goals to produce cost-competitive biofuels.

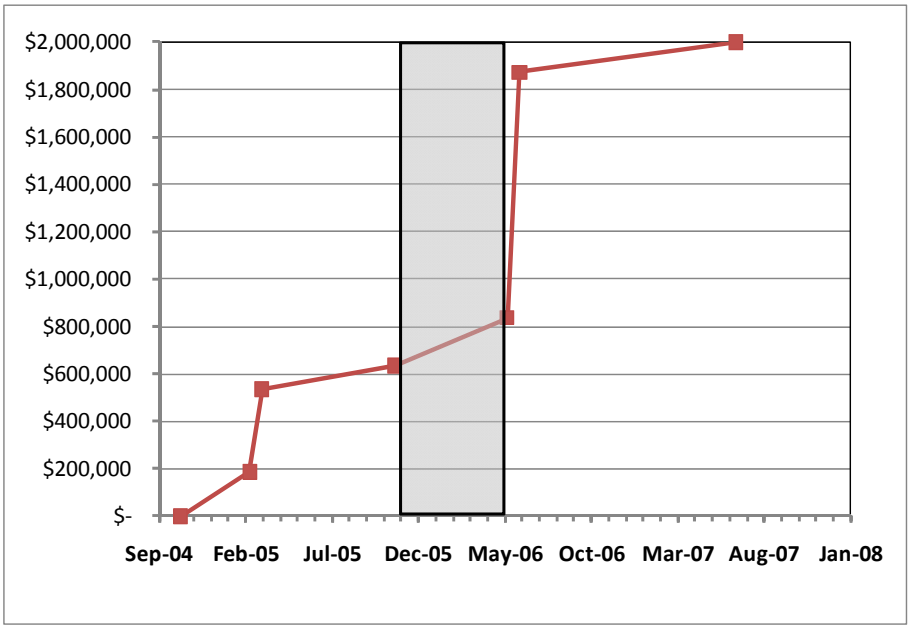

Figure 1: Cumulative Project Funding

Project funding was another challenge that affected project execution and technical progress. From the beginning, the project was incrementally funded on a yearly basis. After the project scope was modified in FY05 to align with biofuels production, the federal budget process left the Biomass Program with a shortage of discretionary funding and no additional funds were added to the project for FY06. This funding interruption resulted in a 6-month (November 2005 through April 2006) Stop Work Order for the project that delayed the design and fabrication of the bench-scale Therminator unit. See Figure 1 for the cumulative project funding with the Stop Work Order period highlighted.

The interruption in funding to the project and the Stop Work Order also required that the subcontract with Cratech be terminated. This coincided with change in management at Cratech. When funding was re-instated for the project RTI was unable to come to an agreement with Cratech to initiate another subcontract. The most significant impact to the project was the loss of a host site to test the Therminator technology with biomass-derived syngas. Cratech was also a major cost share provider to the project.

As the Stop Work Order was lifted and the majority of the project funding was secured the project was without a host site for the technology development and lacked a commitment for the majority of the cost share required for the project. The biomass gasification facility at the University of Utah was selected as the new host site for evaluating the Therminator performance. The original Therminator unit was designed to receive syngas produced from the equivalent of 10 lbs/hr of biomass in a pressurized air-blown gasifier. The University of Utah gasification facility contains a 20 kg/hr (44 lbs/hr) pressurized indirect biomass gasifier. As a result, the original Therminator unit was redesigned to accommodate the roughly 4.5 times higher syngas throughput and add a unit operation to quench the steam used as the carrier gas in the indirect gasifier. This effectively expanded the scope of the original project to provide a larger system for testing the tar cracking technology. Additional cost share was also secured from a grant awarded to RTI by the Biofuels Center of North Carolina; a state funded organization mandated to support the goal of replacing 10% of the transportation fuel consumed in North Carolina with biofuels produced in the state with biomass resources available in the state.

The revised project scope was divided up into four main technical tasks as described in the following:

Task 1. Laboratory Testing and Catalyst Scale-up

Laboratory-scale catalyst testing at Clemson University was completed in FY08. Mixed metal oxide catalyst performance will be validated in a laboratory-scale fluidized bed reactor system at RTI with model tar compounds in simulated syngas mixtures.

Task 2. Bench-Scale Therminator Testing

A skid-mounted bench-scale fluidized-bed Therminator capable of operation up to 700ºC (1306ºF) at 150 psia that can accommodate the equivalent of 20 kg/hr of biomass derived syngas was designed, fabricated and integrated with a pilot-scale indirectly heated biomass gasifier.

Task 3. Technology Implementation

The skid-mounted Therminator unit was fabricated and installed at the University of Utah in their biomass gasification facility.

Task 4. Engineering Evaluation and Commercial Assessment

The NREL Mixed Alcohol Design Report was be used as the basis of determining the techno-economic performance of the Therminator. ASPEN Plus process models were developed to with the Therminator as the primary gas cleanup unit operation. Mass and energy balances were calculated around the gas cleanup steps and for the whole, integrated biomass gasification/gas cleanup/fuel synthesis process. A comparative economic analysis of a 2000 tpd biomass gasification/fuel synthesis process with the Therminator tar cracking technology and a steam reforming process for gas cleanup was developed. Each gas cleanup technology was considered for mixed alcohol synthesis and gasoline synthesis using the Methanol-to-Gasoline (MTG) process.

Task 1: Laboratory Testing and Catalyst Scale-up

Clemson University Catalyst Testing

Introduction

Catalyst development, characterization, and testing were performed in the Catalysis Laboratories of the Department of Chemical Engineering at Clemson University. Catalysts investigated included:

- Acid Catalysts - rare earth doped USY (REY), silica-alumina (S-A), and tungstated zirconia (WZ)
- Ammonia Decomposition Catalysts - tungsten oxide and carbide (WO and WC), Fe, Fe_3O_4, Fe carbide, Ni, MnO, Mn carbide, and ZrO_2
- H_2S Sorbents - EX-SO3, zinc titanate

As a benchmark, dolomite, commercial Ni reforming catalysts (HTSR-1 and G-65), a commercial Fe ammonia synthesis catalyst, and a commercial REY cracking catalyst were also studied.

Catalyst preparations demonstrating significant activity and selectivity for ammonia decomposition and tar cracking were characterized to determine the structure (XRD, Raman, BET, SEM/TEM), adsorption properties (chemisorption, TPD, IR), and reducibility (TPR). Selected catalysts were studied before and after reaction to correlate changes in activity and selectivity with potential changes in structure or surface properties.

The effects of catalyst composition and structure, as well as the impact of gas composition on catalyst activity and selectivity were investigated. Toluene and naphthalene were used as model tar compounds and the reaction gas consisted of various combinations of toluene/naphthalene, NH_3, H_2S, H_2, H_2O, CO, CO_2, CH_4, and N_2 in order to mimic product gas from a biomass gasifier as well as to examine particular reactions and the impact of CO, CO_2, and H_2O on ammonia decomposition, tar cracking, and H_2S removal. Catalyst testing was performed using a fixed-bed micro-reactor with on-line GC and MS analysis. The powerful surface reaction technique, steady-state isotopic transient kinetic analysis (SSITKA), was also applied to determine site activities and the concentration of active sites on the most promising catalysts to guide further catalyst improvement and optimization. Carbon deposition and removal during regeneration was measured gravimetrically (TGA) and by CO_2 analysis during regeneration.

Experimental Methods and Equipment

In the Catalysis Laboratories of the Department of Chemical Engineering, there are general catalyst preparation facilities, 2 Fourier transform infrared spectrometers, a drifts attachment and reaction flow cell for one of the FTIRs, a Micromeritics ASAP 2010 Micropore Analyzer adsorption system; an Altamira TPD/R/O/Rx system, GC/MS, and various reaction systems (1-10 atm). These reaction systems include 1) 3 isotopic transient kinetic reaction systems with on-line GCs and mass spectrometers, 2) a gas phase FTS tubular reactor equipped with electronic mass flow controllers and on-line GCs, 3) an Autoclave Engineers microclave stirred reactor with Robinson-Mahoney configuration, 4) a Parr stirred reactor with helical impeller and high torque motor, and 5) a ReactIR-reaction analysis system equipped with two batch reactors, an overhead IR reflectance sampling system, and a liquid ATR measuring device. The College of Engineering and Science has an excellent central analysis facility that contains several TEM and SEM instruments with light element EDAX, various optical microscopes, SAM, STM, AFM, XRD, and XPS.

The catalyst testing reactor used in this project consists of a stainless-steel plug flow reactor (0.3 in. i.d.) operated at 1 atm in the temperature range from 600 to 700°C. For the ammonia decomposition reaction, the flow rates of the gases decided are H_2: 10.4 sccm, CO: 17 sccm, CO_2: 15.3 sccm,

10%NH_3/He: 1 sccm and N_2: 42.3 sccm. For tar decomposition, the flow rate of toluene/N_2 will be 25 sccm. A GC system with a FID detector was used to measure reaction products as a function of reaction conditions and time on stream.

Catalyst Preparation

The WC catalyst was obtained from Alfa Aesar while the WZ catalyst was provided by Magnesium Electron, Inc. A commercial Fe-based NH_3 synthesis catalyst (Amomax-10) was obtained from Sud-Chemie.

WC was characterized as received while it was pretreated before use in reaction studies in the presence of an 80/20 mixture of H_2/CO at 650 °C for 1 h. Prior to characterization or use in reaction, WZ was calcined at various temperatures in the range 450-900 °C in static air (where WZ900 indicates WZ calcined at 900 °C). The temperature was ramped to the desired calcination temperature at 15 °C/min and held there for 3 h. For WZ, the pretreatment was carried in a flow of He at 650 °C for 1 h and then the catalyst was cooled down to the desired reaction temperature. Amomax-10 was pretreated in the flow of pure H_2 at 650 °C for 1 h.

Since the study of the effect of calcination temperature of WZ on toluene decomposition showed that WZ calcined at 900 °C gave the best steady-state activity, WZ900 was chosen as the support for Pt incorporation. Several catalysts with different Pt loadings were prepared by incipient wetness impregnation. Suitable amounts of $H_2PtCl_6 \cdot 6H_2O$ (Alfa Aesar) were dissolved in distilled water to give desired Pt metal loadings of 3%, 5%, and 10 wt % in the catalysts. The solution was then added drop wise to the support until incipient wetness, and the resulting catalysts were oven-dried at 100 °C for 12 h followed by calcination in static air at 500 °C for 3 h. It has been reported in the literature that a calcination temperature for PtWZ above 500 °C could result in the migration of zirconia species over Pt, resulting in reduced H2-chemisorption.18 Hence, in the present study, 500 °C was chosen as the final calcinations temperature for PtWZ. The catalysts with 3%, 5%, and 10 wt % Pt loadings are henceforth referred to as 3PtWZ, 5PtWZ, and 10PtWZ, respectively.

About 50-55 mg of catalyst was placed at the center of the reactor sandwiched between quartz wool with a thermocouple at the bottom of the catalyst bed. After pretreatment, the H_2/CO flow was turned off, a flow of He was turned on, and the reactor was allowed to cool to the desired reaction temperature. A stream of 4000 ppm of NH_3 in He (total flow rate: 100 sccm) was fed to the reactor after the reaction temperature was reached. For reaction runs in the presence of syngas, flows of 10% H_2 and 15% CO were used to replace some of the He while keeping the total flow rate at 100 sccm and the concentration of NH_3 4000 ppm. The effluent from the reactor was analyzed using a Varian CP-3800 GC equipped with three columns (Poraplot, CPSil5CB, and CP-Molsieve 5A) and two parallel detectors (one TCD and one FID).

Mears' criterion for external diffusion indicated no external mass transfer effects existed at the reaction conditions used for both the catalysts. Calculation of Weisz-Prater parameters for WC and WZ indicated that there were no internal mass transfer effects at the reaction conditions used in the present study.

Nano-crystalline Zinc titanate ($ZnTiO_3$) sorbent with high BET surface were synthesized by a simple co-precipitation method using aqueous solutions of $Zn(NO_3)_2$ and titanium oxysulfate as metal precursors and aqueous ammonia as a precipitant. In this method, an aqueous solution (A) containing equimolar amounts of $Zn(NO_3)_2$ and titanium oxysulfate and a solution B containing aqueous NH_3 are added drop wise simultaneously to a reaction vessel containing a desired amount of deionized water. The precipitation was performed at a constant pH between 6 and 10 under vigorous stirring at room temperature. The precipitate was then aged at 70^{o}C for about 1 h under stirring and filtered, washed and dried at 100^{o}C overnight. The dried precipitate was calcined between 500°C and 700°C for 2h to obtain

$ZnTiO_3$ nanopowders. The performance of this catalyst will be compared to the bench-mark EX-S03 catalyst.

Ammonia Decomposition

Temperature programmed reaction (TPRx)

Temperature programmed reactions (TPRx) were carried out for NH_3 decomposition on both tungsten carbide (WC) (Alfa Aesar) and a commercial ammonia synthesis catalyst (Amomax-10) (Süd-Chemie). The TPRx studies were carried out in a stainless-steel plug flow microreactor (0.3 in. i.d.). The catalyst (50-55 mg) was sandwiched between quartz wool and placed at the center of the reactor with a thermocouple at the bottom of the catalyst bed.

WC catalyst was pretreated in the flow of various gases including pure H_2, pure CO, and an 80/20 mixture of H_2/CO. Amomax-10 was pretreated in the presence of H_2 only. All the pretreatments were carried out at 650°C for 1 h (after a ramp of 5°C/min from 30°C). After pretreatment, the catalyst was cooled to RT in a flow of He. Temperature programmed reaction was then carried out at 1 atm with a temperature ramp of 5°C/min to 450°C and a ramp of 1°C/min from 450 to 650°C. The reactants were fed to the reactor with a NH_3/He ratio of 4/96 (total flow rate = 100 sccm). The effluent from the reactor during reaction was analyzed by a gas chromatograph (GC) (Varian CP-3380). In the GC, the products were separated by a 6-ft long 80/100 mesh Hayesep Q column (Alltech) at 35°C.

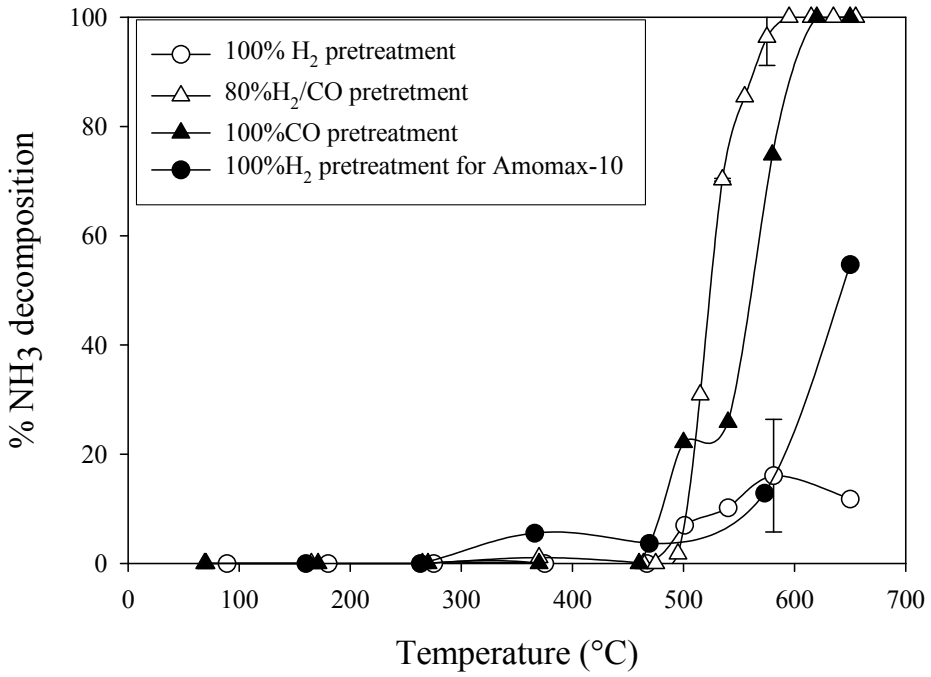

Figure 2: TPRx profiles for various pretreatments on WC and Amomax-10 catalysts

Figure 2 shows TPRx profiles of NH_3 decomposition for various pretreatments on the WC and Amomax-10 catalysts. The NH_3 decomposition reaction started at 475-490°C on WC independent of the pretreatment method. For the pretreatment of WC with H_2/CO mixture, the % decomposition increased sharply with temperature and reached 100% at 580°C. However, the maximum conversion obtained following H_2 pretreatment was only ~10%, even at 650°C. The pretreatment in the presence of CO

resulted in 100% decomposition at 600°C. According to Ribeiro et al.[5, 6], H_2 may react with the carbidic carbon in WC forming CH_4 during the pretreatment. This may lead to loss of active sites on the surface of the catalyst resulting in smaller catalytic activity following pretreatment with only H_2. The Amomax-10 catalyst showed a conversion of ca. 60% at 650°C indicating the pretreatment with pure H_2 gives a better result with Amomax-10 than with WC.

For NH_3 decomposition on an unpretreated catalyst, the TPRx curve was close to that of the catalyst pretreated in H_2/CO. The activity dependence on catalyst treatment is H_2/CO ≈ unpretreated, > CO>>H_2. Pretreatment of the catalyst with H_2 should remove carbon (both "free" or "polymeric" and carbidic carbon) from the surface[5]. The behavior of the catalyst treated with H_2 resembles that of tungsten metal [7]. The most relevant feature during CO pretreatment was the release of a small amount of CO_2 at temperatures above 400°C with a maximum at ca. 550°C, which could be related to disproportionation of CO (or the Boudouard reaction) [8, 9] in low yield.

$$2CO \rightarrow CO_2 + C \qquad [1]$$

Any carbon deposited on the surface as a consequence of reaction was small as SEM analysis of WC samples treated in CO did not show appreciable formation of carbonaceous deposits [5]. The major product observed during pretreatment of WC with H_2-CO was CH_4 with a small amount of CO_2. One possible reaction is:

$$2CO + 2H_2 \rightarrow CH_4 + CO_2 \qquad [2]$$

Decomposition of CH_4 or CO and even the Boudouard reaction might be the source of the carbon deposited on the WC surface as seen by SEM (Figure 5). The pretreatment in H_2/CO seems to result in two opposite effects: partial reduction of WC (by H_2) and carburization of the surface by CO to yield WC and perhaps W_2C domains [10-14].

The WC catalyst showed 100% conversion for NH_3decomposition at 650°C. The kinetics of the catalytic NH_3 decomposition reaction was investigated at selected temperatures in the range of 475-525°C. The catalysts were pretreated in a flow of 80/20 mixture of H_2/CO; the method that produced the most active catalyst, at the reaction temperature for 1 h. Following pretreatment, the reaction was carried out at 1 atm with 4000 ppm of NH_3 in He. The variation in % NH_3 decomposition as a function of time on stream (TOS) for various temperatures is shown in Figure 3.

The variation in percent NH_3 decomposition as a function of time-on-stream (TOS) at selected temperatures is shown in Figure 3. The inlet concentration of NH_3 was 4000 ppm. For this series of experiments, the WC catalyst was pretreated in H_2-CO. The reaction was characterized by an induction period. At 475°C, activation of the catalyst took more than 2 h. The length of the induction period decreased with temperature, requiring less than 40 min at the highest temperature studied (525°C). For reaction temperatures ≥ 500°C, significant initial activity was observed that increased during the induction period. At 650°C, complete decomposition of NH_3 was observed at 5 min TOS. Any induction phenomena were masked by this. No deactivation of the catalyst was observed for 12 h TOS at any of the temperatures.

This induction period may result from coke deposits formed during pretreatment that initially block the active sites. As the temperature increases, the concentration of these coke deposits may convert into active WC species as carbon diffuses into bulk WC phases. The rate of diffusion increases as reaction temperature increases so the induction period is shorter at higher temperatures. A slight deactivation after the initial increase in the activity was also observed at 500 and 525°C.

A comparison of %NH_3 decomposition on WC and Amomax-10 at 500°C as a function of TOS is shown in Figure 4.

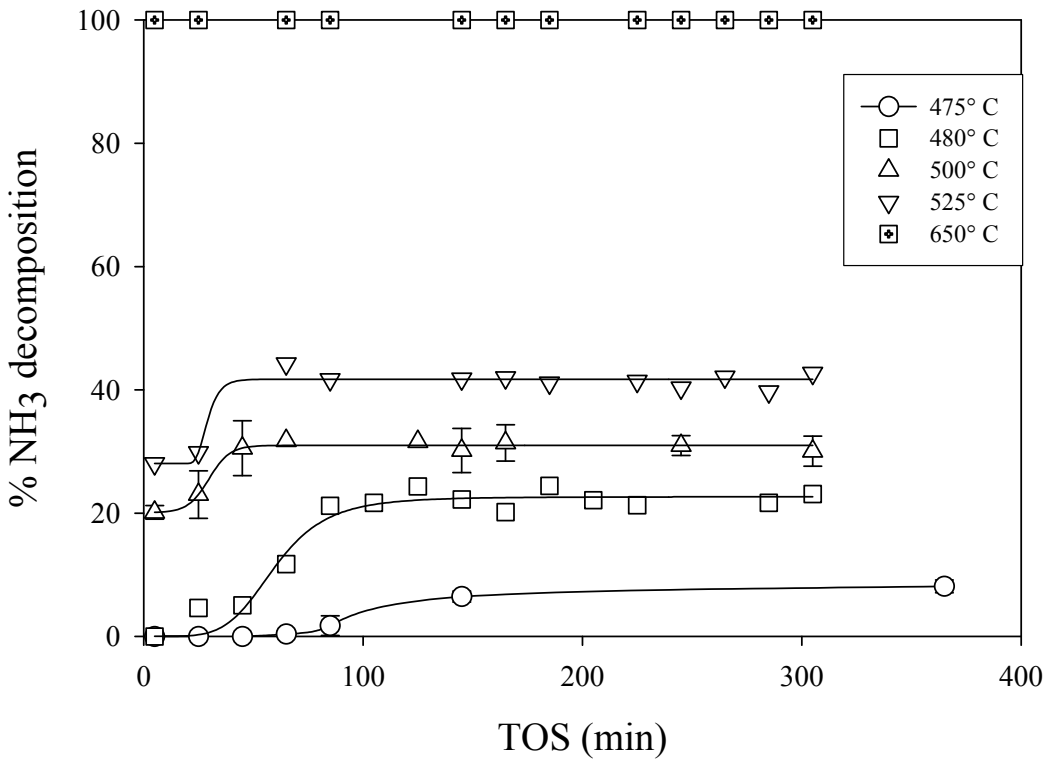

Figure 3: Time-on-stream behavior of the WC catalyst for NH_3 decomposition

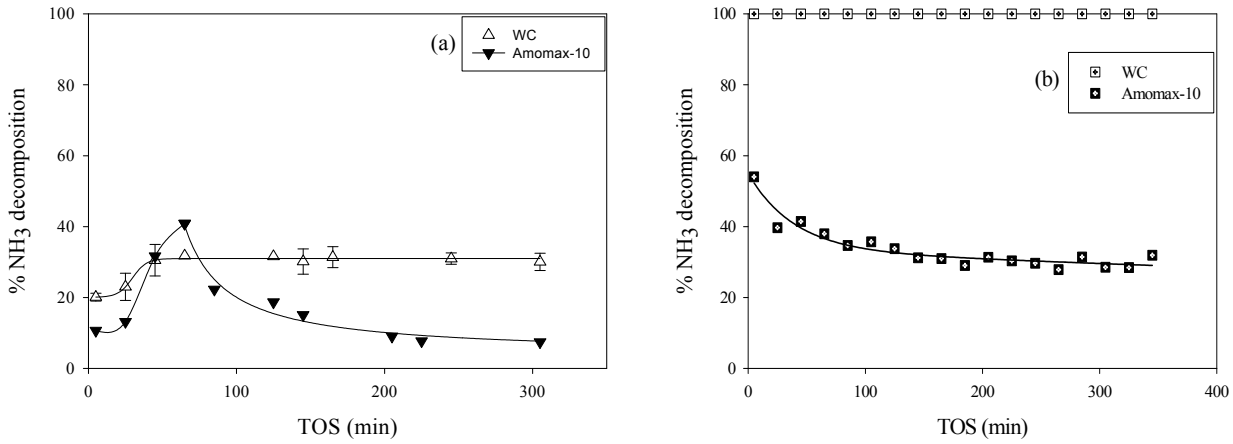

Figure 4: %NH_3 decomposition as a function of TOS for WC and Amomax-10 catalysts at a) 500°C and b) 650°C.

The Amomax-10 catalyst also demonstrated an induction period. However, it showed rapid partial deactivation after 60 min TOS and attained a steady-state NH_3 decomposition value of 8% after 5 h TOS. The deactivation was more prominent compared to that of the WC catalyst at the same temperature. The steady-state value for WC catalyst was 30%, three times that of Amomax-10. At 650°C, the induction period for Amomax-10 was very short and the Amomax-10 partially deactivated until NH_3 conversion stabilized at 30% after 5 h TOS (Figure 4b). At the same temperature, the WC catalyst showed no signs of deactivation

The activation energy for WC catalyst was calculated from the rate of reaction at steady state in the temperature range of 475-490°C. The value was 120 kJ/mol after 300 min TOS. The apparent activation energy for NH_3 decomposition at steady state on WC, calculated from experiments with 1000 ppm NH_3, keeping maximum conversion lower than 25%, was 140 kJ/mol.

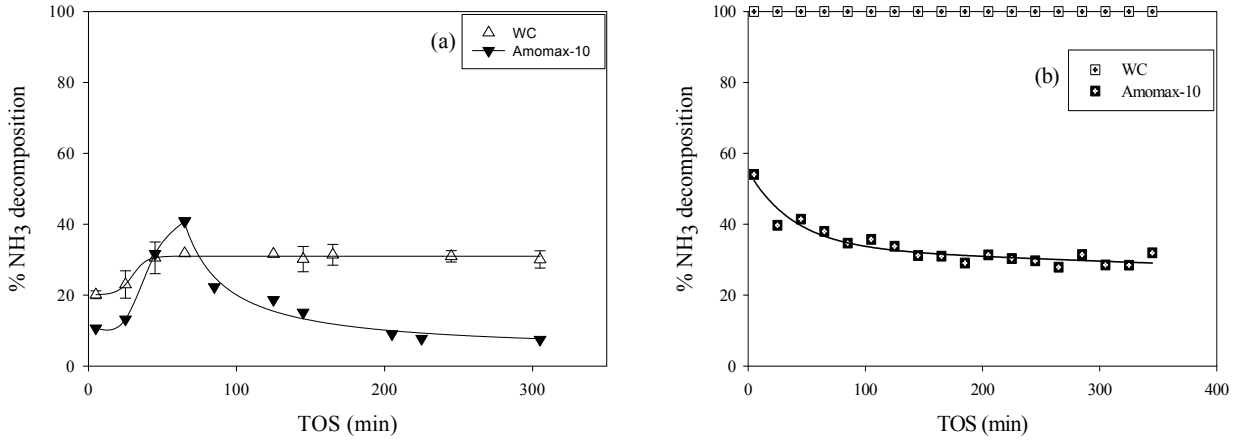

Figure 4: %NH_3 decomposition as a function of TOS for WC and Amomax-10 catalysts at a) 500°C and b) 650°C.

Catalyst activation has been observed for NH_3 decomposition on a reduced Ru catalyst (at 530°C) by Friedlander et al. [15, 16]. These authors argued that activation was due to the time required by the NH_3 molecules to reconstruct the metal surface favorable for the reaction. In the present study, we hypothesize that something similar was occurring during the induction period, perhaps with the formation of a surface with a stoichiometry WxCyNz, modifying the electronic properties of the surface.

The role played by the carbon deposits observed after H_2-CO pretreatment is not clear. This pretreatment was the best for NH_3 decomposition even though at least some of this extra carbon remained on the surface after reaction. So the question remains whether ammonia decomposition is happening in spite of the carbon deposits or, at least partly, because of them.

Temperature programmed desorption experiments by Ribeiro et al. [5, 6] have shown that NH_3 desorbs as N_2 from WC surfaces at temperatures above 430°C with a peak in the vicinity of 500°C. Desorption of N_2 from well characterized single crystal Fe surfaces occurs at around 630°C [17]. This indicates that adsorption of N_2 is stronger on Fe than on WC. If N_2 desorption is assumed to be the rate controlling step [18], then the catalytic activity would decrease as the strength of N adsorption on the surface increases, and it would be even more affected by bulk nitridation. Thus, bulk nitridation might be the reason for partial deactivation of Amomax-10 during TOS experiments. Although Amomax-10 is a good NH_3 synthesis catalyst, our results indicate that it is not the best catalyst for the decomposition of NH_3, in agreement with recent findings by Boisen et al. [18].

Ammonia Decomposition Catalyst Characterization

BET, SEM, EDX, TPRx, and TOS reaction experiments were used for characterizing and testing the WC catalyst. The WC catalyst was pretreated in the presence of H_2, CO, and H_2-CO to study the effect of these pretreatment on NH_3 decomposition.

The SEM micrographs of a fresh sample (as received-without pretreatment) and a sample after the NH_3 decomposition reaction at 500°C are shown in Figure 5 and Figure 6, respectively. The crystals of fresh WC were characterized mostly by flat surfaces with some surface defect structures. The sample after reaction showed deposits of an amorphous material on the irregularities on the crystal surface (Figure 6). Energy dispersive X-ray spectroscopy (EDX) experiments on the same fresh WC sample

showed 64 atom % carbon. However, the EDX analysis of the amorphous material had 89 atom % carbon confirming the presence of carbon which was likely deposited during pretreatment and not removed during reaction. Another interesting observation from the EDX analysis of the fresh WC sample was that the surface composition differed from the bulk composition. XRD analysis confirmed that the bulk composition of the fresh WC catalyst was W_1C_1, however the EDX analysis showed that the surface composition might be W_1C_2.

The BET surface area of fresh WC catalyst as received was 1.5 ± 0.3 m^2/g. EDX analysis of the fresh sample indicated an overall composition of $W_{0.4}C_{0.6}$ that we take as a rough estimate of the presence of a small carbon excess. The SEM micrographs of WC catalyst after pretreatment with H_2 or CO were similar to those of the fresh WC catalyst. On the contrary, micrographs of the WC samples pretreated with H_2-CO (Figure 7) showed selective deposition of a material on the crystal edges, pits, and crevices. An EDX analysis showed that the atomic W/C ratio in the amorphous region was 11/89, confirming that the amorphous material was carbon rich. Although the material deposited on the pits looked "amorphous" at the micrometer scale, when observed with a higher magnification, they showed fibril structures (Figure 8). Some material also deposited on the relatively flat sections of the crystal (Figure 9). However, the morphologies of the deposits on the flat surface and on the pits were different.

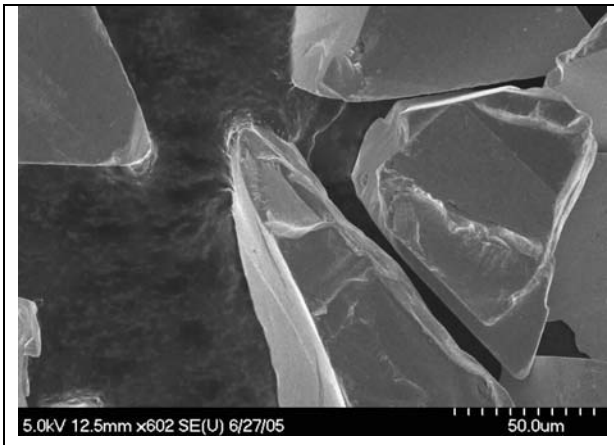

Figure 5: SEM micrographs of fresh, as received WC catalyst.

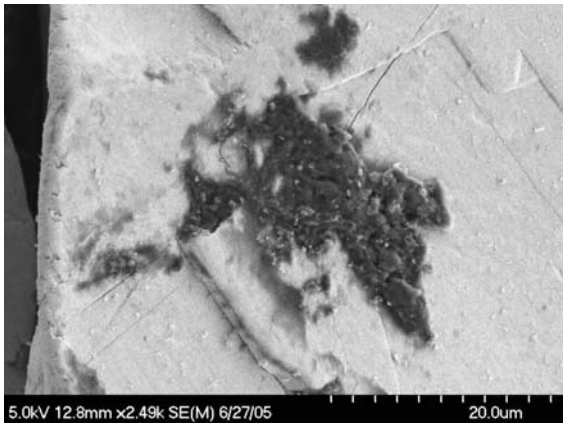

Figure 6: SEM micrographs of WC catalyst after pretreatment and reaction.

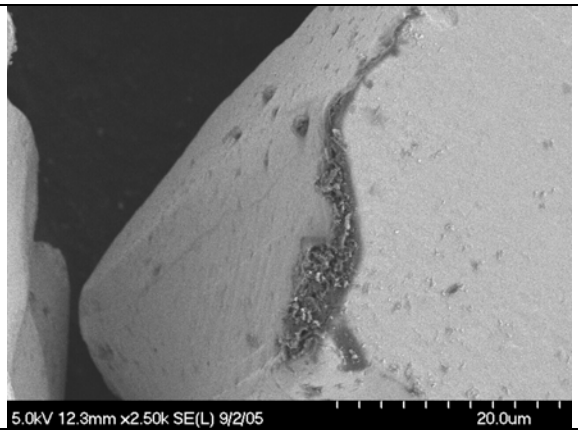

Figure 7: SEM micrograph of WC catalyst after H_2-CO pretreatment (20 µm resolution)

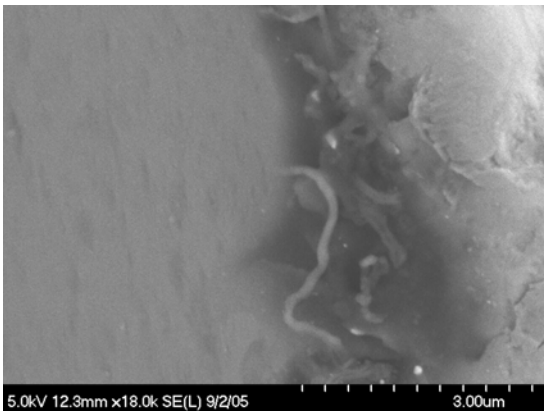

Figure 8:SEM micrograph of WC catalyst after H_2-CO pretreatment (3 µm resolution)

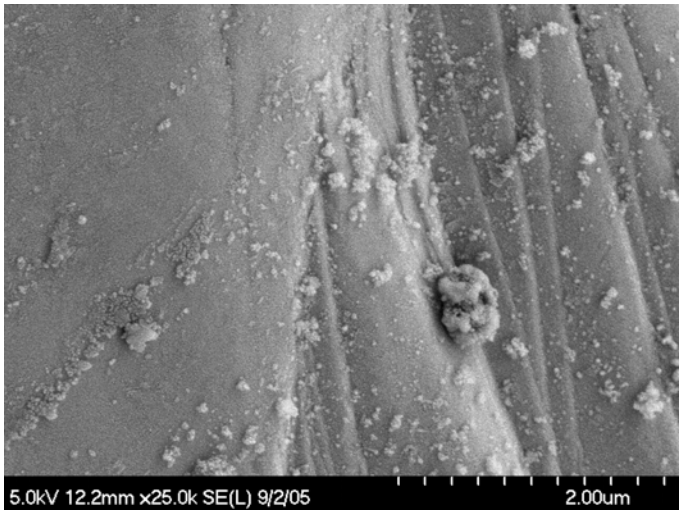

Figure 9: SEM micrograph of WC catalyst after H_2-CO pretreatment (2 µm resolution)

Effect of Gasification Gas Components on Decomposition of NH_3

Since the NH_3 decomposition reaction is of interest within the frame of removal of NH_3 from gasification gas streams, it is important to study the effects of H_2 and CO. These two gases are not only reducing species but may also block the active sites for NH_3 decomposition by chemisorption.

The influence of the presence of H_2 and CO on the TPRx profiles for the decomposition of NH_3 is shown in Figure 10. As a reference, the normal TPRx (NH_3 in helium) is also shown. For all runs, the catalyst was pretreated with an 80/20 mixture of H_2-CO. The profiles for the reaction in helium and in 14 % CO were almost identical. For the reaction in the presence of 10% H_2, the TPRx curve shifted toward higher temperatures. The curve reached a small plateau near 580°C and then the NH_3 decomposition increased to attain 100% conversion at 620°C.

The TOS behavior of NH_3 decomposition on WC at 525°C in the presence of He, 10% H_2, and 14% CO is shown in Figure 11. An induction period was evident in all cases but it was much longer when H_2 was present compared to the other two cases.

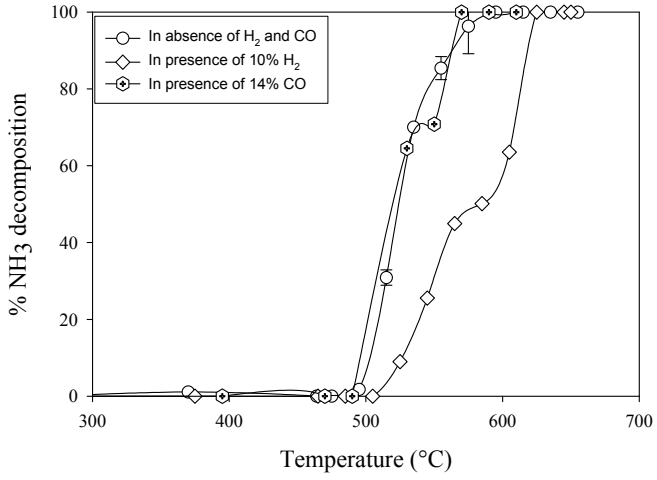

Figure 10: TPRx profiles for NH_3 decomposition in the presence of He, 10% H_2, 14% CO.

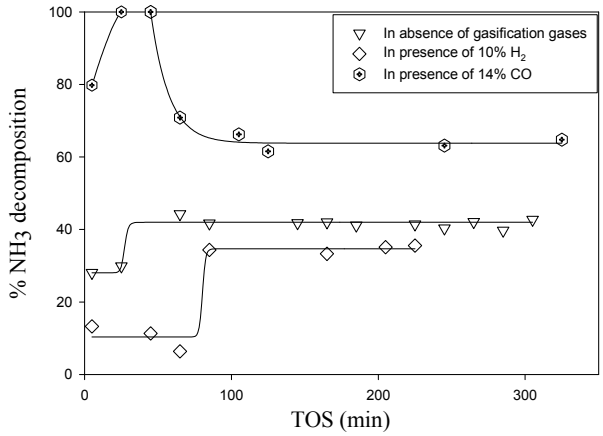

Figure 11: TOS behavior of WC catalyst for NH_3 decomposition at 525°C in the presence of He, 10% H_2, and 14% CO.

In all three situations, the reaction attained steady state but the reaction profile in CO was complex achieving 100% conversion at 25 min and then decaying slowly to finally attain a steady-state value of 60% after 6 h TOS. Overall, CO had a positive impact on NH_3 decomposition while the presence of H_2 hampered the reaction. It is possible that CO helps to maintain a fully carburized surface while H_2 contributes to a partial reduction of the WC surface.

Tar Cracking Catalysts

Tungsten-based catalysts, ultrastable Y (USY) zeolite, and Pt/γ-Al_2O_3 were evaluated for tar cracking activity in the fixed bed microreactor system using toluene as a surrogate tar compound. The tungsten-based catalysts were tungsten carbide (WC), tungstated zirconia (WZ), and Pt supported on tungstated zirconia (PtWZ). Toluene conversion over these catalysts was measured as a function of temperature and reactor gas composition. The gas compositions studied included inert (He), and various syngas components, H_2, CO, and CO_2, plus various blends. Ammonia was also added to various blends to investigate the simultaneous tar cracking and ammonia conversion performance of the selected catalysts. The experiments revealed that WZ calcined at 900°C was the most active for toluene hydrocracking at 700°C and incorporation of 5 wt% Pt to WZ calcined at 900°C was the most effective. Hence, these catalysts were also investigated for simultaneous NH_3 and toluene removal. The selected catalysts are referred to as WC, WZ900 and 5PtWZ. 5 wt% Pt/ γ-Al_2O_3 (5PtAl) also showed extremely high activity for toluene cracking.

Toluene cracking in the presence of 10% H_2

The time-on-stream behavior of WC for toluene cracking in 10% H_2 in He is shown in Figure 12. Methane and benzene were the only products of the reaction. At 700°C, low CH_4 and benzene concentrations were measured and no significant catalyst deactivation was observed. At 800°C, the catalyst showed considerable activity for both CH_4 and benzene formation and slight deactivation was observed. Carbon balance indicated that deactivation was caused by coke deposition during initial time-on-stream. These results indicated that WC could be a potential inexpensive catalyst for hot gas clean-up because it was also an excellent catalyst for NH_3 decomposition and has a sulfur tolerance.

The rates of formation of CH_4 and benzene on USY in the presence of 10% H_2 from 575 to 800°C are shown in Figure 13a and Figure 13b, respectively. These reactions were conducted at differential reaction conditions with toluene conversions maintained below 10%. From the figure it was observed that at 575°C, very low formation of CH_4 and benzene was observed. But the rates of formation increased

with TOS without any deactivation and steady-state rates of 4 μmole/g cat/s for CH_4 and 15 μmole/g cat/s for benzene were observed after 4 h TOS.

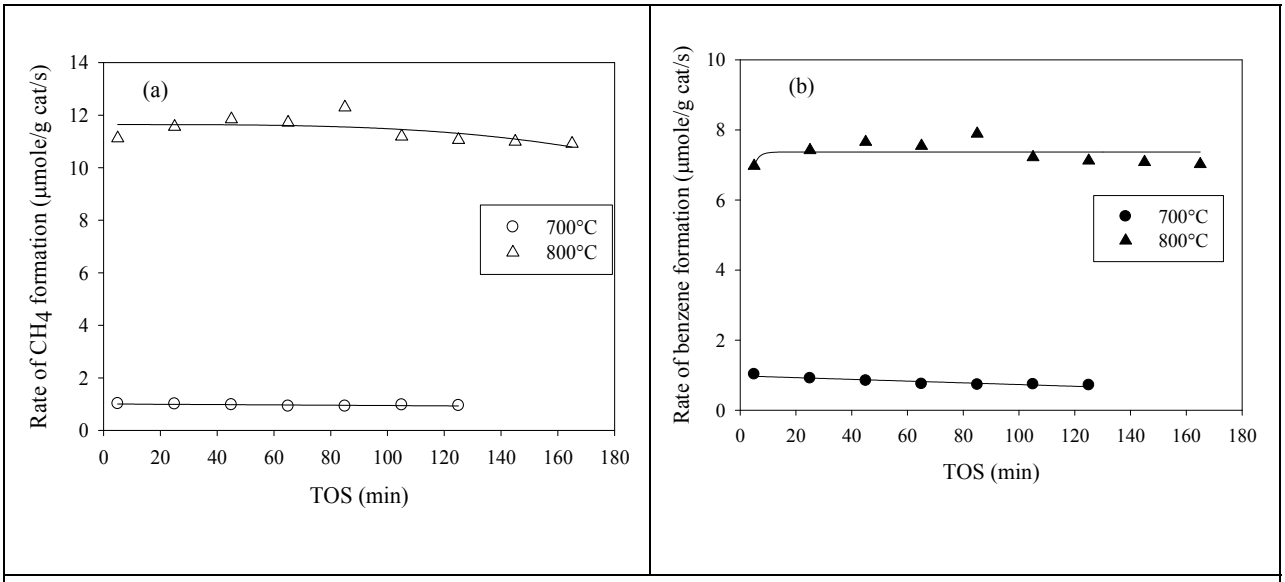

Figure 12: TOS behavior of WC for toluene cracking in the presence of 10% H_2; a) rate of CH_4 formation, b) rate of benzene formation.

A different behavior was observed at temperatures above 650 °C. The catalyst showed an induction period in which the rates increased to achieve a maximum value at 25 min TOS followed by a rapid partial deactivation. This behavior was observed till 800 °C. The possible cause of the partial deactivation observed after 650 °C could be the coke deposition on highly acidic sites of USY catalyst. Another possibility was the collapse of the zeolite structure at these high temperatures.

In order to investigate the precise reasons for the observed partial deactivation, the BET surface area of the catalyst after reaction at 700 °C was determined. The surface area of the fresh catalyst was 548 m^2/g while the surface area of the catalyst after reaction was only of 40 m^2/g. This significant loss of surface are suggests that coke deposits blocked the pores of the zeolite or the zeolite structure collapsed causing catalyst deactivation.

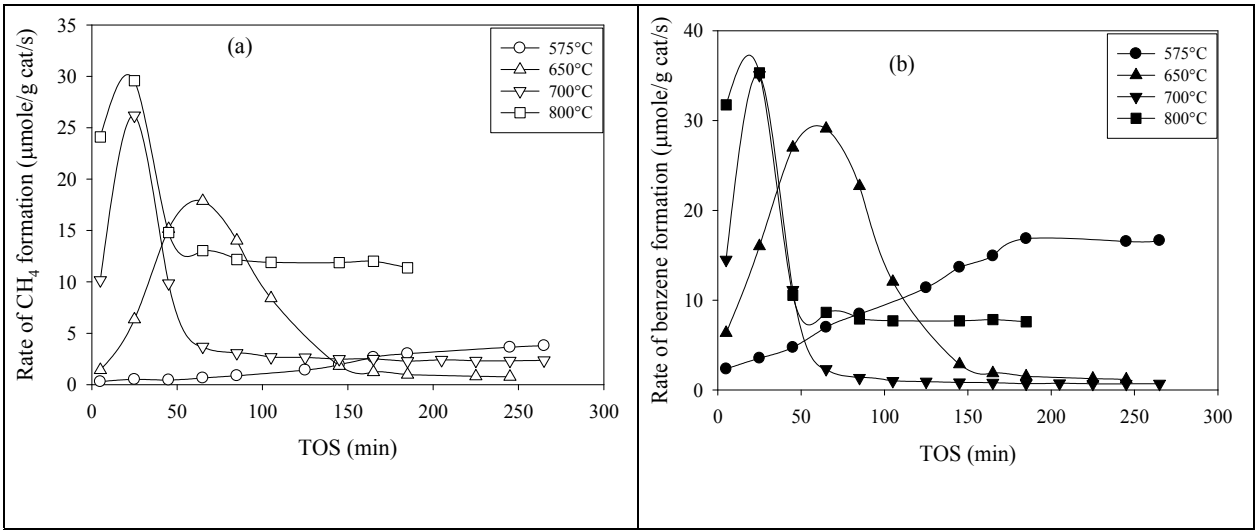

Figure 13: TOS behavior of USY for toluene cracking in the presence of 10% H_2; a) rate of CH_4 formation, b) rate of benzene formation.

Several reaction runs were conducted at 650, 675, and 700 °C under integral reaction conditions to get higher toluene conversions during initial TOS. The conversion of toluene as a function of TOS at these temperatures is shown in Figure 14.

The catalyst showed an induction period similar to that observed with differential conditions. The highest conversion was observed at 25 min TOS followed by a rapid partial deactivation. The catalyst showed ca. 10% conversion at steady-state at all these temperatures. As discussed earlier, the possible reason for this partial deactivation could be coke deposition on the active acid sites of the catalyst. The superficial residence time, maximum conversion, and k (the first order rate constant) at maximum conversion are shown in Table 1. The k values are used to calculate the apparent activation energy as shown in Figure 15.

The superficial residence time at these conditions was ca. 0.02 s, corresponding to a first-order rate constant of ca. 45 s^{-1}. From Figure 4, it was observed that there could be a possibility of mass transfer limitations at these reaction conditions. The apparent activation energy obtained was ca. 11 kcal/mol.

Table 1: Superficial residence time, maximum conversions, and k at maximum conversion in 10% H_2 for USY at different temperatures.

Reaction temperature (°C)	Superficial RT (sec)	Max. conversion (%)	k at max conv. (s^{-1})
650	0.0189	49	36
675	0.0186	57	45
700	0.0178	58	49

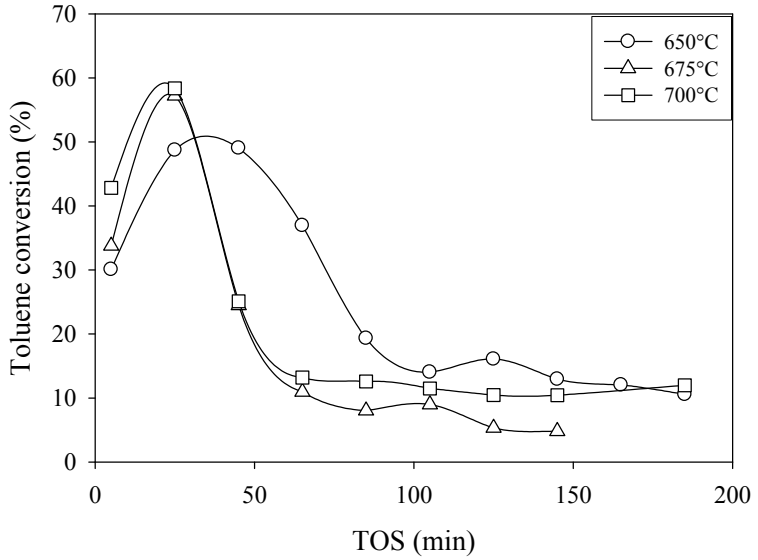

Figure 14: Toluene conversion over USY in 10% H_2 as a function of TOS at different temperatures.

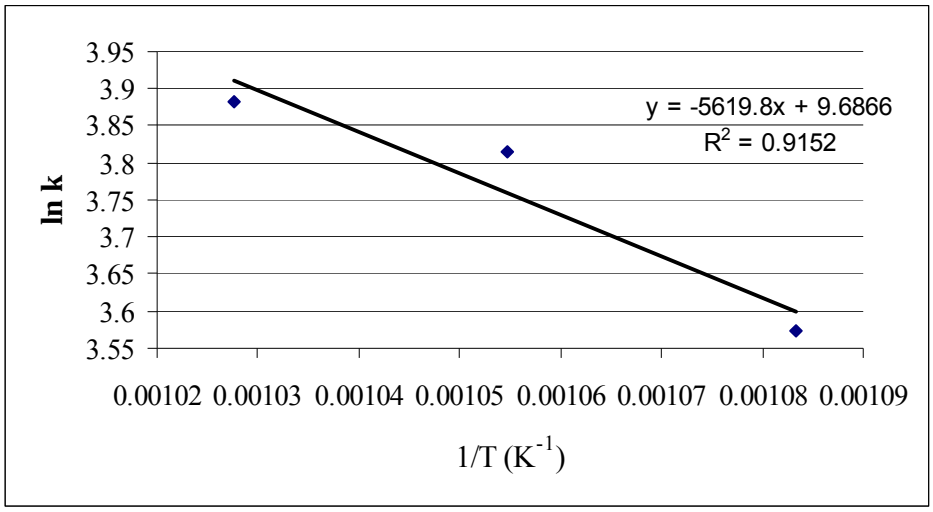

Figure 15: Arrhenius plot for toluene conversion over USY

A comparison of steady-state rates of CH_4 and benzene formation over WZ, 5PtWZ, and USY at different temperatures is shown in Figure 16 and Figure 17, respectively. At lower temperatures (< 575°C), only 5PtWZ showed considerable activity. After 575°C, WZ and USY showed considerable activity for toluene cracking in the presence of 10% H_2. WC did not show any activity until 700°C. After 700°C, the activity increased, and at 800°C, all the catalysts showed similar activities for both CH_4 and benzene formation. At 575°C, the rate of formation of benzene was higher than that of CH_4 on USY. Although the precise reason for this surprising behavior is still unclear, one possible explanation could be coke formation from CH_4 as per the following reaction:

$$CH_4 \rightarrow C + 2H_2$$

Thus, all catalysts were equally active for toluene cracking in the presence of 10% H_2 at temperatures greater than 700°C. It is only below 600°C that significant differences in the activity were observed.

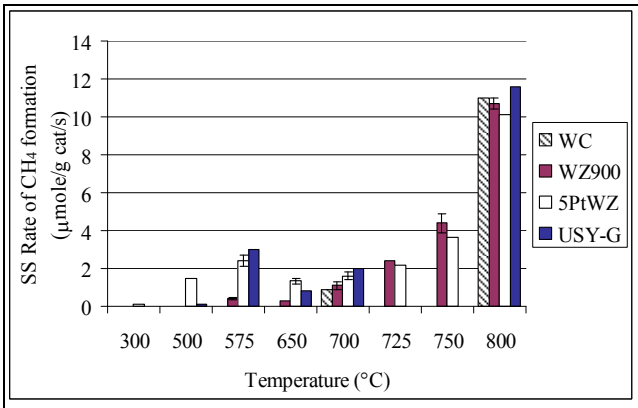

Figure 16: Comparison of steady-state rates of CH_4 formation over WC, WZ, 5PtWZ, and USY from 300 to 800°C

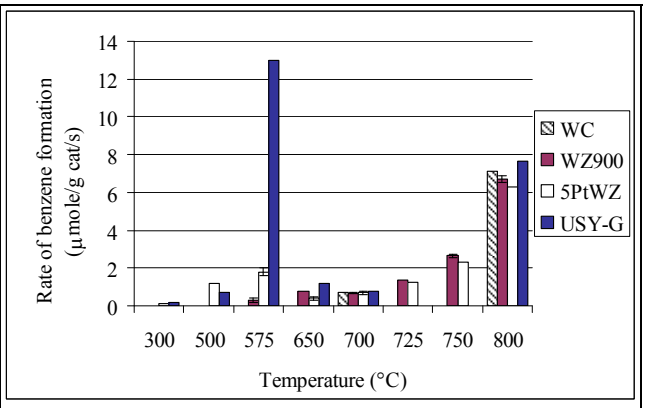

Figure 17: Comparison of steady-state rates of benzene formation over WC, WZ, 5PtWZ, and USY from 300 to 800°C

Although, WC, WZ, 5PtWZ, and USY show considerable activity for toluene hydrocracking to CH_4 and benzene after 600°C, another Pt-based catalyst, Pt/γ-Al_2O_3 (PtAl), was investigated for tar

cracking as well. The PtAl catalyst is extremely active for toluene hydrocracking. The catalyst yielded 350 µmole/g cat/s of CH_4, as shown in Figure 18, and 180 µmole/g cat/s of benzene, as shown in Figure 19, at 5 min TOS. This is an order of magnitude higher rates of CH_4 and benzene formation than on other catalyst studied (WC, WZ, 5PtWZ, and USY). A small partial deactivation was observed followed by a steady-state activity, which again was an order of magnitude greater than that of WC, WZ, 5PtWZ, and USY at similar conditions. As 10% H_2 was present in all the reaction runs, there was a highly likely possibility of dissociative adsorption of H_2 on Pt particles resulting in more ring opening and hydrogenolysis and leading to increased CH_4 formation.

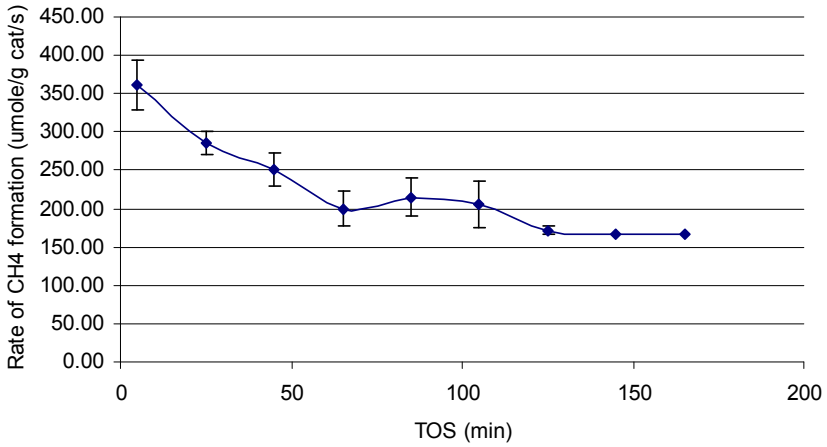

Figure 18: Rate of CH_4 formation during toluene decomposition in 10% H_2 over 5% Pt/Al_2O_3 at 575°C

The TOS runs were conducted on PtAl at different temperatures ranging from 300 to 800°C and the steady-state rates of CH_4 and benzene formation at these temperatures are shown in Figure 8. From the figure, it was observed that the rates of product formation increased monotonously from 300 to 575°C. After 575°C, a sudden drop in steady-state activities was observed, with the lowest activity at 800°C. Although the least activity was observed at 800°C, it was still greater than other catalysts investigated at those conditions.

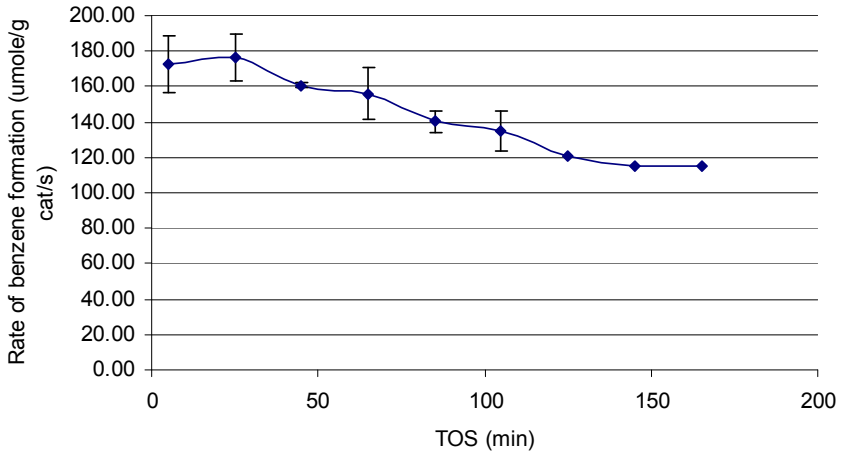

Figure 19: Rate of benzene formation during toluene decomposition in 10% H_2 over 5% Pt/Al_2O_3 at 575°C

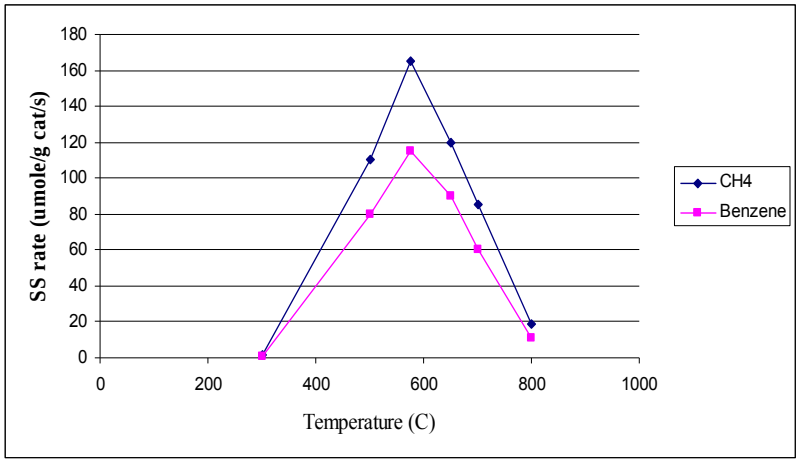

Figure 20: Steady-state rates of CH_4 and benzene formation from toluene decomposition over Pt/Al_2O_3 at different temperatures in 10% H_2.

A comparison of steady-state rates of CH_4 and benzene formation on PtAl, 5PtWZ, and WZ at 575 and 700°C is shown in Table 2. A comparison of CH_4/benzene ratio is also made. From the table, it was observed that at these temperatures, PtAl was much more active compared to 5PtWZ and WZ. These results indicated that incorporation of Pt was effective at 575°C, but the possibility of the presence of strong metal-support interactions (SMSI) in case of 5PtWZ might be responsible for poor activity compared to a catalyst in which SMSI were absent (PtAl, in this case). At higher temperature (700°C), the effect of Pt incorporation was nullified, as both WZ and 5PtWZ showed similar activities, but still the activities were lower compared to PtAl. These results indicated that PtAl was highly active catalyst for toluene cracking in the presence of 10% H_2.

The catalyst screening results showed that WC was active for toluene cracking in the presence of 10% H_2 at 800°C. USY showed an induction period at temperatures greater than 650°C, followed by a partial deactivation to attain a steady-state activity for CH_4 and benzene formation. At 575°C, no deactivation was observed for USY. The presence of 10% H_2 and 15% CO had a negative impact on the activity of USY at 575°C. WC, WZ, 5PtWZ, and USY displayed similar activities for toluene cracking in the presence of 10% H_2 at temperatures greater than 700°C. $Pt/\gamma\text{-}Al_2O_3$ was highly active catalyst for toluene cracking in the presence of 10% H_2. The activity was an order of magnitude more compared to WC, WZ, 5PtWZ and USY at 700°C.

Table 2: Comparison of steady-state rates of CH_4 and benzene formation on PtAl, 5PtWZ, and WZ at 575 and 700°C.

Temperature (°C)	SS CH_4 rate (µmole/g cat/s)			SS benzene rate (µmole/g cat/s)			CH_4/benzene		
	PtAl	5PtWZ	WZ	PtAl	5PtWZ	WZ	PtAl	5PtWZ	WZ
575	66.13	2.4	0.4	115.36	1.8	0.3	1.44	1.33	1.33
700	1.43	1.6	1.6	57.6	0.7	0.7	1.41	2.29	2.29

Toluene cracking in the presence of gasification gases

The TOS studies of toluene cracking and NH_3 decomposition were conducted in a plug flow micro-reactor at 1 atm and 700°C. The catalyst was placed at the center of the reactor sandwiched between quartz wool. Before the reaction, the temperature was raised in the presence of He to the desired reaction temperature at the rate of 5°C/min. The total flow rate was 100 sccm, consisting of 10% H_2, 15% CO, 15% CO_2, 10% H_2O, 4000 ppm of NH_3, 3000 ppm of toluene with balance He. The effluent from the reactor was analyzed using a Varian 3800 GC equipped with three columns and two detectors (a TCD and a FID).

The TOS behavior of WC in the presence of various gasification gases is shown in Figure 21 and Figure 22. CH_4 and benzene were the only products of the reaction in the presence of gasification gases. From the figure it is observed that when only He and toluene were present in the inlet stream, very low activity for toluene cracking to CH_4 and benzene was observed. However, as soon as 10% H_2 was introduced, the activity for both CH_4 and benzene formation increased by a factor of 2. The activity did not change a lot with the introduction of 15% CO, 15% CO_2, and 4000 ppm of NH_3. The highest activity for benzene formation was observed when all the gasification gases were present in the inlet stream. The rates of CH_4 formation were also higher when all gases were present.

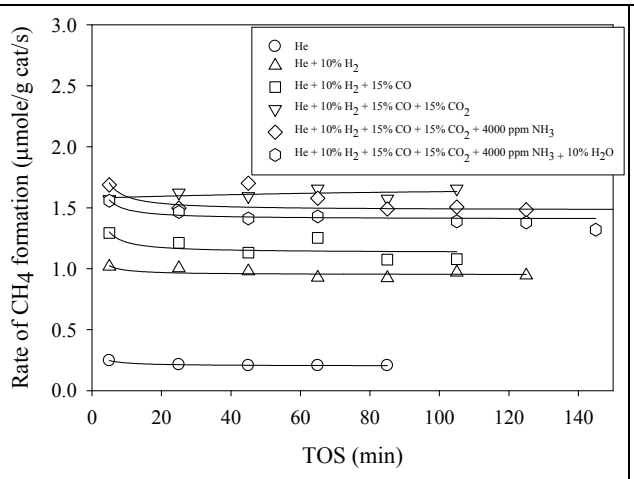

Figure 21: Rate of CH_4 formation during toluene decomposition over WC at 700°C as a function of gas atmosphere.

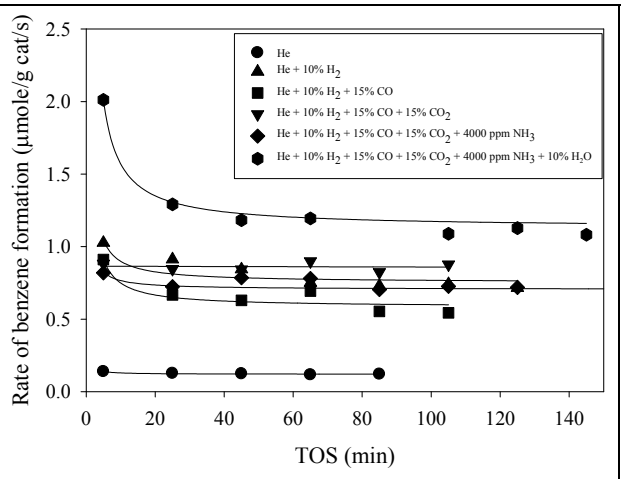

Figure 22: Rate of benzene formation during toluene decomposition over WC at 700°C as a function of gas atmosphere.

The high activity in the presence of H_2O and CO_2 could possibly be due to the introduction of O into the WC matrix resulting in the formation of WO_x acid sites, which is a common phenomenon for WC [5, 7, 19]. This *in situ* formation of acid sites could be responsible for more cracking of toluene to benzene and CH_4 resulting in higher rates of reaction as observed in Figure 21 and Figure 22. These results indicate that WC can effectively crack toluene to benzene and CH_4, even in the presence of gasification gases.

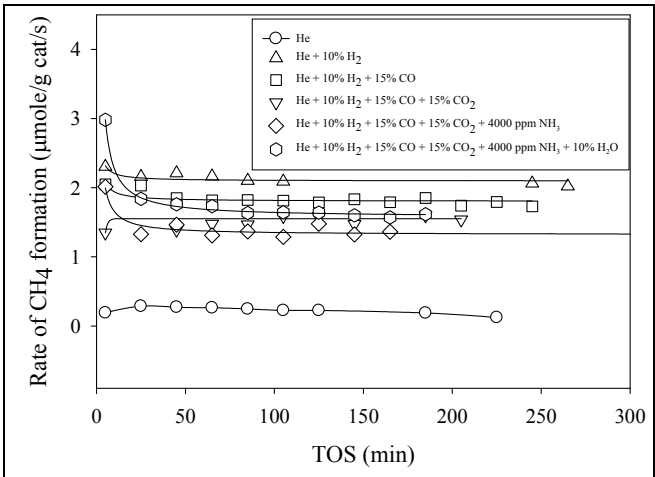

Figure 23: Rate of CH_4 formation during toluene decomposition over WZ900 at 700°C as a function of gas atmosphere.

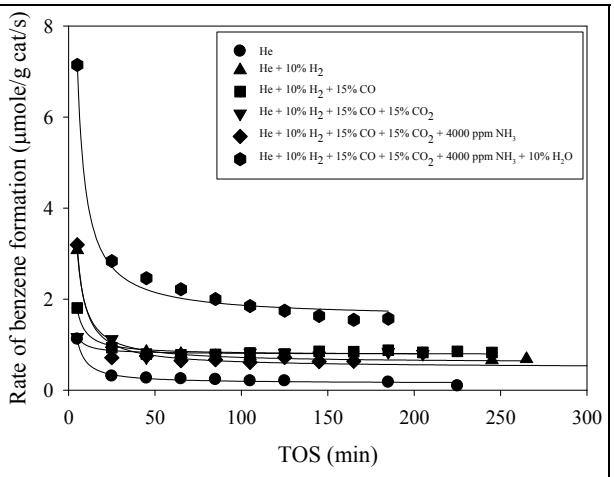

Figure 24: Rate of benzene formation during toluene decomposition over WZ900 at 700°C as a function of gas atmosphere.

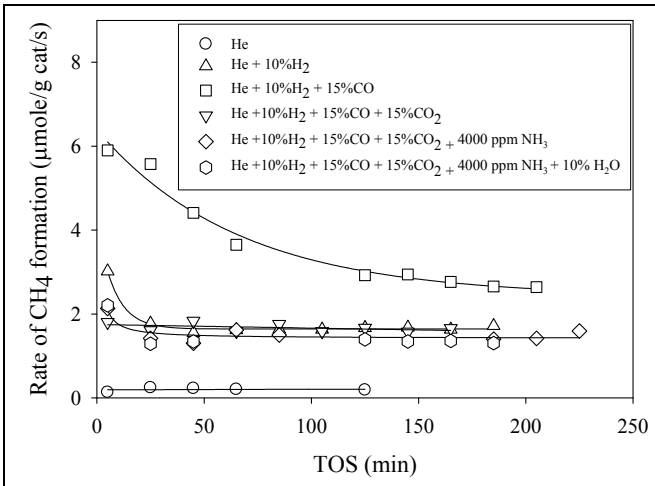

Figure 25: Rate of CH_4 formation during toluene decomposition over 5PtWZ at 700°C as a function of gas atmosphere.

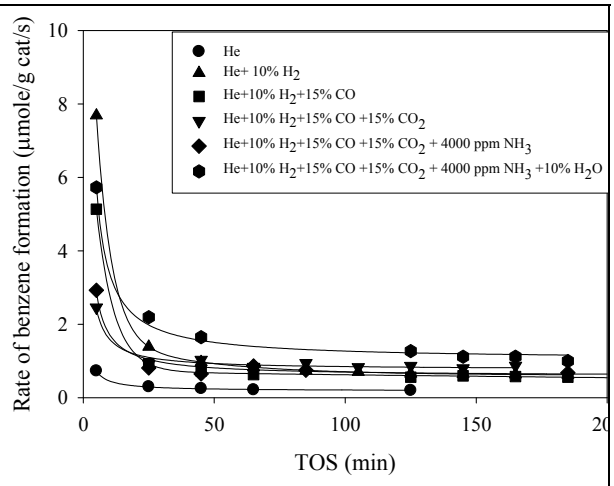

Figure 26: Rate of benzene formation during toluene decomposition over 5PtWZ at 700°C as a function of gas atmosphere.

The activity for toluene decomposition over WZ900 (Figure 23 and Figure 24) and 5PtWZ (Figure 25 and Figure 26) was low in a helium atmosphere. For both catalysts, negligible CH_4 and benzene formation was observed with only He and toluene were present in the inlet reaction stream. The toluene decomposition activity increased over both catalysts; WZ900 and 5PtWZ, with the introduction of the gasification gases. For WZ900, the highest activity for CH_4 formation was observed when only 10% H_2 was present (Figure 23). Methane formation was slightly lower with the introduction of CO, CO_2, NH_3 and H_2O. In case of benzene formation, the highest rate of reaction was observed when all gasification gases were present indicating that WZ900 could also be a potential candidate for tar removal from gasification gases. An initial partial deactivation was observed for both CH_4 and benzene formation as seen in Figure 23 and Figure 24 Coke deposition is the most probable reason for this partial deactivation as active sites of the catalyst are blocked.

In the case of 5PtWZ, the highest rate of CH_4 formation was observed in the presence of 10% H_2 and 15% CO (Figure 25). There is a possibility of CH_4 formation by reaction between H_2 and CO, and hence, the actual rate of CH_4 formation from toluene might be lower than the observed rate. The catalyst showed a similar behavior for both CH_4 and benzene formation in the presence of other gasification gases (Figure 25 and Figure 26). Similar to WC and WZ900, an initial partial deactivation was observed, probably due to coke deposition.

Previously, USY showed more activity at 575°C without any deactivation compared to other catalysts tested in 10% H_2 (Figure 13), therefore, the catalyst was investigated further to study its behavior in the presence of H_2 and CO. The TOS behavior of USY for toluene cracking in the absence and presence of 10% H_2 and 15% CO is shown in Figure 27 and Figure 28. The rate of formation of CH_4 is shown in Figure 27 and the rate of benzene formation is shown in Figure 28. From the figures, it was observed that in the absence of H_2 and CO, USY showed a significant conversion of toluene to CH_4 and benzene. The activity increased with TOS, and no deactivation was observed. After 3 h TOS, 5 µmole/g cat/s of CH_4 and 20 µmole/g cat/s of benzene was formed.

When 10% H_2 was introduced in the inlet stream, a similar behavior was observed, although the rates were lower than those in the absence of H_2. This suggested that at 575°C presence of 10% H_2 had a negative impact on the behavior of USY for toluene cracking. When 15% CO was co-fed with 10% H_2, the rates of CH_4 formation displayed a small increase compared to those in the presence of 10% H_2 only, while benzene formation did not show any significant change in the activity. These observations indicated that presence of 10% H_2 and 15% CO had a negative impact on the toluene cracking activity of USY at 575°C and at 1 atm pressure.

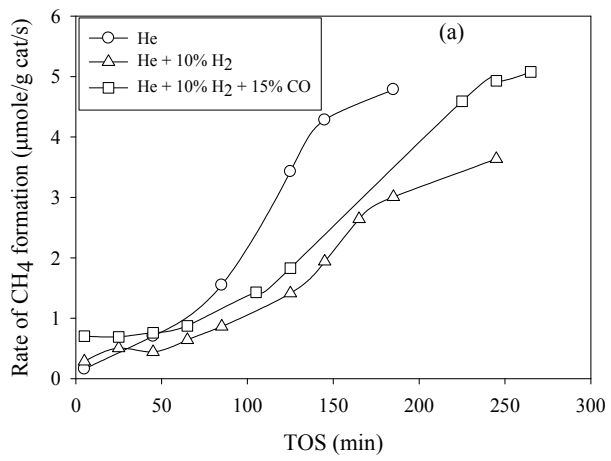

Figure 27: Rate of CH_4 formation during toluene decomposition over USY at 575°C as a function of gas atmosphere.

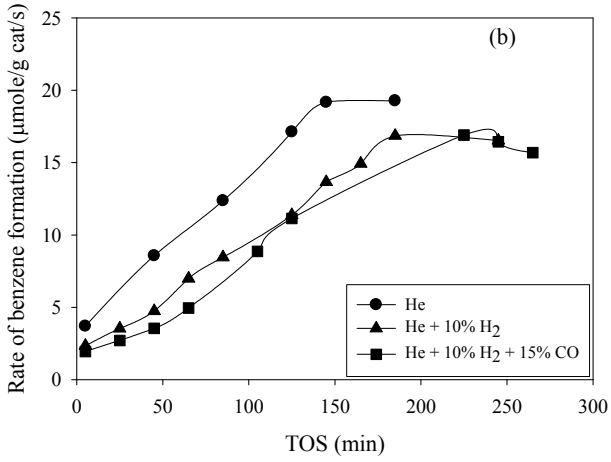

Figure 28: Rate of benzene formation during toluene decomposition over USY at 575°C as a function of gas atmosphere.

A comparison of steady-state rates of CH_4 and benzene formation on a "per-gm-catalyst" basis at 700°C and 1 atm in the presence of H_2, CO, CO_2, NH_3, and H_2O are shown in Figure 4. For comparison, the rates of CH_4 and benzene formation on ultra-stable Y zeolite at similar reaction conditions are also shown in Figure 29. From the figure it is observed that all the W-based catalysts showed rates of CH_4 and benzene formation comparable to that on USY.

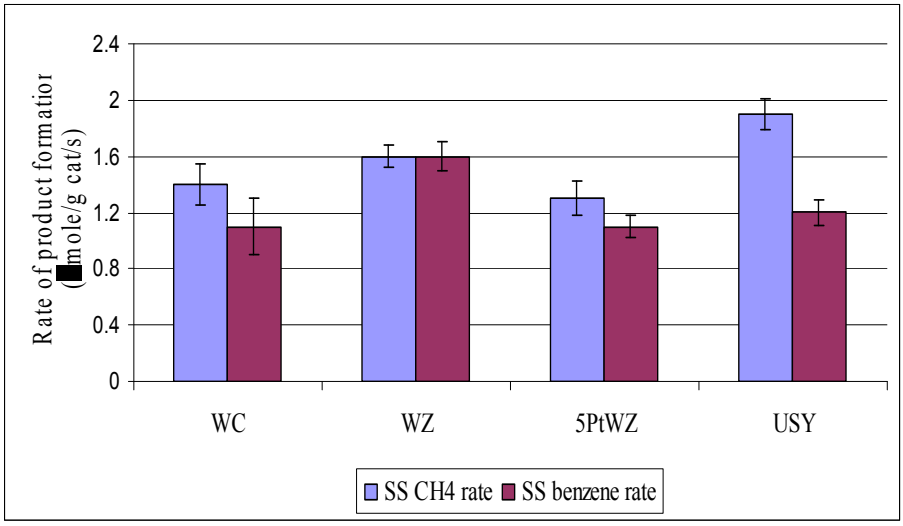

Figure 29: Comparison of SS rates of product formation on a "per-gm-catalyst" basis at 700°C and 1 atm on WC, WZ900, 5PtWZ, and USY.

Although the rates in Figure 29 are compared on a "per-gm-catalyst" basis, all these catalysts had different surface areas as determined by BET. Hence, the rates of CH_4 formation are also compared on a "per active surface area" basis as shown in Figure 5. From the figure it is observed that only WC was highly effective for toluene cracking on a per active surface area basis. Both WZ900 and 5PtWZ showed very little activity for both CH_4 formation as well as benzene formation. The least activity was observed for USY as seen from Figure 30. Thus from Figure 29 and Figure 30, it can be concluded that WC is an effective catalyst for toluene cracking in the presence of gasification gases on both "per gm" and " per active surface area" bases.

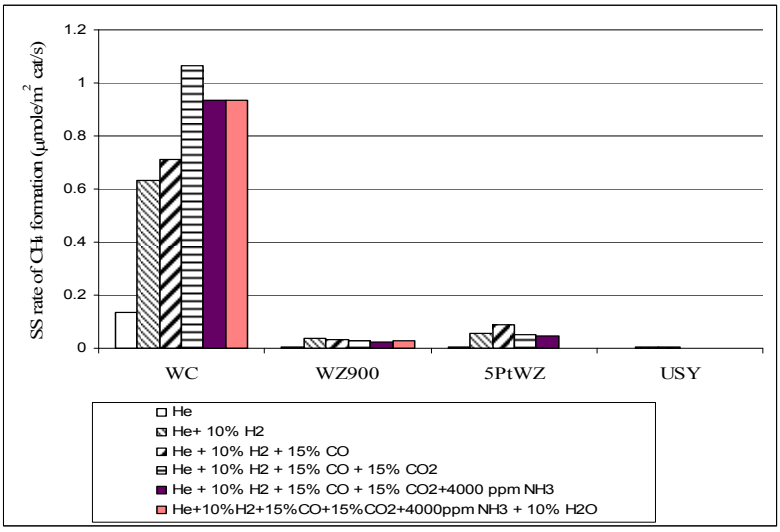

Figure 30: Comparison of rates of SS rate of CH_4 formation on various catalysts on "per active surface area" basis at 700°C and 1 atm.

Decomposition of NH_3 in the presence of gasification gases on WC, WZ900, and 5PtWZ

As discussed earlier, all W-based catalysts showed satisfactory performance for toluene cracking in the presence of gasification gases. Figure 31 shows the performance of these catalysts for NH_3 decomposition at 700°C and 1 atm in the presence of H_2, CO, CO_2, toluene, and H_2O.

From the figure it is observed that all catalysts showed a higher activity at 5 min TOS. But after 5 min TOS, an initial partial deactivation was observed for WZ900 and 5PtWZ. Both catalysts deactivated and did not show any activity for NH_3 decomposition after ca. 100 min TOS. On the other hand, WC showed ca. 50% conversion at 5 min TOS followed by a small deactivation to attain a steady conversion of ca. 30%.

The partial deactivation observed for all catalysts is due to coke deposition on the active sites as a result of toluene cracking. The results indicate that WC can satisfactorily decompose NH_3 to N_2 and H_2 even in the presence of other gasification gases. Thus, WC is a potential candidate for the simultaneous removal of NH_3 and tars from biomass gasification gas.

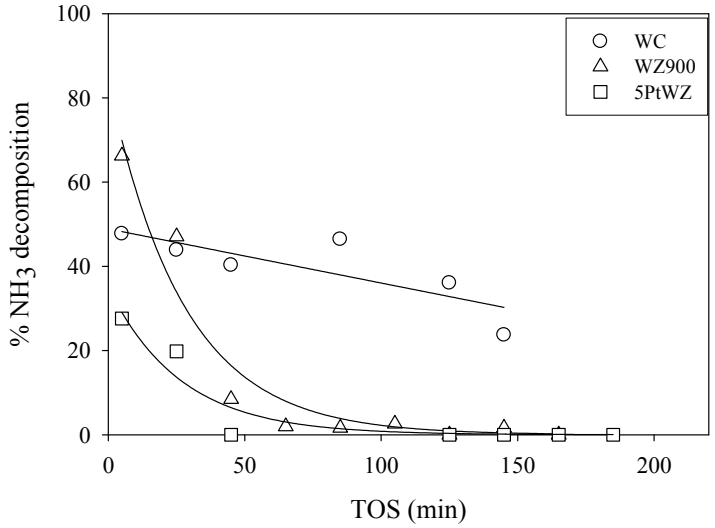

Figure 31: TOS behavior of WC, WZ900, and 5PtWZ for NH3 decomposition at 700°C and 1 atm in the presence of gasification gases.

In previous studies, 5PtAl showed extremely high activity for toluene cracking to CH_4 and benzene. Hence, this catalyst was further explored to study its performance for simultaneous NH_3 and toluene removal in the presence of other gasification gases. The conversion of toluene and rates of formation of products on 5PtAl at 700°C, 1 atm and in the presence of various gasification gases are shown in Table 3.

From the table it is observed that, when only He and toluene were present in the inlet stream, a small conversion of toluene was observed to CH_4 and benzene. When 10% H_2 was introduced, the toluene conversion increased to ca. 38%. Presence of Pt and H_2 is known to increase the cracking activity [10]. When CO was co-fed with H_2, the toluene conversion dropped to 10% but the rate of CH_4 formation was higher, possibly due to the reaction between H_2 and CO. When CO_2 and NH_3 were introduced to the reaction stream along with H_2 and CO, the conversion increased to ca. 90% with more selectivity towards CH_4 (ca. 60%). Complete conversion of 3000 ppm of toluene at the reaction conditions used in the present study was observed with CH_4 being the dominant product when H_2O was also introduced in the inlet stream along with the other gases. 5PtAl showed ca. 60% conversion for NH_3 decomposition in the presence of H_2, CO, CO_2, toluene, and H_2O which was constant for ca. 5 h TOS (data not shown).

Thus, the results indicate that 5PtAl is a highly effective catalyst for simultaneous NH_3 and toluene removal in the presence of other gasification gases. Although it is a highly active catalyst, the performance of 5PtAl would undoubtedly be affected by the presence of H_2S in the inlet stream. However, if H_2S was removed prior to passing the gasification stream over 5PtAl, then it should be an extremely active catalyst for simultaneous NH_3 and toluene removal.

Table 3: Performance of 5PtAl in the presence of various gasification gases

Condition	SS toluene conversion (%)	SS rate of CH_4 formation (µmole/g cat/s)	SS rate of benzene formation (µmole/g cat/s)
He	10	0.55	0.6
He + 10% H_2	38	81	60
He + 10% H_2 + 15% CO	10	80	13
He + 10% H_2 + 15% CO + 15% CO_2	92	80	51
He + 10% H_2 + 15% CO + 15% CO_2 + 4000 ppm NH_3	92	80	50
He + 10% H_2 + 15% CO + 15% CO_2 + 4000 ppm NH_3 + 10% H_2O	100	100	15

WC showed significant activity for simultaneous removal of NH_3 and toluene in the presence of H_2, CO, CO_2, and H_2O at 700°C and 1 atm. The activity was comparable with a commercial ultra-stable Y zeolite. A small initial partial deactivation was observed for both CH_4 and benzene formation. The possible reason for this initial partial deactivation is coke deposition on the active sites of the catalyst. On a per-m^2-active surface area basis, WC was extremely active for toluene cracking compared to other W-based catalysts and even the commercial USY zeolite. 5 wt% Pt/γ-Al_2O_3 also displayed extremely high activity for both NH_3 decomposition and toluene cracking at 700°C and 1 atm in the presence of other gasification gases.

Tar Cracking Catalyst Development

Biomass gasification product gas consists mainly of CO, H_2, CO_2, H_2O, N_2, and hydrocarbons. Minor components of the product gas include tars, sulfur and nitrogen oxides, alkali metals, and particulates. Tars are high molecular weight hydrocarbons that can range from 0.1 to 20 wt% in the biomass-derived syngas. Excessive tar levels in biomass-derived syngas potentially threaten the successful application of downstream syngas utilization processes such as compressors, catalytic fuel synthesis, and wastewater treatment.

The main objective of this effort is to develop a tar cracking catalyst that can achieve >99% tar cracking conversion in a laboratory-scale fluidized bed reactor. Catalyst characterization tools will be used to assist in catalyst development and understanding deactivation mechanisms (coking, sulfur-poisoning and attrition).

Catalysts tested for tar cracking activity include spent FCC, olivine, Zeolites (USY, etc.), and nickel-based materials. Tar cracking experiments at RTI were performed in a fluidized-bed reactor system. The process flow diagram of the reactor system is shown in Figure 32. The reactor is a 2" OD quartz tube fluidized bed reactor with a quartz frit (7 um pore diameter) to support the catalyst and distribute the feed gas. The reactor is housed in a 3-zone furnace to maintain a constant reactor and catalyst bed temperature. The temperature profile throughout the reaction zone and catalyst bed is measured with a 1/8" thermocouple inserted in a ¼" protection tube. The reactive feed mixture was obtained by mixing individual components (H_2, CO, CO_2) to manipulate the syngas composition. An HPLC pump delivers feed water for steam production in the vaporizer while a tar solution is fed using a syringe pump. A nitrogen carrier gas fed to the vaporizer preheater sweeps water vapor and tars into the reactor. Nitrogen is also used as an internal standard in dry gas analysis. The effluent from the reactor passes through an in-line filter to trap any entrained catalyst particles at the exit of the reactor. Product gas lines downstream of the quartz reactor are heat traced to maintain the gas temperature at 350°C. The solids-free product gas enters a metal condenser maintained at approximately 13°C to trap all condensable vapors. A slipstream is withdrawn upstream of the condenser to draw a hot product sample for tar sampling using a Solid Phase Adsorption (SPA) cartridge. Hot sampling using SPA is used to quantify the

tar content in the product stream. Any uncondensed water and tar vapors remaining in the process gas leaving the metal condenser are trapped in an impinger filled with ice. A slipstream of the dry, tar-free product gas is withdrawn downstream of the impinger and sampled with an on-line micro GC capable of sampling product gas every 3-4 minutes.

To begin a series of catalyst testing experiments, a known amount of bed material (inert or catalyst) is loaded into the quartz tube reactor and the system is preheated to the desired temperature while fluidizing the catalyst bed with nitrogen. Once the operating temperature is achieved, water is fed into the reactor using an HPLC pump. The surrogate tar mixture is fed into the reactor once the steam flow rate is stable.

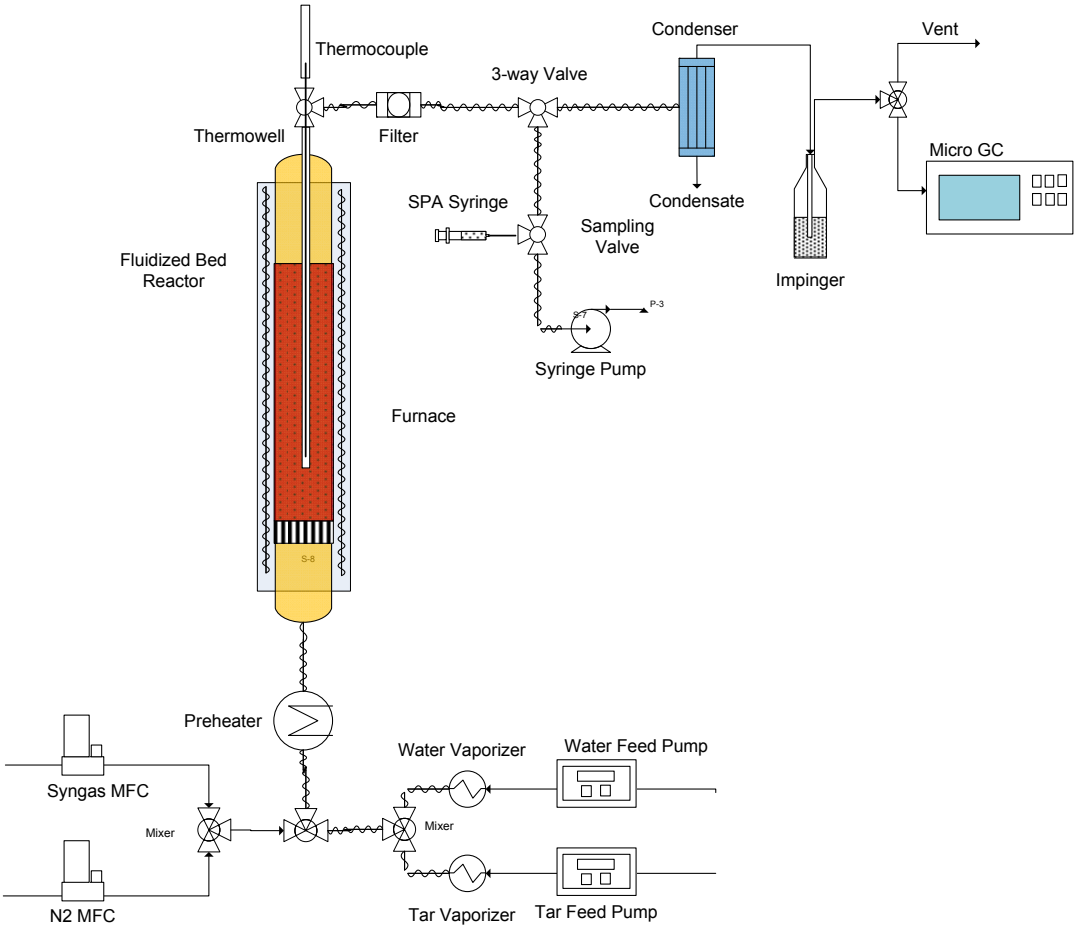

Figure 32: Fluidized bed reactor system for tar cracking experiments

Tar Analysis

A Solid Phase Adsorption (SPA) method has been modified to qualitatively and quantitatively analyze tars and condensable products. Approximately 60 ml of hot product gas is extractively sampled through a silica-based amino phase (NH_2) cartridge where all the tar in the sampled gas will be adsorbed on the active phase. The amine active phase is strongly polar and thus posses very good gas phase trapping efficiency.

Tar adsorbed on the SPA cartridge is extracted by using eluotropic solvents (i.e. solvents of increasing polarity). The SPA column is first extracted with dicholoromethane (DCM) to desorb nearly all aromatic hydrocarbons. Phenolic compounds not desorbed with the first solvent are recovered with a

DCM-isopropanol extraction. The third and final extraction is with isopropanol. The extracted liquid fractions are analyzed by GC-MS.

Tar cracking experiments

The operating conditions used for the tar cracking experiments are as below:

Reaction temperature	600-700 °C
Reaction pressure	1 atm
Gas composition	60% N_2/Syngas and 40% H_2O (mol%)
Tar content	35 g/Nm^3
H_2S concentration	100 ppmv

The thermal efficiency of the syngas clean-up process improves when the clean-up process temperature is matched with the gasifier outlet temperature to eliminate the need of cooling or heating the product gas. For this purpose, tar cracking reactions were operated at 600-700°C. Although a reaction temperature of 600°C is more appropriate, reactions were also operated at 700 °C to understand the effect of temperature on catalyst performance. The feed to the reactor will consist of 60 mol% gas, either N_2 or syngas based on the experiment, 40 mol% water and 35 g/Nm^3 of tar to simulate syngas produced during atmospheric pressure indirect steam gasification of biomass. The gas phase products from the cracking of tar, present in small concentration in the feed, will be masked by the feed syngas and thus difficult to analyze in the GC. Since accurate analysis of the product gas is critical to gauging catalyst performance, screening experiments will be conducted with nitrogen as the feed gas. A simulated multicomponent mixture was used to represent tar. The tar mixture was composed of five hydrocarbons: 25 wt% toluene; 25wt% phenol; 25.0wt% p-cresol; 12.5wt% naphthalene; and 12.5wt% methylnaphthalene.

Baseline tar cracking experiments were carried out using silicon carbide as the inert material under both nitrogen and syngas flow using the operating conditions as discussed above. The dry product gas composition observed during the tar cracking experiment at 600 °C using SiC bed material is shown in Figure 33. For the first hour nitrogen was used as the carrier gas to allow the bed to thermally equilibrate and flows to stabilize. After one hour the gas feed was switched from nitrogen to a syngas blend. The composition of syngas is indicated by solid lines in Figure 33. Tar cracking in the presence of syngas was performed for an hour. The product gas composition matches the inlet syngas composition indicating the absence of tar cracking products in the gas phase over SiC. The SPA method was used to measure the tar content in the product gas stream and estimate tar conversion. Figure 34 presents the tar content in the product gas stream and the solid line at 35 g/Nm^3 indicates the feed tar concentration. A high degree of scatter was observed in the product gas tar content numbers with most of the data points below the feed concentration. Observations after the experiment indicated that the scatter in the data was caused by incomplete vaporization of the surrogate tar mixture and water in the preheater.

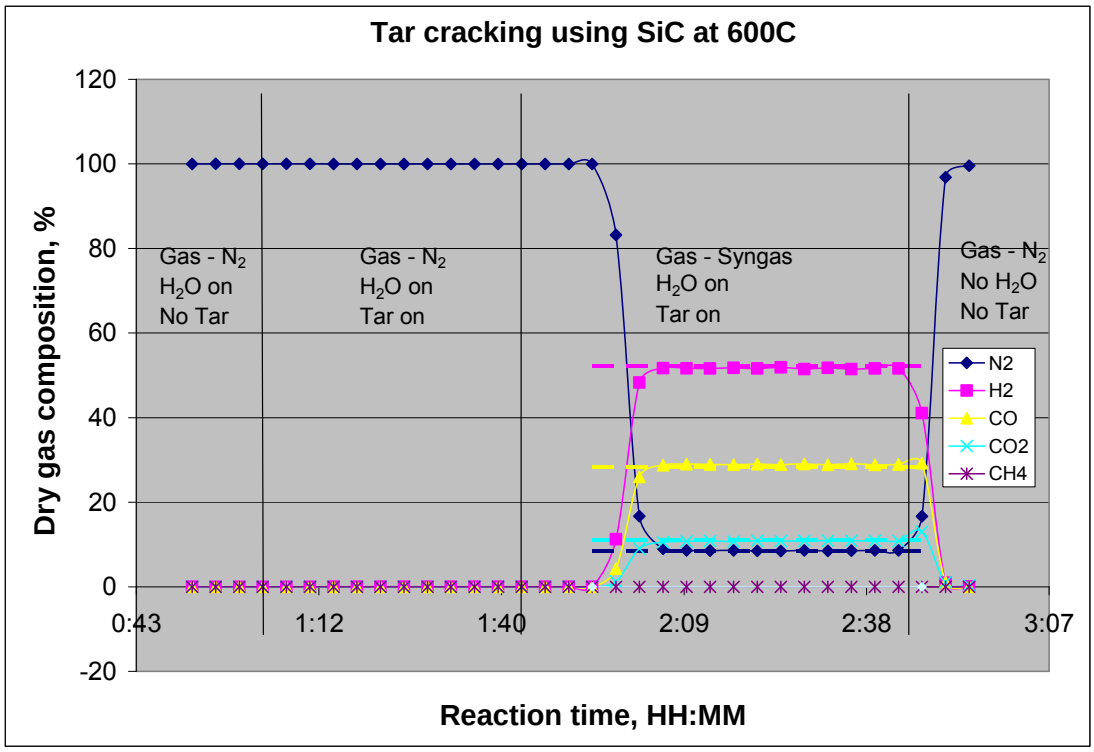

Figure 33: Product gas composition during tar cracking using SiC

- Several modifications were made to the reactor system to address the problem of incomplete liquid vaporization in the preheater and the tar sampling technique was modified to improve the tar trapping efficiency of the method.
- Length of the liquid feed line entering the preheater was increased to feed the liquids deeper in the preheater section. This causes the liquid to come in contact with gas at higher temperature and thus increases liquid vaporization.
- Earlier, two different preheaters were used for heating syngas and vaporizing liquids. It was found that one preheater was sufficient to heat syngas and also vaporize the liquids. Flowing both gas and liquid through the same preheater increased gas velocity through the preheater and thus the heat transfer coefficient.
- Based on some additional tests, it was observed that benzene and toluene were not adsorbing completely on the SPA cartridge. This problem was resolved by using two SPA cartridges in series to sample hot product gas. However, instead of having to extract two cartridges for one data point 150mg of coconut shell charcoal was added to a SPA cartridge to trap the highly volatile tars (benzene and toluene). Addition of charcoal did improve the quantification of toluene and benzene.
- The amount of product gas sampled for tar analysis was reduced from 60 ml to 30 ml.

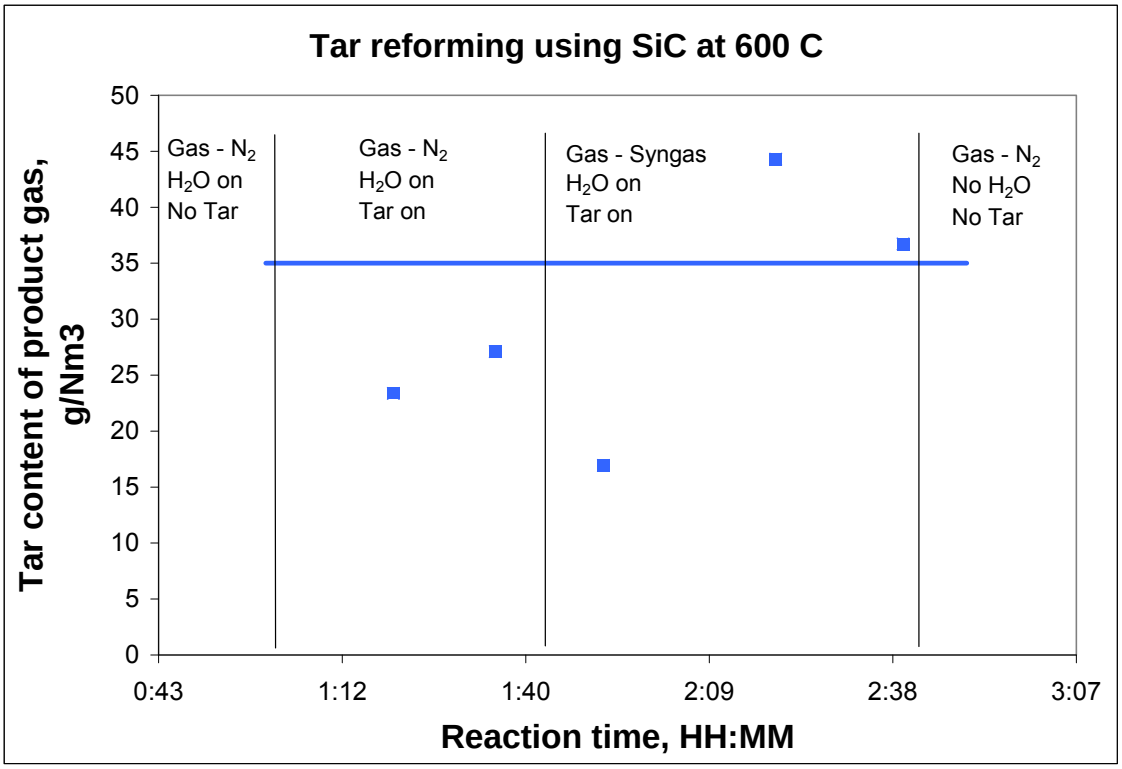

Figure 34: Tar content in the product stream during tar cracking at 600 C using SiC bed material

The baseline tar cracking experiment was repeated after these modifications were made in the system. The tar concentration in the product stream is shown in Figure 35. An improvement in the quantification of the product gas tar content was observed. The modified system and tar sampling method will be used as a standard in all the next experiments.

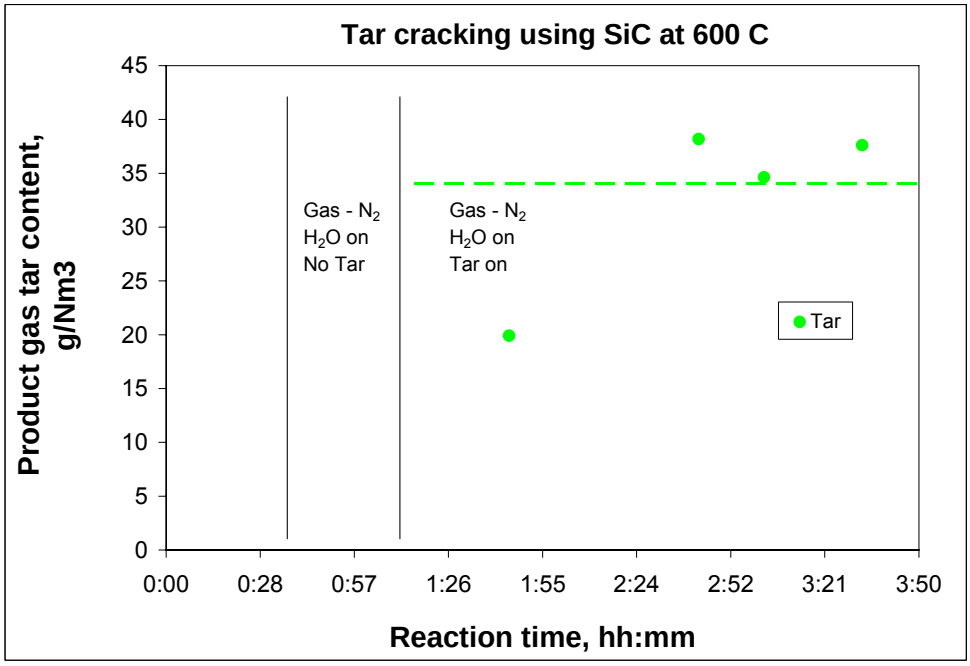

Figure 35: Tar content in the product stream during tar cracking at 600 C using SiC bed material

Catalyst Screening Tests

The following catalysts were screened for tar cracking activity:

- Olivine
- Spent FCC
- USY
- ZSM-5
- Commercial FCC
- Ni/Al_2O_3
- $Ni/ZnO-Al_2O_3$

Olivine sand from AGSCO Corporation was supplied by the National Renewable Energy Laboratory (Golden, CO). Zeolites USY (CBV-600) and ZSM-5 (CBV-5524G) were purchased from Zeolyst Inc. It was not possible to use these materials as received because they were powders with particle size <20 μm and would not fluidize in the catalyst testing reactor. Consequently, fluidizable catalyst particles were prepared by spray drying the zeolites with kaolin clay and silica sol to obtain catalyst particles with a size distribution in the rage of 60-80 μm. The zeolite concentration used in the spray drying slurry was 35 wt%. The commercial FCC material was supplied by GRACE Davison. The two nickel-based materials, Ni/Al_2O_3 and $Ni/ZnO-Al_2O_3$, were experimental materials produced at RTI.

Initially, catalyst screening experiments were conducted in a simulated syngas mixture containing H_2, CO, and CO_2. The high concentration of these components made it difficult to quantitatively measure the amount of tar cracking products. Consequently, catalysts were tested under an inert atmosphere to probe the tar cracking reaction pathways.

All the catalysts listed above have different bulk densities and particle size which require different gas velocities to fluidize. In order to present a direct comparison of the catalyst performance, screening experiments were conducted at a constant gas hourly space velocity (GHSV) of 1635 hr^{-1}. This corresponds to a gas residence time of 2.2 sec which is similar to the design basis used in the pilot-scale Therminator unit. The different operating parameters required for catalyst screening experiments at 600 °C to target the desired residence time are summarized in Table 4. The tar conversion achieved during the catalyst screening experiments at 600 and 700 °C is presented in Figure 36.

Table 4: Operating conditions for tar cracking catalyst screening experiments at 600 °C

	Olivine	Spent FCC	ZSM-5	USY	FCC	Ni/Al_2O_3	$Ni/ZnO-Al_2O_3$
Bed density, lb/ft^3	136	68.3	51.2	45.4	60.5	89.0	94.0
Residence time, sec	2.2	2.2	2.2	2.2	2.2	2.2	2.2
Catalyst weight, g	840	194	65	64	92	100	100
Feed flow, accm	10500	4800	2150	2400	2600	1900	1800
$W/F_{A,0}$, g/sccm	0.256	0.128	0.096	0.085	0.114	0.167	0.176
$W/F_{A,0}$, g/accm	0.080	0.040	0.030	0.027	0.036	0.052	0.055

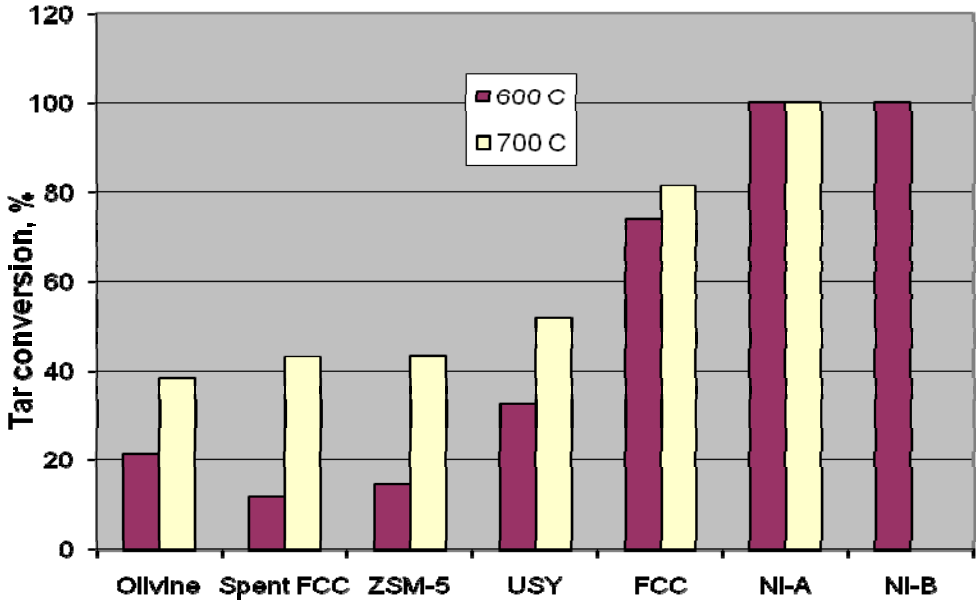

Figure 36: Tar conversion at 600 and 700 °C observed during catalyst screening in N_2

Tar conversion was calculated using the amount of tar observed in the product stream, as measured by the hot sampling method, compared to the amount of tar fed in to the reactor. Olivine has good reforming activity at temperatures above 800 °C. However, at 600-700 °C it is not very active as the tar conversion ranged from 20-39 % respectively. From the four zeolite materials tested for tar cracking activity, tar conversion was highest when using the commercial FCC catalyst as the bed material at both 600 (74% conversion) and 700 °C (81% conversion). Compared to the commercial FCC catalyst, which uses zeolite USY, spray dried USY showed significantly lower conversion (33% and 52%, respectively) at 600 and 700 °C. The higher activity of the commercial FCC catalyst might be due to higher zeolite concentration in the catalyst or due to the use of an active binder material. The relative tar cracking activity of the zeolite catalysts at 600 °C increased in the order - Spent FCC<ZSM-5<Olivine<USY<FCC. On the other hand, the Ni catalysts on two different supports, alumina and zinc aluminate, presented almost complete tar conversion even at 600°C. These results were based on the measurement of tar in the product stream using SPA cartridge for sampling and a GC-MS for detection. This tar measurement process has a detection limit corresponding to 99.5% conversion of tar. When using the Ni catalysts for reaction, no peaks corresponding to feed tar were observed in the GC-MS confirming >99.5% conversion of tar.

Higher reaction temperature increased tar conversion for all catalysts. The effect of temperature was more pronounced in case of catalysts with low activity compared to catalysts with high activity.

Catalyst selectivity towards cracking and reforming can be measured using the ratio of cracking reaction products (carbon as coke + carbon as gaseous hydrocarbons) and reforming reaction products (CO and CO_2). Based on this metric, all zeolite catalysts had a higher yield towards cracking than reforming. When using FCC catalyst for tar cracking, 93% of the carbon in the product is laid down on the catalyst as coke and only 7% is present in the gas phase. The high selectivity of FCC catalyst towards coke formation is similar to the other zeolite catalysts tested. At 600 °C, the cracking yield was the highest for spent FCC followed by commercial FCC, USY and ZSM-5. On the contrary, although 100% tar conversion was observed in case of both the Ni catalysts, selectivity towards coke was substantially reduced. Selectivity towards coke formation for Ni-ZnAl catalyst was 46% whereas for Ni-Al it was even lower (23%). At 700 °C, selectivity towards reforming increased for almost all catalysts.

The quality of the catalyst screening data was verified by determining the carbon balance. The carbon balance for the catalyst screening experiments is summarized in Table 5. Apart from the experiment with olivine at 700 °C, the feed carbon was well accounted for with the carbon balance ranging between 85-115%. The liquid portion represents carbon from all the liquid hydrocarbons, reactants and products, as analyzed with the GC-MS. Carbon in the gas phase is from CO, CO_2, CH_4 and other light hydrocarbons. The concentrations of other hydrocarbons periodically detected in the product stream were insignificant. Carbon deposited on the catalyst as coke was measured using thermogravimetric analysis (TGA).

Table 5: Distribution of feed carbon in the product stream and overall carbon balance during tar cracking reactions for different catalyst

Catalyst	Reaction temperature (°C)	Product yield, %		Unconverted tar in product, %	Product gas flow rate, sccm	Total carbon balance, %
		Coke	Gas			
Olivine	600	5.4	0.7	78.6	7	84.7
	700	4.8	3.9	61.7	22	70.4
Spent FCC	600	24.7	1.6	88.0	6	114.3
	700	26.8	7.2	56.9	19	90.9
ZSM-5	600	14.6	3.8	85.1	4	103.5
	700	30.1	6.5	56.6	7	93.2
USY	600	35.1	3.6	67.4	5	106.2
	700	36.6	11.8	48.0	12	96.4
FCC	600	68.8	5.4	25.7	9	99.8
	700	59.4	18.7	18.6	24	96.7
Ni/Al_2O_3	600	*23.9*	77.1	0.0	81	101.0
	700	*24.4**	75.6	0.0	52	-
$Ni/ZnO\text{-}Al_2O_3$	600	*45.6**	54.4	0.0	54	-

*****_Coke deposition on Ni-based catalysts is determined by difference pending results from TGA analysis._

The amount of individual tar components in the liquid products during the catalyst screening experiments at 600 and 700 °C are shown in Figure 37 and Figure 38, respectively. Apart from the feed tar constituents, benzene was the only other hydrocarbon detected in the product stream. During tar cracking, benzene can be produced by the demethylation of toluene or dehydroxylation of phenol. Other possible reactions include demethylation and dehydroxylation of cresol to produce phenol and toluene respectively. Methylnaphthalene can also undergo demethylation to form naphthalene. All these hydrocarbons have the potential to contribute in some combination of reforming and coking reactions. Thus, benzene is produced during the reaction, cresol and methylnaphthalene are only consumed during the reaction whereas toluene, phenol and naphthalene are produced as well as consumed during the reaction.

Conversion of methylnaphthalene to naphthalene via the demethylation reaction was observed with all catalysts at 600 °C. A corresponding increase in the naphthalene content was observed with all catalysts except for olivine. Catalyst activity for methylnaphthalene conversion (demethylation+coking) decreased in the order NiAl=NiZnAl>FCC>USY>spent FCC>ZSM-5>Olivine. At 600 °C, except when using olivine, almost all cresol was converted. Cresol conversion was limited to about 45% over olivine.

With all the catalysts, a decrease in cresol concentration was accompanied with an increase in toluene concentration whereas the phenol concentration remained unchanged. This concludes that dehydroxylation of cresol is more favored compared to demethylation. It is also observed that the phenol concentration remains fairly stable with all the catalysts with low activity where as the amount of toluene decreases and that of benzene increases with increasing conversion. Even with zeolites that have high tar cracking activity (USY and FCC) the phenol concentration in the product stream was much higher compared to toluene. This indicates that the zeolite catalysts are less active towards phenol dehyroxylation compared to demethylation of toluene. As a result, phenol conversion of about 45-50% was observed when using USY, ZSM-5 and spent FCC, 35% with olivine while the conversion was around 85% with FCC catalyst. The two most unreactive hydrocarbons were benzene and naphthalene. No liquid hydrocarbons were detected in the product stream when using the Ni catalysts. Based on these results the increase in reactivity of the individual tar components is observed in the following order: benzene < naphthalene < phenol < toluene < methylnaphthalene < cresol.

At 700 °C, higher conversion of all hydrocarbons was observed. Methylnaphthalene conversion increased more than 2-fold over ZSM-5, spent FCC and USY whereas it was unchanged using olivine. In the case of spent FCC, increasing the temperature increased conversion of toluene and phenol to produce benzene. Similar behavior was observed when using ZSM-5.

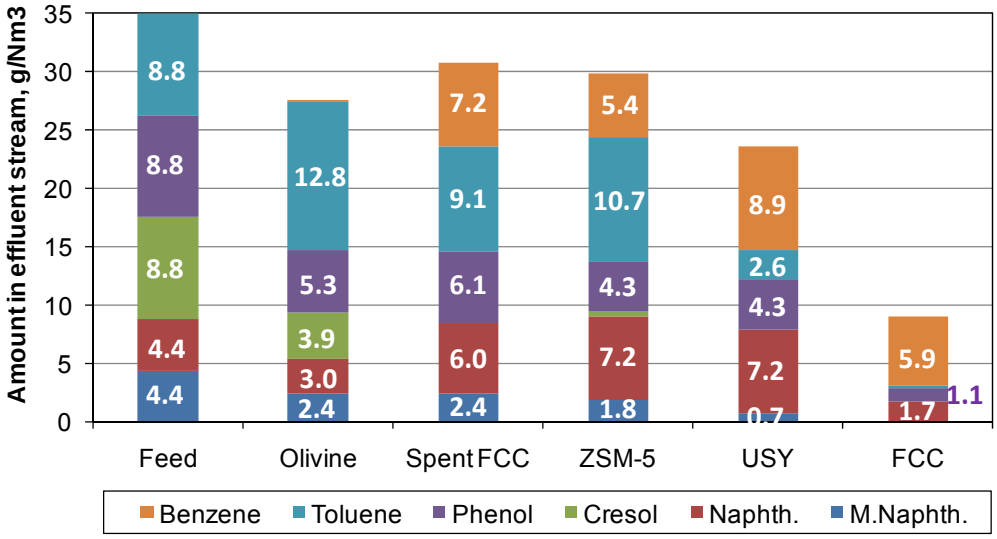

Figure 37: Comparison of amount of tar constituents in the product stream during tar cracking reactions at 600 °C in N_2

The N_2-free dry product gas composition observed during the tar cracking experiments at 600 and 700 °C is shown in Table 6 and Table 7, respectively. No CO and a very small amount of CO_2 was detected in the product stream using Spent FCC, while significant quantities of H_2 and CH_4 were detected indicating very low activity towards reforming reaction. USY, which was the most active in-house non-metallic catalyst, produced equal quantity of CO and CO_2 combined and CH_4. With the use of FCC catalyst, about 63% of the carbon in the product stream is CO and 10% is CO_2 indicating the occurrence of reforming reaction. The remaining 27% of carbon is seen as CH_4, a product of cracking reaction. In case of Ni-alumina catalyst, of the 77% of product carbon in gas phase, 90% is as CO_2 and the rest 10% is as CO. This indicates high reforming and shift activity of Ni-Alumina catalyst at 600 °C. The Ni-ZnAlumina catalyst also presented high reforming and shift activity as evident by 93% of gas phase carbon present as CO_2 and the rest 7% present as CO. The concentrations of CO and CO_2 were higher at higher temperature whereas the amount of CH_4 was lower. This indicates that with increase in reaction temperature reforming activity of all catalysts increased significantly.

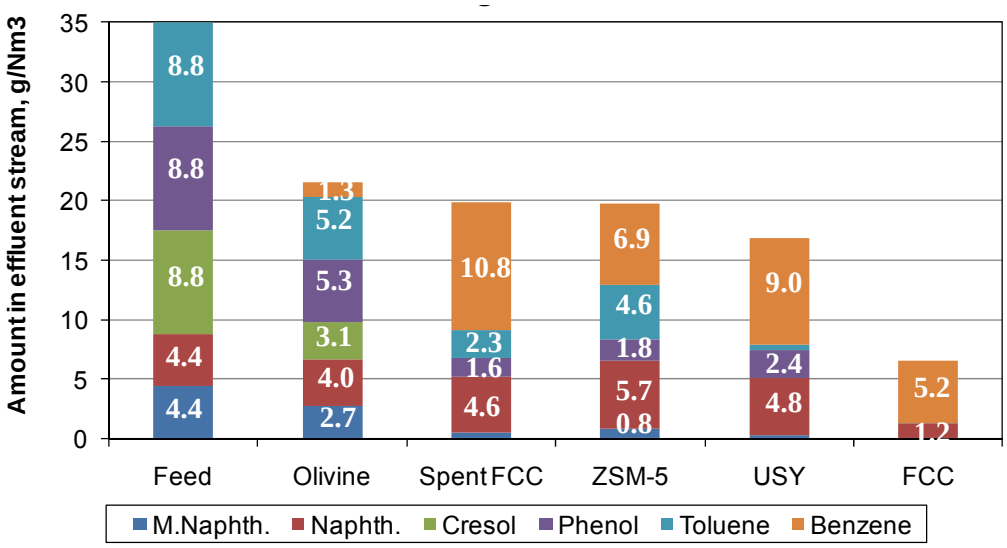

Figure 38: Comparison of amount of tar constituents in the product stream during tar cracking reactions at 700 °C in N_2

Component	Syngas composition, %	
	Feed	Product
H_2	27	18.5
CO	54	1.6
CO_2	14	55.4
CH_4	0	17.3
N_2	5	7.3

Table 6: Dry product gas composition during tar cracking experiments at 600 °C

	N_2-free dry product gas composition, vol%			
	H_2	CO	CO_2	CH_4
Olivine	79.4	0.0	20.6	0.0
Spent FCC	79.7	0.0	2.5	17.8
ZSM-5	60.8	26.5	6.9	5.9
USY	65.8	13.2	3.4	17.5
FCC	73.0	16.9	2.6	7.4
Ni/Al_2O_3	68.9	3.2	27.9	0.0
$Ni/ZnAl_2O_4$	57.1	3.1	39.7	0.1

The FCC catalyst was the most active zeolite catalyst and the Ni-alumina had the highest overall tar cracking activity. Consequently, these two catalysts were chosen for further analysis. At first, effect of sulfur poisoning in the presence of H_2S in raw syngas was studied. A feed gas consisting of 200 ppm H_2S in N_2 was used during these reactions. Tar cracking activity remained stable over a 6 hr period for both catalysts. Since the screening reactions were performed using N_2 as feed gas, it was important to know whether these catalysts hold their activity in the presence of syngas. For these experiments, a syngas comprising of 27% H_2, 54% CO, 14% CO_2 and 5% N_2 was used. Tar conversion with FCC catalyst dropped from 74% to 68% in presence of syngas whereas, in case of Ni/Al_2O_3 catalyst, no drop in tar

conversion was observed. However, the Ni/Al_2O_3 catalyst changed the feed syngas composition significantly. The change in syngas composition up on reaction is shown in the following table.

The significant change in the feed syngas composition seems to be predominantly due to two reactions: water-gas-shift and methanation. As a result, CO concentration drops from 54% to 1.6% whereas concentration of CO_2 increases from 14 to 55.4% and CH_4, which was not present in the feed, increases up to 17.3%. The observed change in the quality of syngas is undesirable for the application of producing liquid fuels due to the decreased CO and H_2 concentration.

Table 7: Dry product gas composition during tar cracking experiments at 700 °C

	N_2-free dry product gas composition, vol%			
	H_2	CO	CO_2	CH_4
Olivine	67.8	9.8	19.6	2.9
Spent FCC	68.3	22.9	2.9	6.0
ZSM-5	63.8	25.6	3.1	7.5
USY	60.9	29.3	3.5	6.4
FCC	63.3	30.4	2.0	4.3
Ni/Al_2O_3	64.9	2.2	32.8	0.0

Component	Syngas composition, %	
	Feed	Product
H_2	27	38.8
CO	54	14.3
CO_2	14	35.9
CH_4	0	3.3
N_2	5	4.4

In summary, the$Ni\text{-}Al_2O_3$ catalyst completely converts tar although it also alters the syngas composition. The commercial FCC catalyst on the other hand, does not alter the feed syngas composition but is only able to achieve 74% tar conversion. In order to target complete tar conversion with minimal effect on the raw syngas composition, a physical mixture of both these catalysts was tested. The idea is to use enough Ni catalyst to maximize tar conversion while minimizing methanation to control the syngas composition. A physical mixture of 70 wt% FCC and 30 wt% $Ni\text{-}Al_2O_3$ had the least methanation activity although significant shift activity as indicated by below. The high shift activity in the absence of the methanation reaction is favorable since it increases the H_2/CO ratio of the syngas from 0.5 to 2.7 which is desirable for liquid fuel synthesis process. Complete conversion of tar was observed during tar cracking reaction at 600 °C using the above mentioned 70-30 wt% physical mixture of FCC and Ni/Al_2O_3.

Task 2: Bench-scale Therminator Testing

Cold Flow System Design and Operation

The cold flow model of the Therminator was constructed to understand the solids circulation and how best to control and operate the unit. To better control the solids circulation, it was decided to use a loop seal as shown in Figure 39 instead of using two control valves as originally considered. Layout drawings of the cold flow unit are shown in Figure 40. The cold flow unit was built by Particulate Solids Research Institute (PSRI) for RTI to use as a model for its hot, pressurized Therminator. The cold flow unit was fabricated from transparent PVC pipe so that the flow of the solids could be observed. An attrition resistant equilibrium FCC catalyst in sufficient quantity was obtained as the primary catalyst for developing circulation both in the cold flow reactor and in the hot Therminator reactor. The properties of this catalyst are shown in Table 8. Compressed air was used as the fluidizing, aeration, and transport gases.

This cold flow unit was run for about three months and provided operational data and experience invaluable for transfer to the hot flow unit. Below is a list of the major observations that were used to develop recommendations for design of the hot flow unit.

- A slide valve in between the reactor and regenerator is not absolutely necessary. A 3/8" diameter circular orifice allowed solids to flow in the range desired. A solids control valve on the hot, pressurized unit was found to be economically infeasible.
- The cyclones on the unit would have to be more properly sized and carefully fabricated. The miscellaneous pipe fittings used to fabricate the cyclones on the cold flow unit proved to be inadequate.
- The circulation of the solids proved to be very robust in that it continued to circulate despite process changes that may have affected the flow.
- The flow rate of the solids was directly affected by the flow rate of the riser gas.

Table 8: Properties of Equilibrium FCC Catalyst

Microactivity Test Activity	75
Coke factor	1.0
Gas Factor	1.3
Ni (ppmw)	204
V (ppmw)	153
Fe (wt%)	0.32
Total Surface Area (m^2/g)	175
Zeolite Surface	114
Al_2O_3 (wt%)	38.9
Sodium (wt%)	0.27
Re_2O_5 (wt%)	1.29
Particle Size Distribution (wt%)	
0 to 40 μm	7
0 to 80 μm	60
Average Particle Size (μm)	72
Average Bulk Density (g/cc)	0.87
Pore Volume (cc/g)	0.3

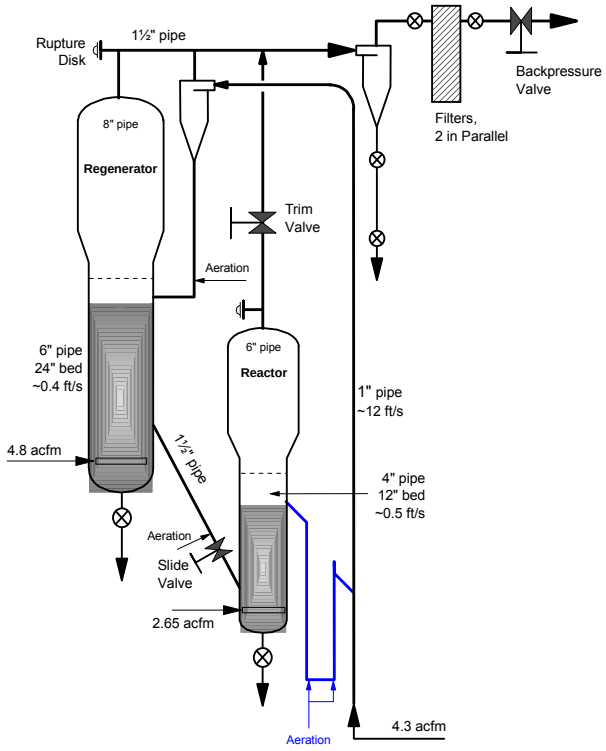

Figure 39: Therminator cold flow reactor with loopseal option

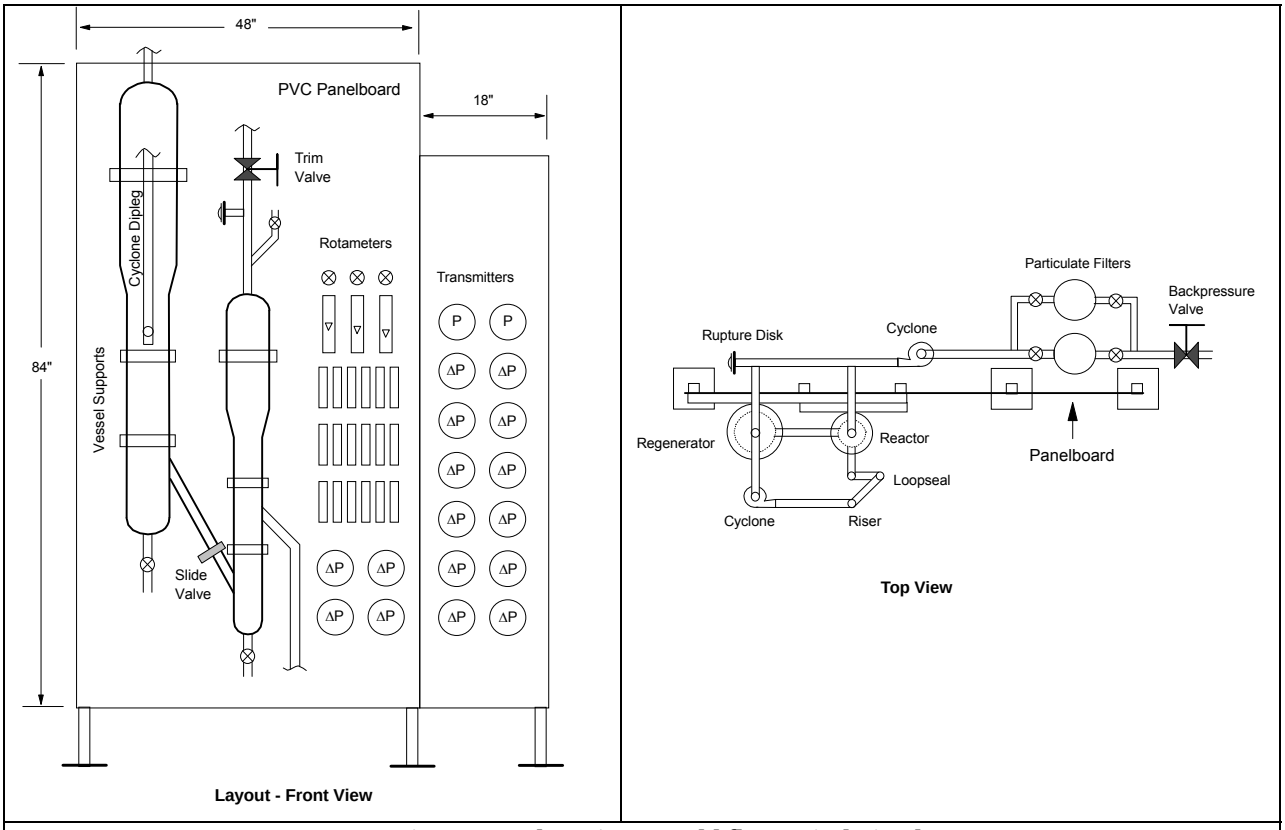

Figure 40: Therminator cold flow unit design layout

RTI Biomass Therminator Gas Cleanup Design Evaluation

The Therminator process was designed to operate at a pressure of approximately 20 psig and a temperature of approximately 1200°F. The biomass gasifier at the University of Utah produces syngas at a rate of between 2000 and 2600 SCFH at the fluidized bed absorber freeboard pressure of 20 psig. The syngas from the gasifier is heated to approximately 650°C (1200°F) via a heater before entering the 12-in-diameter absorber. This temperature is approximately 50°C (90°F) above the reaction temperature in order to provide enough excess heat to drive the endothermic cracking reaction.

In the absorber, the syngas fluidizes the catalyst in a nearly turbulent fluidized bed to give sufficient heat and mass transfer to absorb the hydrogen sulfide from the syngas. The cleaned syngas is separated from the catalyst in an internal cyclone before exiting the absorber. The syngas then is routed to a quench to reduce the temperature of the syngas stream and to remove tar, ammonia, and hydrogen sulfide. A pressure control valve for the process is located downstream of the quench system. After the pressure control valve, the gas is sent to a burner.

The spent catalyst from the absorber is transferred to a solids transfer regenerator loop. Air will be used as the regeneration gas in this loop. The solids from the absorber are passed through a loop seal and then into the bottom of a 4-in-diameter fluidized bed called the mixing zone where most of the regeneration occurs. The solids density in the mixing zone is expected to be approximately 20 lb/ft^3 at a superficial gas velocity of approximately 5 ft/s. The riser will be approximately 2 inches in diameter, and is expected to have a suspension density of approximately of 0.8 lb/ft^3. The gas velocity in the riser will be approximately 19 ft/s.

The catalyst from the riser is separated from the riser gas in a cyclone and then discharged into a dipleg below the cyclone. Catalyst from the dipleg is returned to the mix zone via an automatic L-valve or loop seal. A certain fraction of the recirculating catalyst is drawn off of the dipleg and returned to the absorber via a standpipe. A slide valve in the standpipe controls the rate at which the catalyst is recirculated back to the absorber.

One of the key things that must be evaluated in any solids transfer system is the pressure balance around the solids transfer loop or loops. Based on the drawings in the Figure 41, the pressure balances around the three flow loops in the process are derived as follows.

Pressure Balances

1. Overall Loop Balance:

$$P_{cy2/out} - P_{absorb/out} - \Delta P_{cy1} - \Delta P_{loop\ seal} + \Delta P_{mix\ zone} + \Delta P_{riser} - \Delta P_{cy2} = 0$$

$$\Delta P_{cy2/absorber} - \Delta P_{cy1} - \Delta P_{loop\ seal} + \Delta P_{mix\ zone} + \Delta P_{riser} + \Delta P_{cy2} = 0$$

The element in this flow loop that will adjust so that the pressure drop will balance is the loop seal. The seal height in the loop seal will change automatically so that the pressure drop will balance around the flow loop. This pressure balance can be written as:

$$\Delta P_{mix\ zone} + \Delta P_{riser} + \Delta P_{cy2} + \Delta P_{cy2/absorber} - \Delta P_{cy1} = \Delta P_{loop\ seal}$$

Therefore, in order for the system to operate satisfactorily, the loop seal must be designed correctly so that it can absorb or develop the required pressure drop to balance the pressure drop around the flow loop.

2. Riser/Dipleg Loop Balance:

$$\Delta P_{mix\ zone} + \Delta P_{riser} + \Delta P_{cy2} + \Delta P_{orifice} = \Delta P_{cy2\ dipleg}$$

For this pressure balance loop, the device that will adjust to balance the loop pressure drop is the dipleg below the riser cyclone.

3. Standpipe/Absorber Loop Balance

Pcy2/out – Pabsorb outlet + ΔPcy2 + ΔPsp – ΔPslide valve – ΔPabs bed1 – ΔPcy1 = 0

ΔPcy2/absorber + ΔPcy2 + ΔPsp – ΔPslide valve – ΔPabs bed1 – ΔPcy1 = 0

If the pressure balance is written in terms of the standpipe, then:

ΔPslide valve + ΔPabsorber bed1 + ΔPcy1 - ΔPcy1/absorber - ΔPcy2 = ΔPstandpipe

In this pressure balance loop, the pressure drop across the absorber bed (ΔPabsorber bed1) is only the pressure drop of that part of the absorber bed above where the solids from the standpipe enter the bed. If the solids enter near the top of the absorber bed, then this pressure drop will be small. If the solids are added to the absorber bed near the bottom, then the pressure drop will be larger.

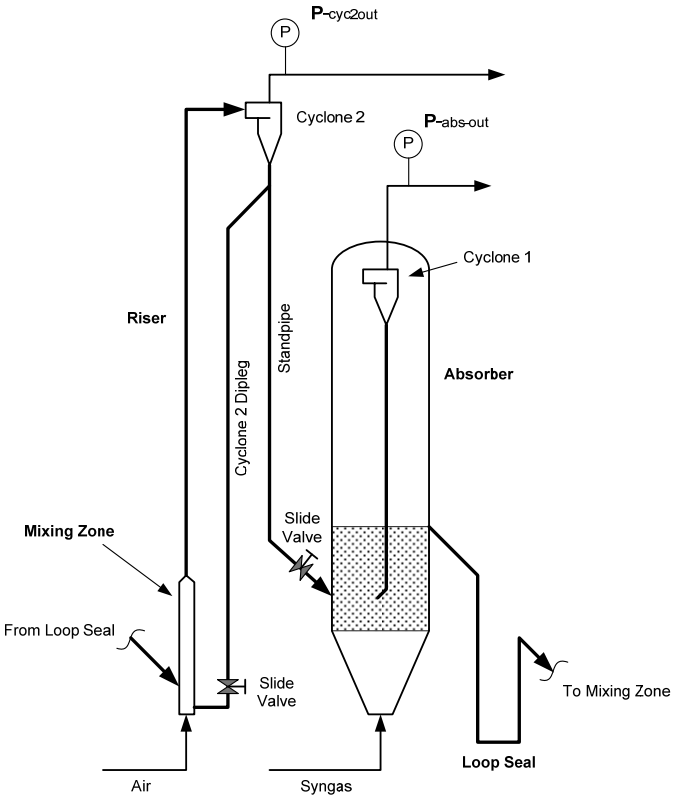

Figure 41: Schematic Drawing of Proposed Therminator Process Flowsheet

The regenerator dipleg is angled off of the dipleg/standpipe (hereafter referred to as the standpipe) that routes the regenerated catalyst back to the absorber. This configuration allows a longer length of pipe below Cyclone 2 to allow more pressure drop to be taken in the standpipe. The riser cyclone, Cyclone 2, is located above the absorber to yield a standpipe height of approximately 7 feet, with a distance between the cyclone outlet and the overflow height for the dipleg to be approximately 1.5 to 2 feet, to allow the pressure balance in this loop to be achieved. T

All three pressure balances must be satisfied in the unit. As can be seen from the balances above, in two of the three pressure drop balances (the overall loop balance and the dipleg/standpipe/absorber loop balance), the difference in pressure between the outlet of the riser cyclone (Cyclone 2) and the pressure at the outlet of the absorber is important. This pressure differential (between the outlet of Cyclone 2 and the outlet of the absorber bed) will normally be set to a particular value and controlled. To determine what value should be used, three cases were considered:

Case 1: Pcy2 – Pabsorber bed = 0 (ΔPcy2/absorber = 0)

Case 2: Pcy2 > Pabsorber bed (ΔPcy2/absorber > 0)

Case 3: Pcy2 < Pabsorber bed (ΔPcy2/absorber <0)

To evaluate the various cases, actual values for the pressure drops need to be inserted into the pressure balance equations. Therefore, the following values of the various components of the pressure drop have been selected.

ΔPcyclone

A nominal (conservative) value of 0.5 psi will be used in the calculations for both the riser cyclone (Cyclone 2) and the cyclone in the absorber (Cyclone 1).

ΔPriser

The assumed density in the riser in the *Preliminary Design Package* is 0.8 lb/ft^3. This density is equivalent to 0.8/144 = 0.0056 psi/ft. The riser length in the table in the *Preliminary Design Package* and the riser length shown in the 3D drawing are different. In the former, it was listed as 10 feet, in the latter drawing it is closer to 7.5 or 8 feet. It will be assumed that the riser is approximately 8 feet in length. Therefore, the riser pressure drop is approximately 0.0056 x 8 = 0.045 psi.

ΔPmixing zone

The density in the mixing zone was supplied by RTI as 20 lb/ft^3 (0.139 psi/ft). The length of the mixing zone is 5 feet. Therefore, the pressure drop across the mixing zone is approximately 0.69 psi.

ΔPabsorber bed

The absorber expanded bed height is assumed to be approximately 3.3 feet. The assumed bed density will be taken to be 36 lb/ft^3. This is equivalent to t density of 36/144 = 0.25 psi/ft. Therefore, the total pressure drop across the absorber bed is: 0.25 psi/ft x 3.3 ft = 0.825 psi.

ΔPslide valve

The pressure drop across the slide valve in the standpipe will be assumed to be 0.5 psi.

ΔPorifice

There is an orifice at the bottom of the dipleg below the riser cyclone. It will be assumed that the pressure drop across this orifice will be 0.5 psi.

The loop seal, the dipleg below the riser cyclone, and the standpipe transferring solids between the riser dipleg and the absorber are devices that can adjust to differences in pressure drop in order to balance the differential pressures in the system. It will be assumed that the density in the loop seal and the riser cyclone dipleg (when the solids in them are fluidized) will be 36 lb/ft^3 (0.25 psi/ft). It will be assumed that the density in the standpipe joining the absorber bed with the riser cyclone dipleg will be 36 lb/ft^3 (0.25 psi/ft) when it is building pressure.

The pressure balances for the various cases are shown below in Table 1, for values of Pcy2 – Pabs bed (ΔPcy2/abs) of 1, 0 psi and -0.25 psi. All values shown are in psi.

This pressure balance analysis indicates several things. For Case 1 (ΔPcy2/absorber = 1 psi) for the ***Overall Loop Balance***, the required solids level in the dipleg section of the loop seal is nearly 7 feet. This means that the solids level in the loop seal downleg would be approximately 7 feet above the solids discharge of the loop seal. This is not possible with the overflow loop seal that you have now and the height available for the unit (assumed to be 16 feet).

For Case 2 (ΔPcy2/absorber = 0), the required loop seal height is nearly 3 feet. This may be possible, but it would mean a modification to the loop seal that would give a very small loop seal upleg height.

For Case 3 (ΔPcy2/absorber = -0.25 psi), the required solids level in the loop seal downleg is approximately 2 feet. This means that the solids level in the loop seal downleg needs to be approximately 2 feet above the loop seal discharge. This can be done, but not with the loop seal design shown in the Therminator 3D drawing. This shows a very short length of loop seal above the discharge location of the loop seal. However, by lowering the loop seal discharge height approximately 2 feet, it would be possible to operate the loop seal with this pressure differential between the Cyclone 2 outlet and the Absorber outlet.

Therefore, based on the results discussed above, it would be better to have ΔPcy2/absorber be slightly negative (the pressure at the outlet of the absorber would be higher than the pressure at the outlet of Cyclone 2) because it would minimize problems with loop seal design.

For the ***Riser/Dipleg Loop Balance***, ΔPcy2/absorber is not involved in the pressure balance. This pressure balance has been set up to determine the height of the riser cyclone dipleg required to balance the pressures in this flow loop. For the assumptions made, the results show that the dipleg height must be approximately 7 feet above the orifice at the bottom of the dipleg to achieve pressure balance.

For the ***Standpipe/Absorber Loop Balance***, the three cases for the pressure difference between the outlet of Cyclone 2 and the outlet of the absorber bed must again be considered. However, during the analysis of this pressure drop balance, it was found that it was difficult to achieve the required pressure balance in this loop while still being able to maintain the pressure balance in the ***Overall Loop Pressure Balance*** as well. Therefore, as explained above when discussing the pressure balance for this loop, it is recommended that the configuration shown in Figure 1 be adopted. In this figure, the regenerator dipleg is angled off of the standpipe used to route the regenerated catalyst back to the absorber. This configuration allows a longer dipleg length to allow more pressure drop to be taken in the standpipe. As also mentioned with this configuration, it will also be necessary to raise Cyclone 2 (the riser cyclone) approximately 2 feet to allow the pressure balance in this loop to be achieved. Raising Cyclone 2 approximately this amount gives a standpipe height of approximately 7 feet, with a distance between the cyclone outlet and the overflow height for the dipleg to be approximately 1.5 to 2 feet.

Also, the Cyclone 2 pressure drop in this pressure balance is not the entire Cyclone 2 pressure drop. The only pressure drop that applies in this case is the pressure drop from the bottom of the cyclone through the gas outlet tube. This pressure drop has been estimated to be 30% of the total Cyclone 2 pressure drop. Therefore, this pressure drop is: 0.3 x 0.5 psi = 0.15 psi.

There is one other difference in this pressure balance loop that must be explained. The absorber bed pressure drop that applies in this analysis is only that part of the absorber bed pressure drop above where the standpipe enters the absorber. It would be better for the pressure drop to have this entrance be as high in the absorber bed as possible. However, a high entrance may cause the regenerated catalyst to bypass quickly into the loop seal. If this is not a problem, the standpipe can be added higher in the bed. Another possibility exists. To prevent solids bypassing, sometimes a vertical baffle is added to the bed to force the entering solids to move down to the bottom of the bed before flowing upward to the outlet again.

Also, as explained above, the pressure drop analysis for this loop is calculated in a different manner. The height of the angled and vertical sections of the standpipe is estimated to be approximately 7 feet. For a maximum standpipe fluidized bed density of 36 lb/ft^3 (0.25 psi/ft), the maximum pressure drop that this standpipe can generate is 7 x 0.25 = 1.75 psi. Therefore, the pressure drop required in the standpipe for Cases 1, 2 and 3 are 0.35, 1.35 and 1.6 psi, respectively. Because the standpipe can generate 1.75 psi, it is possible for the standpipe to operate in pressure balance for all cases. However, the "best" case for operation of the ***Overall Loop Pressure Balance*** described above is for Case 3. Even

for Case 3, there is a small "reserve" pressure drop of 0.15 psi. Therefore, it is recommended that the differential pressure between the Cyclone 2 outlet and the absorber outlet be set to approximately -0.25 psi.

Table 9: Pressure Balances

	Case 1	*Case 2*	*Case 3*
Overall Loop Balance			
ΔPcy2/absorber	1.0	0	-0.25
ΔPcy1	0.5	0.5	0.5
ΔPmix zone	0.69	0.69	0.69
ΔPriser	0.045	0.045	0.045
ΔPcy2	0.5	0.5	0.5
Req'd loop seal ΔP, psi	1.74	0.74	0.49
Req/d seal height, ft	6.96	2.96	1.96
Riser/Dipleg Loop Balance			
ΔPmix zone	0.69	0.69	0.69
ΔPriser	0.045	0.045	0.045
ΔPcy2	0.5	0.5	0.5
ΔPorifice	0.5	0.5	0.5
Dipleg ΔP required, psi	1.74		
Dipleg length required, ft	6.96		
Standpipe/Absorber Loop Balance			
ΔPcy2/absorber	1.0	0	-0.25
ΔPcy1	0.5	0.5	0.5
ΔPbsorber bed**	0.5	0.5	0.5
ΔPslide valve	0.5	0.5	0.5
DP in cyclone 2	0.15	0.15	0.15
DP standpipe req'd, psi	0.35	1.35	1.6
Max standpipe DP possible, psi	1.75	1.75	1.75
** Absorber bed height above the entrance of the standpipe is assumed to be 2 feet			

The system shown in Figure 41 will be very sensitive to the amount of solids inventory in the system. It will be necessary to have the inventory set up so that there is enough solids to fill up the dipleg to the solids level required for pressure balance. If the inventory is too low, the seal height in the dipleg may be too short to develop the solids flows required. If it is too great, then the riser cyclone dipleg length will be much greater than required and may not operate in the fluidized bed mode (which is the desired mode). Too great an inventory could also cause the solids in the dipleg to back up into Cyclone 2. Therefore, it is recommended that a hopper with a valve be added to the unit so that solids can be added to the unit to maintain the inventory in the system at the correct amount. Also, a discharge nozzle and hopper are recommended to be added as well so that the solids can be removed from the unit when required. The solids could be added either into the dipleg below the riser cyclone or even into the absorber.

The following instrumentation was included to control the unit and monitor the system operation.

Differential Pressure Transmitters

1. Across the mix zone
2. Across the riser
3. Across the riser cyclone (inlet to outlet)
4. From Cyclone 2 solids discharge to the entrance to the dipleg (to determine if the solids back up into this section)
5. Above the orifice to the entrance of the dipleg
6. Across the orifice
7. Across Cyclone 1 (inlet to outlet)
8. Across the absorber bed
9. Across the absorber bed gas distributor
10. Across Cyclone 1 dipleg
11. Across the downleg section of the loop seal
12. Across the upleg section of the loop seal
13. Between the pressure at the outlet of Cyclone 2, and the pressure at the outlet of the absorber
14. Between the standpipe inlet to the absorber and the absorber freeboard

Other Considerations

1. The diameter of the Cyclone 1 (absorber cyclone) dipleg should be at least 1.5 inches in diameter. A 2-in-diameter dipleg would be better. Starting the unit up requires a pressure seal in this dipleg.
2. The distance between the two sides of the loop seal were desinged as short as possible to prevent solids from defluidizing in the horizontal section.
3. An aeration point was added immediately above the orifice in the dipleg to control the solids flow through it.

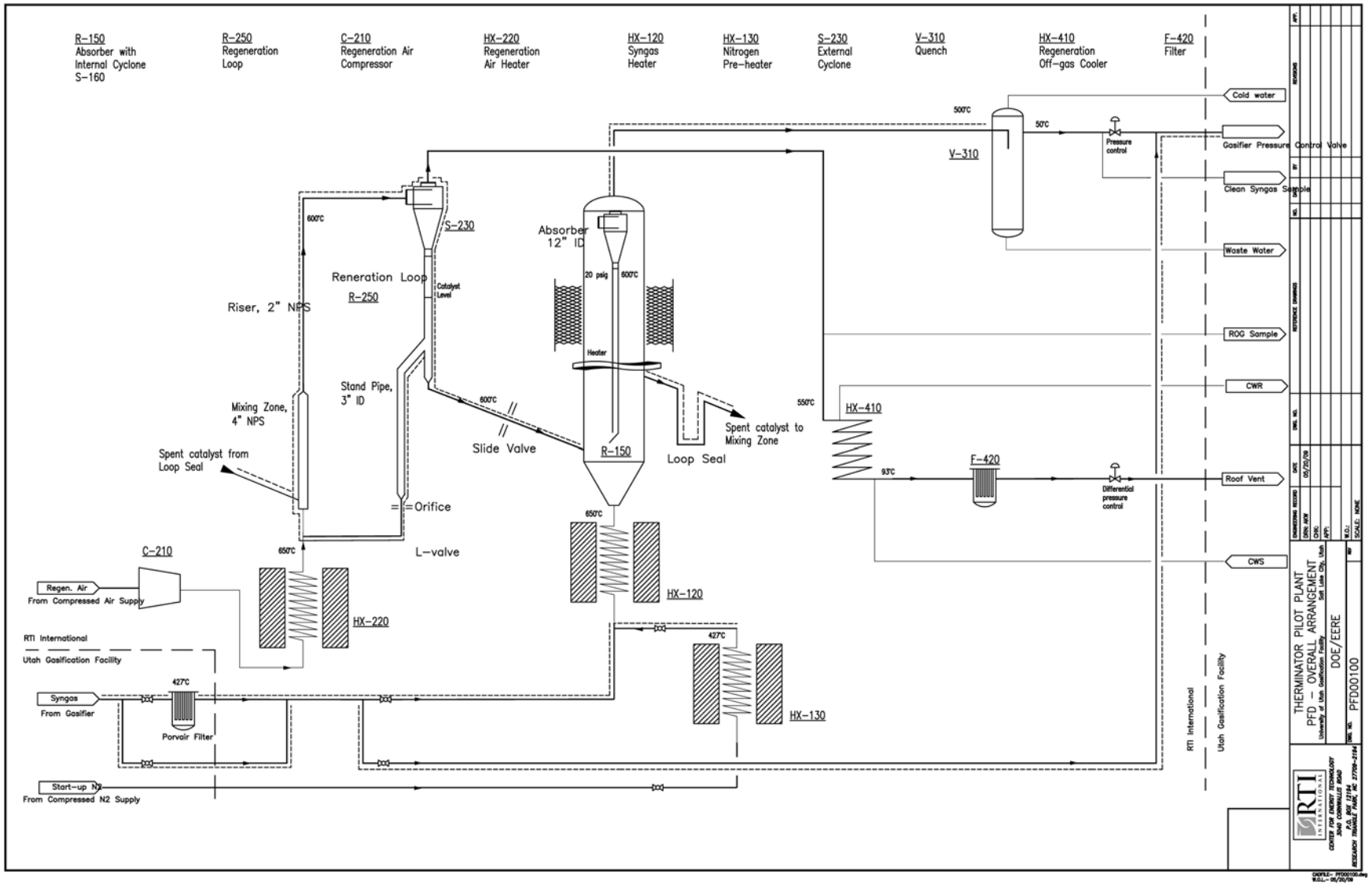

Figure 42: Process Flow Diagram for Therminator System

Therminator Operating Philosophy

The process Flow Diagram for the Therminator system is shown in Figure 42. The Therminator consists of a fluidized bed absorber (R-150) coupled with a circulating regeneration loop (R-250) for cracking tars. A fluidizable attrition-resistant catalyst like FCC is chosen for this cracking process. The catalyst moves from the absorber to the regeneration loop through a loop seal where it is circulated multiple times before it returns to the absorber through a diagonally-positioned standpipe. The slide valve in the angled standpipe controls the overall solids circulation rate and therefore the split ratio between the solids flow rates in the regeneration loop and to the absorber.

The Therminator is sized so that it can treat the full wet/syngas stream (in the following referred to as simply syngas) produced in an indirectly-heated gasifier at the gasification facility of the University of Utah in Salt Lake City. The nominal gasifier throughput is 20 kg/hour of biomass (17 wt% moisture) and a total steam-to-biomass ratio of 1. The syngas to be treated will range between 2800 and 2900 SCFH at an absorber freeboard pressure of 20 psig. The Therminator will be installed downstream of a hot gas filter and upstream of the existing afterburner. The pressure is maintained using one automatic back-pressure control valve in each of the two exit gas lines, the cleaned syngas line, and the regeneration off gas (ROG) line. The control valves should be set up in a cascade configuration. The syngas valve will have a pressure set point, while the ROG valve will "float" and maintain a set pressure differential across the regenerator and absorber exit gas lines.

The syngas leaves the gasifier hot gas filter (Porvair) at 800^{o}F (427°C) and is re-heated to 1202^{o}F (650°C) in a circulation heater (HX-120) before entering the absorber. This temperature is 122^{o}F (50°C) above the reaction temperature of 1112^{o}F (600°C) in order to provide sufficient excess heat to drive the endothermic cracking reaction. In the reactor, the syngas works as fluidization gas to create a bubbling regime. The bubbling, almost turbulent, fluidization regime ensures sufficient heat and mass transfer between the syngas and the catalyst. The clean syngas is separated from the entrained catalyst particles by means of an internal cyclone before exiting the reactor. It then passes to a quench (V-310) for final tar, and ammonia scrubbing and temperature reduction. The pressure control valve is located downstream of the quench. At this point the cleaned syngas is directed to the afterburner, which is part of the existing gas treatment in the Utah gasification facility.

Air or diluted air is used as regeneration gas for the spent catalyst. The air is drawn from the building, compressed, and pre-heated to 1202^{o}F (650°C) in a circulation heater (HX-220) before it is injected into the regeneration loop riser. The ROG is separated from the circulating solids in an external cyclone and is then cooled to 200^{o}F (93°C) in a heat exchanger (HX-410) and filtered (F-420) upstream of the back pressure control valve. The temperature of the vent gas is at 200^{o}F (93^{o}C). The design provides the means to mix the regeneration air with nitrogen in order to reduce the oxygen content in the regeneration gas if required. Please refer to the PFD for the process flow path and equipment locations.

The catalyst used to clean the syngas is continuously circulated through the reactor and regeneration loop. The catalyst from the regeneration loop enters the reactor bed and travels upwards via aide from the syngas until it reaches the overflow point. At this point, the catalyst travels through a loop seal which prevents the regeneration gas from contacting the syngas. From the loop seal, the catalyst material is transported vertically through a 4-in NPS mixing zone and a 2-in NPS riser by the regeneration gas. The catalyst regeneration happens predominantly in the mixing zone. The ROG and catalyst separate in the cyclone and the solids enter a 3-in NPS vertical dipleg. A fraction of the catalyst is transferred from the vertical dipleg back into the reactor via an angled standpipe while the rest stays in the loop for repeated regeneration. The slide valve in the angled standpipe controls the overall solids circulation rate and therefore the split ratio between the solids flow rates in the regeneration loop and to the absorber. The regeneration loop is sized for a multiple-pass catalyst regeneration regime. The catalyst remaining in the regeneration loop works its way vertically downward in the dipleg, through an orifice, and an L-valve to the regeneration gas pick-up point to complete the loop. Aeration gas (air or nitrogen) is fed to the bottom of the L-valve to assist in transporting the solids from the standpipe into the mixing zone. A provision will be made to add a catalyst make-up charge port at the top flange of the reactor. Make-up catalyst addition will occur during scheduled unit shutdowns.

Therminator Vessel Sizing Philosophy

The gasifier at the University of Utah Gasification Facility is based on indirectly-heated steam gasification. The gasifier is a bubbling bed with the required superficial velocity of the fluidizing gas being provided by adjusting the flow rate of dilution steam to the gasifier. The location of the facility is at high altitude (approximately 5500 ft elevation) so the atmospheric pressure is low – approximately 12.5 psia.

The Therminator operating pressure is set at 20 psig to provide sufficient pressure driving force for the operation of the Therminator unit. The mechanical design pressure of the Therminator reactor/regenerator vessel, heaters, and quench vessel are set at 150 psig. Please refer to Table 10 for design pressure information. The mechanical design pressure allows the unit to run at a future operating condition of 110 psig. The mechanical design temperature limit for the Therminator reactor & regenerator vessels is set at 1292°F (700°C). Preliminary material selection points toward 316 or 316/316L grade stainless steel.

The bubbling bed Therminator reactor has been sized at nominal 12-in NPS in order to achieve a superficial velocity of 1.5 ft/sec at the nominal operating pressure and temperature of 20 psig and 1112°F (600°C). The aspect ratio of the bubbling bed was chosen to be 3:1, resulting in a gas residence time of 2.2 seconds.

The solids residence time is a function of the rate of transfer of solids to the regenerator loop. The Therminator is designed with separate absorber/reactor and regeneration loops. As configured, the solid transfer rate is an independent, controllable variable. Having the regenerator loop circulation be independent of the absorber/reactor gas flow is desirable, from the standpoint of uncertainty in the gasifier operation. For the cases that are being considered, the solids residence time ranges from 15 minutes to 128 minutes.

Major Equipment Design Philosophy

Table 10: Process Conditions for Major Equipment

Tag #	Equipment Name	Inlet Temperature		Outlet Temperature		Operating Pressure	Design Pressure	Flow		
		°F	°C	°F	°C	PSIG	PSIG	SCFM	ACFM	GPM
HX-120	Syngas heater	800	427	1202	650	20	150	65	70	
HX-130	Nitrogen Preheater	68	20	800	427	20	150	65	70	
HX-220	Regen Air heater	68	20	1202	650	20	150	60	27	
C-210	Regen Air Compressor	68	20	68	20	20	TBD	20	9	
HX-410	Regen Off-Gas Cooler	1112	600	200	93	20	TBD	9	12	
V-310	Quench Vessel	1112	600	115	46	20	150	52	70	
HX-330	Quench Heat Exchanger	100	38	95	35	20	TBD	0		8
F-360A/B	Liquid Filter	100	38	100	38	20	TBD	0		8
P-320	Quench system pump	100	38	100	38	20	TBD	0		8

HX-120 Syngas heater

Syngas leaves the gasifier, passes through a Porvair hot gas filter then enters the syngas pre-heater HX-120). The syngas pre-heater will heat syngas in order to provide sufficient excess heat to drive the endothermic cracking reaction within the reactor. See Table 10 for process conditions. After the syngas is heated up to operating temperature, it is fed into the bottom of the reactor.

HX-130 Nitrogen pre-heater

Hot nitrogen will be fed into the absorber during start-up. The nitrogen will be heated from ambient temperature to an intermediate temperature in HX-130 before passing through the syngas heater

(HX-120). The syngas heater will then heat the nitrogen up to the operating temperature of the Therminator reactor vessel. See Table 10 for process conditions.

HX-220 Regeneration air heater

Air is used as regeneration gas for the spent catalyst. The air is drawn from the building, compressed, and pre-heated in order to provide sufficient excess heat for catalyst regeneration. The air is then introduced into the mixing zone of the regeneration loop. See Table 10 for process conditions.

All heaters are electrically-heated circulation-type design. The instrumentation and controls will include a thermocouple located at the outlet nozzle for temperature control. In addition, one thermocouple will be located on the internal element sheath for over-temperature protection. The sheath elements and shell will be constructed of alloy and stainless steel material respectively. Spare internal elements must be available onsite in the event that the heater elements burn out.

HX-410 Regeneration Off-Gas Cooler

The regeneration off-gas (ROG) is separated from the circulating solids in an external cyclone and is cooled prior to venting. See Table 10 for process conditions. Preliminary equipment sizing and selection indicated that a natural draft design is suitable.

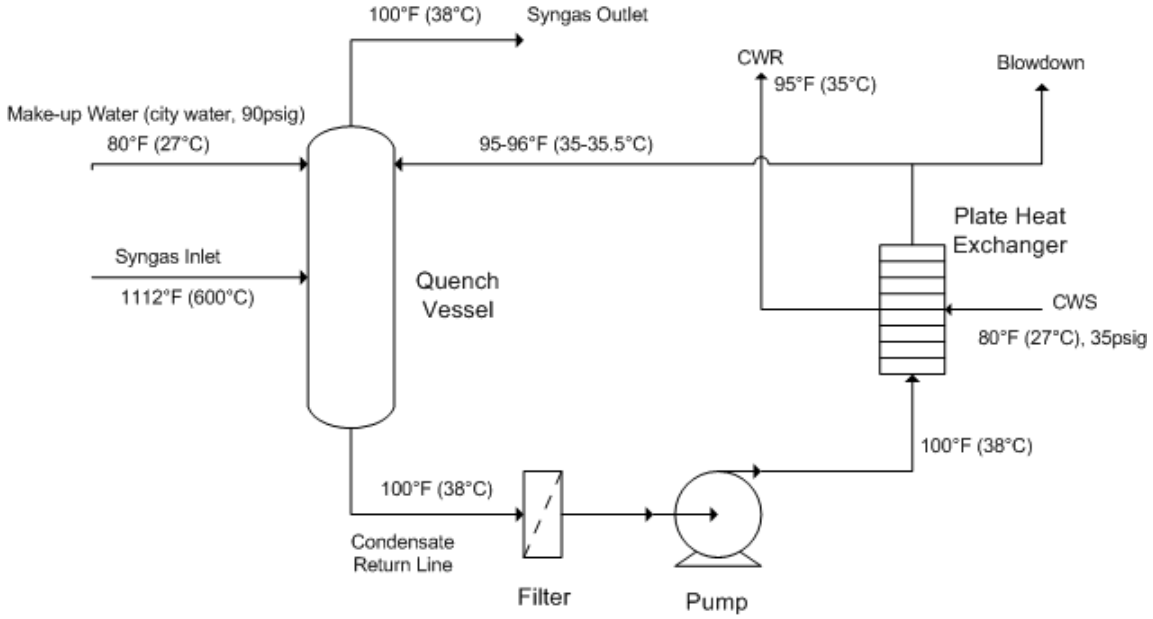

Figure 43: Quench System PFD

Quench System

The clean syngas is separated from the entrained catalyst particles by means of an internal cyclone before exiting the reactor. It then passes through a quench system for final tar, ammonia, and hydrogen sulfide scrubbing and to condense water. Please refer to Figure 43 for the PFD of the quench system.

V-310 Quench Vessel

The clean syngas enters the quench vessel where it is cooled by a water spray. The water is sprayed into the vessel by either one or two nozzles, pointing in the direction of the gas stream. The non-condensable components in the gas stream leave the top of the vessel and then pass through a coalescing filter. The condensable components are cooled, exit the bottom of the vessel and travel through the condensate return line. The condensate then passes through a redundant liquid filter (F-360A/B), circulation pump, and heat exchanger before returning to the spray nozzle at the quench vessel. Please refer to Table 10 for the quench system process conditions and Figure 43 for the PFD of the quench

system. Preliminary sizing of the quench vessel indicates the volume to be approximately 35 gallons to provide a 2-min liquid holdup time. The quench vessel will be in a vertical orientation and equipped with a coalescing wire mesh pad located near the top of the vessel. Please refer to Table 10 for the quench system process conditions and Figure 1 for the PFD of the quench system.

P-320 Quench Pump

The circulation pump will recycle the condensate from the filter outlet through the heat exchanger and back into the vessel through the spray nozzle(s). Please refer to Table 10 for the quench system process conditions and Figure 1 for the PFD of the quench system.

HX-330 Quench Heat Exchanger

Cooling water is supplied at 10 GPM to the heat exchanger at a maximum (summer) temperature of about 80°F (27°C) and is returned at 95°F (35°C). Preliminary sizing and selection indicates that a plate-type heat exchanger with an area of 41ft^2 would be suitable for this application due to the high potential of particulate fouling. This is not the final design and other designs will be considered. Please refer to Table 10 for the quench system process conditions and Figure 43 for the PFD of the quench system.

The blow-down stream (0.2 gpm) exits the return loop into a drain. Make-up water (city water) is introduced into the vessel through a spray nozzle and is controlled by the condensate level in the vessel.

Instrumentation and controls are detailed in the P&IDs.

C-210 Air Compressor

The air compressor pressurizes air prior to introduction into the regeneration loop. The air compressor should be sized for 20 SCFM at 20 psig. Commercial compressors are available at 120 psig. The air pressure is reduced across a control valve to the operating pressure of the Therminator unit prior to entering the regeneration air pre-heater. The Utah facility currently uses a compressor with 100 cfm capacity and discharge pressure of 100 psig. Should 100 cfm be sufficient capacity for supply to the Therminator and other processes within the facility, then a new compressor will not be required.

Band Heaters

Electric band heaters are used to maintain an internal reactor temperature of 1112°F (600°C). Band heaters are available commercially up to 15" diameter and 1382°F (750°C) rating.

Heat Tracing

High temperature heat tracing is required on process lines that contain condensable tars. In general, the heat tracing must maintain a temperature of 1112°F (600°C), except the process line between the Porvair filter and the syngas pre-heater (HX-120) and between the nitrogen pre-heater (HX-130) and the syngas pre-heater (HX-120), which are maintained at 800°F (427°C).

S-230 Cyclone

The regeneration loop includes a cyclone that separates the circulating solids from the regeneration off-gas.

S-160 Cyclone

The absorber includes an internal cyclone to separate the solid particles from the syngas. A dipleg will be attached to the internal cyclone and is submerged within the absorber bed. A trickle valve will be attached to the bottom of the dipleg to prevent syngas gas from entering the cyclone and thus lowering the efficiency.

Control Philosophy

The Therminator unit will be only semi-automated. Operators will be required for its operation, both in the control room and at the unit. The unit will require "hands-on operation" to include:

- Turning hand valves to set up flow paths
- Adjusting hand-operated control valves for flows that do not need continuous modulation (i.e., standpipe slide valves)
- Monitoring liquid level glasses
- Reading pressures on pressure gages
- Taking samples (schedule and type TBD)
- Draining coalescing filters

Remotely actuated control valves are shown where continuous modulation is required – i.e., back pressure control. Also, actuated valves are shown for e-stop isolation and nitrogen flooding.

Hardware:

- NEC classification: Unclassified (but all wiring should be in conduit – flexible or rigid – for physical protection.
- Electrical panels with I/O modules should be located on the equipment skid/frame. Data connection to the existing control room will be by Ethernet.
- All control equipment must be Opto 22.
- Transmitters will be isolated from the process lines with manifolds (3-valve manifolds for DP transmitters). Additional process interface valves (PIVs) to isolate the impulse lines are NOT required.
- Temperatures should be measured with thermocouples (T/Cs). The T/C wire can be run directly to the I/O modules in the panels on the skid. Temperature transmitters are not required.
- Continuous data logging of P, DP, T, flow rates
- Over-temperature protection high-high switches are to be independent of the central control system. (Not shown on P&ID but should be included in the cost estimate.
- Main control room Human Machine Interface (HMI) programming will be supplied by the site.

Normal Startup and Shutdown:

1. Purge unit with nitrogen to remove air and moisture.
2. Start solid circulation using nitrogen in R-150 and R-250 loop.
3. Gradually heat up the syngas path to operating temperature by passing the startup nitrogen through HX-130 N2 Preheater and HX-120 Syngas Preheater.
4. Gradually heat up the regeneration path to operating temperature by passing nitrogen through HX-220 Regen Air Heater.
5. Introduce syngas into the R-150 loop: modulate FV-104 to increase syngas, and modulate FV-102 to decrease nitrogen.
6. Monitor operation of the solids circulation, as the high-steam syngas will have different transport properties than the nitrogen.
7. Introduce air into the R-250 regeneration loop: modulate FV-204 to increase air, and modulate FV-206 to decrease nitrogen.
8. Normal shutdown: reverse above procedures.
9. For Emergency Shutdown the unit will be flooded with nitrogen.

Task 4. Engineering Evaluation and Commercial Assessment

In the early phases of the proejct, Cratech prepared a preliminary heat and material balance for two biomass integrated gasification combined cycle (IGCC) power plants with each plant producing a net 6.8 MW of electrical power. One of these biomass gasification plants operates at 98% carbon conversion. The design of the two plants is based on Cratech's biomass IGCC technology. For the plant gasifying biomass at 83% conversion, the gasifier and material feed systems were based on the direct scale up of acutal data produced by a small scale gasifier equivalent to 550 kW biomass IGCC plant. The desing of the biomass IGCC plant operating at 98% cabron cnversion is an extrapolation of data collected from Cratech's small scale gasifier [20]. The design of the two 6.8 MWe biomass IGCC process will serve as a baseline cases against which future designs of the biomass IGCC processes incorporating the Therminator and a mix of energy products will be compared.

Design Basis

A representative feed material was selected for the biomass gasifier. Of the three basic categories of biomass: wood, lignin-rich agricultural waste, or animal waste, wood was chosen as the feed material for a baseline evaluation because of its availability as well as its cost. For a true commercial embodiment, the feed material for such a process would be dictated by convenience and necessity. An agricultural processing plant which produces a waste by-product of fuel value is one such example.

It was also determined that this wood would be used to generate electricity using an integrated gasification combined cycle (IGCC). An IGCC would be an efficient and effective method for converting biomass of low heating value such as wood into usable energy. The specific amount of power generated has not been determined, but the capacity will not exceed 20 MWe. Above 20 MWe, procurement of enough feed materials becomes difficult. By choosing a capacity less than 20 MWe, the co-generation of wholesale electricity from a waste by-product of an existing process becomes more attractive [20].

Process Overview

The following section describes the process envisioned as a baseline for the evaluation of a commercial embodiment IGCC utilizing the Therminator. Refer to the PFD in Figure 44 for the process overview. The raw, woody biomass as received will be of various shapes, sizes, and quality. The pneumatic conveying system used to transfer the biomass into the gasifier requires that the maximum size of the chips be no larger than 2 cm x 2 cm x 0.5cm [20]. A specific operation for sizing and screening the biomass has not yet been determined, but will be required for a commercial embodiment using forest residue as a feed material.

Wood typically contains moisture levels of about fifty percent [21], but ideally the feed material should contain about fifteen percent moisture for ideal gasification conditions [20]. Reduction of the moisture level below fifteen percent would reduce the overall efficiency as well as deprive the gasifier of water vapor. The Cratech gasifier does not have to have a steam feed, but depends on moisture in the feed material to provide the water required for the gasification reaction.

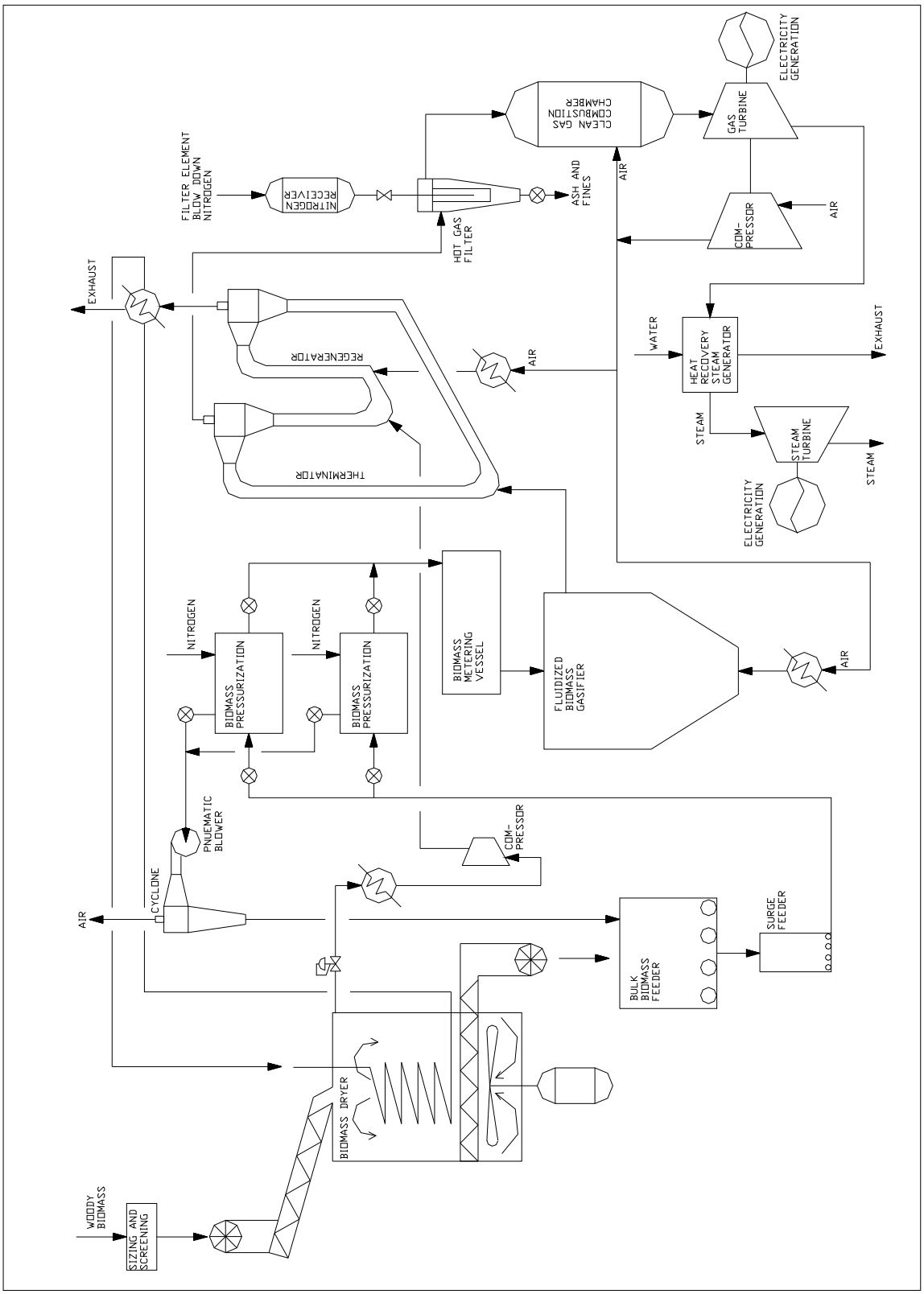

Figure 44: Schematic of Preliminary Biomass IGCC Utilizing the Therminator

The basic principle of the biomass drying operation was taken from a DOE report done by Weyerhaeuser which outlines the design basis for a wood fueled biomass IGCC. The report describes a commercially available indirect steam heated dryer which produces low pressure steam from the evaporated wood moisture. The dryer consists of a rotary pressure lock system which feeds the biomass

into a drying chamber. The drying chamber has steam coils and a convection fan. The pressure is maintained by a back pressure regulator at the steam exit. The dried biomass then exits the chamber via a second rotary airlock for later use. A mass and energy balance for a biomass dryer was performed on the basis of reducing the moisture level in the biomass from fifty to fifteen percent in a dryer with a thermal efficiency of 85%. Table 11 below shows the mass/energy balance around the biomass dryer on the basis of one pound of biomass fed.

In addition to water evaporated from the wood, there are numerous other compounds in the steam that exits the dryer. These compounds include low molecular weight alcohols, aldehydes, carboxylic acids, and turpenes [22]. The amount and exact nature of these extracted compounds varies and no baseline concentration profile for this evaluation has been made at this point. In the preliminary design, it has been suggested to compress and heat the steam so that it can be used to fluidize the catalyst material in the regenerator. The water could then be discharged as vapor while the volatile compounds would be incinerated during the regeneration process.

The dried biomass that exits the dryer enters the gasifier feed process. The biomass is pneumatically conveyed into a vessel where it is pressurized before entering the metering vessel. These mechanical processes are proprietary to Cratech and therefore, will not be elaborated.

The woody biomass is gasified in a fluidized gasifier also proprietary to Cratech. Fluidization of the refractory and oxygen source for gasification will be done using air. Oxygen blown gasifiers, although producing gas of higher heating value and smaller volumes, increase the overall complexity significantly (www.iea-coal.org.uk). Further investigation may include the possibility of using an oxygen blown gasifier, but not in this baseline evaluation.

For this evaluation, data published by Faaij et al. [21] will be used as the baseline input/output model for the gasifier. Tables 3 and 4 below show the input/output scheme of the gasifier on the basis of one pound of dried (15% moisture) woody biomass feed.

All outlet components, including ash and un-burned carbon, leaving the gasifier enter the Therminator. In the Therminator it is estimated that 90% of sulfur compounds and ammonia will be removed by the catalyst. It is also assumed that ½ of the tars entering the Therminator are cracked into methane (for simplicity, it will be assumed that methane is the only cracked hydrocarbon). The other ½ of the tars are assumed to deposit on the catalyst surface as coke.

Upon entering the regenerator, it will be assumed that all coke is burned as well as any remaining carbon. The heat of regeneration will be used to heat the Therminator reaction as well as to raise steam from the waste heat.

The clean gas leaving the Therminator goes through a hot gas filter that will be blown down periodically with nitrogen when the pressure drop across it exceeds a present value. Once the gas passes through the filter, it then goes into a gas turbine, which in turn produces steam for the combined cycle. The low heating value of the gas is estimated to be 6.03 MJ/m^3, which is within range of typical low heating value gas fired turbines, which is 5.6-7.5 MJ/m^3. Table 5 outlines how the heating value of the gas was determined.

Table 11: Mass/Energy Balance Around Biomass Dryer

Wood Present in 1 lb biomass			0.5		
Water Present in 1 lb biomass			0.5		
Water Evaporated in 1 lb biomass			0.4118		
	Cool Water	Sat'd Water	Sat'd Steam	LP Steam	Wood Heating
Temp (°F)	60	212	212	317.66	212
Pressure (psia)	14.7	14.7	14.7	54.38	14.7
Enthalpy (BTU/lb)			1150.4	1192.54	
H_{vap} (BTU/lb)		970.3			
C_p (BTU/lb/°F)	1				0.33
ΔT (°F)	152				152
1-->2	76				
2-->3	399.56954				
3-->4	17.353252				
Wood Heating	25.375473				
Total	**518.2983**	**BTU/lb biomass**			
STEAM ENERGY INPUT					
Overall Thermal Efficiency Assumed=			0.85		
	HP Steam	Sat'd Steam	Sat'd Water	Subcooled Water	
lb steam/lb biomass	0.7248086	0.7248086	0.7248086	0.7248086	
Temp (°F)	464	423.79	423.79	413.02	
Pressure (psia)	323.39	321.39	321.39	321.39	
Enthalpy (BTU/lb)	1231.52	1204.05			
H_{vap} (BTU/lb)			803.034		
C_p (BTU/lb/°F)				1	
ΔT (°F)				10.77	
1-->2	19.910493				
2-->3	582.04598				
3-->4	7.8061891				
Total	**609.7627**	**BTU/lb biomass Including Efficiency Factor**			

Table 12: Gasifier Feed [21]

	Fuel Feed to Gasifier (wt%)	1 lb Basis Feed (lb)	Air Feed wt%	Total Air Feed (lb)	Dolomite Feed (lb)	Total Feed to Gasifier (lb)
C	41.192445	0.4119245				0.4119245
H	5.0337	0.050337				0.050337
O	37.165485	0.3716549	0.2315749	0.3242048		0.6958597
N	0.402696	0.004027	0.7555752	1.0578053		1.0618322
S	0.0083895	8.39E-05				8.39E-05
Cl	0.083895	0.000839				0.000839
Ar			0.0128499	0.0179899		0.0179899
H_2O	15	0.15				0.15
Ash	1.105	0.01105				0.01105
Dolomite					0.0268	0.0268
Total	99.991611	0.9999161	1	1.4		2.4267161

Table 13: Mass Balance around Gasifier, 1lb. Basis

Gasifier Outlet				
Vapor Products	MW	vol %	wt%	Total Wt Out (lb)
C_2H_6	30	0.02	0.0002415	0.0005419
C_2H_4	28	0.94	0.0105943	0.0237713
CH_4	16	2.82	0.0181616	0.0407508
CO	28	17.22	0.194078	0.4354704
CO_2	44	12.22	0.2164258	0.4856141
H_2	2	13.25	0.0106667	0.0239339
H_2O	18	13.55	0.0981741	0.2202821
N_2	28	39.2	0.4418036	0.9913147
O_2	32	0	0	0
Ar	40	0.47	0.0075673	0.0169795
NH_3	17	0.27	0.0018476	0.0041455
HCl	36.4	0.03	0.0004395	0.0009863
Total (Not including Tar)			1	2.2437906
Mol Wt of Gas	24.84362 (Estimated Avg.)			
Tar				0.0012
dolomite+ash				0.03785
Char				0.1438756
Total Gas (Including Tar)				2.2449906
Total Output				**2.426716**

Table 14: Heating Value of Syngas Produced from Gasified Wood

Basis of 1 lb of dry feed			
	Gas Exiting Therminator (lb)	Heat of Combustion (BTU/lb)	BTU/lb fed
C_2H_6	0.0005	22373.1	12.12398389
C_2H_4	0.0238	21682.9	515.4308233
CH_4	0.0414	23944.0	990.1046894
CO	0.4355	4348.7	1893.750817
CO_2	0.4856	0.0	0
H_2	0.0239	61495.6	1471.829415
H_2O	0.2203	0.0	0
N_2	0.9913	0.0	0
O_2	0.0000	0.0	0
Ar	0.0170	0.0	0
NH_3	0.0004	9683.3	4.014251921
Heating Value of Gas		**2017.54**	**BTU/lb**
		162.02	**BTU/scf**
		6.03	**MJ/Nm^3**

Tar Cracking Process Development

The process modeling activities in this project mainly consisted of the following:

1. Development of an Aspen Plus® process model for the proposed Therminator process for biomass derived syngas cleanup
2. Evaluation of the process efficiency of the Therminator cleanup process by incorporating it in commercial-scale conceptual designs for two different biofuels production processes:
    i. Mixed alcohol production process (process model reproduced from NREL thermochemical mixed alcohol synthesis report) [1]
    ii. Synthetic gasoline production via dimethyl ether (DME) (process model developed at RTI) [23-25]

Further, the process models were used to evaluate the relative thermodynamic efficiencies and costs for the net product outputs from the biofuel production processes with integrated tar cracking (Therminator) and tar reforming [1].

Therminator Process Model

Figure 46 shows a process flow diagram (PFD) for RTI's Therminator process. A process model was developed using Aspen Plus® software to estimate the material and energy balances for the Therminator process [1]. The data obtained from the process model is used in the design and optimization of the proposed experimental system. The stream data estimated using this process model is shown in Table 16. The following is a brief description of the process model and the assumptions used in it.

The design basis for the pilot-scale biomass syngas cleanup unit is a 142.7 lb/hr syngas with composition and inlet conditions as shown in Table 16 (Stream#1). The Therminator unit operation is being integrated into the gasification research facility at the University of Utah downstream of the indirect, steam gasifier and hot gas candle filter (for aprticulate removal). This syngas composition and flow rate simulate the gasifier (not shown in Figure 46) fed with 44 lb/hr (20 kg/hr, dry basis) biomass with 17 wt. % moisture, 77 lb/hr steam and 5 lb/hr oxygen. The dry syngas contains 54% H_2, 27% CO, 14% CO_2 and 5% CH_4. A tar concentration of 35g /Nm^3 in the dry syngas is also assumed[1]. Naphthalene is used to represent tar in the process model. Further, H_2S and NH_3 concentrations in syngas are assumed to be 110 ppmv and 4000 ppmv (wet basis), respectively. The ambient pressure in this model is set at 12.5 psia (0.863 psia), representative of the University of Utah gasifier.

Syngas from the gasifier section is cooled to 800°F (427°C) and 32.5 psia (2.24 bara) before it enters the ceramic candle filter for particulate removal (Stream # 2). This stream is then heated to 1202°F (650°C) in the syngas heater (HX-120). The hot syngas containing tars, H_2S and NH_3 is treated in the absorber reactor (R-150) at 1112°F (600°C) to eliminate these contaminants. For the purpose of this simulation a zeolite catalyst was used for tar decompostion. 99% of the tar is assumed to be removed as char according to the following reaction:

$$C_{10}H_8 \text{ (Tar)} \rightarrow 4\ H_2 + 10\ C \text{ (Char)}$$

Although, in reality a significant fraction of the decomposed tar is expected to form lighter hydrocarbons and leave the reactor as a part of the syngas, this process design is set to allow for the maximum carbon deposition rate on the catalyst. The rate of catalyst (zeolite) circulation is set to the design specification of 1.0 wt% carbon loading the catalyst. Ammonia is assumed to decompose to nitrogen and hydrogen. The kinetics of this reaction are fast and equilibrium is attained instantaneously over a suitable catalyst at the specified absorber operating conditions.

$$2\ NH_3 \rightarrow 3\ H_2 + N_2$$

H_2S present in the syngas is absorbed using a zinc titanate sorbent. Twice the stoichiometrically required flow rate (for complete H_2S conversion) of $ZnTiO_3$ is input to the reactor to allow for any sorbent deactivation associated with possible coke formation on the sorbent surface. For the operating conditions

and gas residence time inside the absorber reactor, the desulfurization reaction is also expected to reach equilibrium.

$$H_2S + ZnTiO_3 \rightarrow ZnS + TiO_2 + H_2O$$

An internal cyclone in the reactor (R-150) separates any entrained solids from leaving the reactor. For the purpose of the simulation, 100% solid separation efficiency is assumed for this cyclone. In practice, some solids losses are expected due to attrition and a make-up stream (stream # 12) of catalyst/sorbents will be used to replenish these losses. Catalyst-sorbent mixture is continuously recirculated (stream # 5 and 11) between the absorber reactor and regenerator (R-250) blocks. The solids flow rates between the reactors is estimated using design specifications for solids circulation in the pilot-scale unit operation.

In the regenerator unit (R-250), air is used to oxidize the char deposited on the catalyst as well as regenerate the sulfided zinc titanate sorbent at temperatures greater than 1202°F (>650°C). Complete conversion of ZnS and an 80% char removal are assumed:

$$ZnS + TiO_2 + 1.5\ O_2 \rightarrow ZnTiO_3 + SO_2$$

$$C + O_2 \rightarrow CO_2$$

Air (Stream # 6) at 68°F (20°C) and 12.5 psia (0.86 bara) is compressed (C-210) to 32.5 psia (2.24 bara) using a compressor with an isentropic efficiency of 80% and a mechanical efficiency of 95%. Air flow to the regenerator is set at 1.5 times the stoichiometric requirement. In steady state operation of the unit, air entering the regenerator (R-250) is heated by the recycled solids to the desired reaction temperature (>650°C). An air heater HX-220 is included for startup operation to heat the compressed air (Stream # 7) to 1202°F (650°C). The excess heat generated by the combustion reactions are expected to make-up for the heat losses through the regenerator walls. An external cyclone (S-230) is used to separate the solids from the off-gas. The regenerator off-gas (Stream # 9) is then cooled to 250°F (121°C) using a natural draft cooler (HX-410) before being sent to the vent/burner.

The syngas (stream # 3) from the absorber reactor is then quenched with water (stream # 17) at 95°F (35°C) to remove remaining tars, contaminants and elutriated bed material. The syngas exits (Stream # 4) the quench system at 120°F (49°C). Most of the moisture present in the syngas also condenses, and is removed at the bottom of quench unit along with the quench spray water (Stream # 17). Solids present in the liquid stream exiting the quench are filtered in the filter unit. The water stream exiting the filter contains traces of some dissolved gases, tars and other impurities, and is recirculated (Steam # 16) back to the quench spray system after being cooled to 100°F (38°C, Stream # 17). This cooling is accomplished in a heat exchanger with a continuous cold water supply entering at 80°F (27°C, Stream # 13) and leaving at 100°F (38°C, Stream #14). In a steady state operation, no additional make-up water is expected for the quench unit (except for the cooling water supplied to heat exchanger) and an equivalent amount of the water condensing in the quench unit is purged (Stream # 15) continuously along with dissolved impurities. The cleaned syngas (Stream # 4) can be further used for production of synfuel and/or chemicals. Table 15 lists the heat loads and electricity requirements for various unit operations discussed above as estimated using the process model (negative sign represents cooling duty).

Table 15: Heat Loads and Electricity Requirements

Steam Generation	**Btu/hr**
Heat Duty - HX120	23,421
Heat Duty - HX220(startup)	-13,394
Heat Duty - HX410	19,209
Heat Duty - R150	33,763
Power Requirement	**kWe**
Power - C210	0.89
Power - Cpump	0.05

Evaluation of Therminator process Efficiency

The performance of the Therminator technology was compared with a tar reforming syngas cleanup technology that has been reported in the literature (NREL Design Report). The process models were configured with the Therminator gas cleanup unit operation and a tar reforming unit operation as shown in the block flow diagram below (Figure 45). The relative thermodynamic efficiencies and costs were evaluated for the net product outputs for two fuel synthesis options, mixed alcohols or methanol-to-gasoline. The mixed alcohol synthesis was used to validate the RTI model by comparing it with the state-of-the-art in the literature. For consistency and simplicity, no syngas recycle was included in the fuel synthesis block. The methanol-to-gasoline fuel synthesis process was chosen as an alternative because it has a higher single pass conversion efficiency and greater liquid product yield.

Mixed Alcohols Production Process

The conceptual integrated thermochemical ethanol production process described in the NREL report was used as the base case for this study. The input biomass has 50% moisture and the biomass feed rate is 2000 dry tonnes/day. A block flow diagram of the NREL thermochemical ethanol production process [1] is shown in Figure 45.

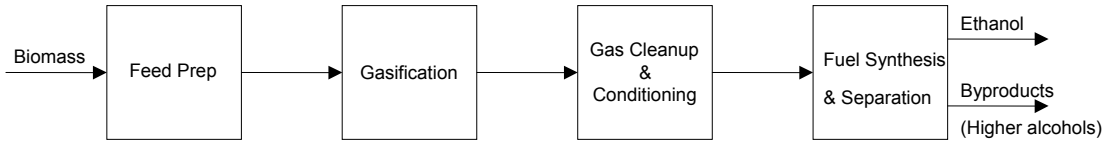

Figure 45. Biomass gasification system with gas cleanup and fuel synthesis

In the feed prep section, the biomass feedstock is dried to 5 wt% moisture using flue gas from the char combustor (gasification block). The gasification section utilizes an indirectly-heated biomass gasifier to generate raw syngas and char from the dry biomass. The solids (char) that are formed from the gasifier are separated from the gas stream in a series of cyclones and sent to the char combustor. The gas cleanup section consists of a tar reformer, an amine based acid gas removal system (to remove CO_2 and sulfur), and a quench system (to remove particulates and other trace contaminants plus knock out the water). The cleanup section also includes a 5-stage intercooled compressor system to compress the clean, dry syngas to 420 psia, for the fuel synthesis step.

The fuel synthesis block includes a fixed bed reactor that converts the clean syngas to mixed alcohols. The effluent stream containing a wide range of alcohols and unconverted syngas is cooled to condense and separate the liquid products. The condensed alcohols are then sent to two distillation columns where the ethanol is separated from the other alcohols. The unconverted syngas and methanol are recycled to the gas conditioning section. A small fraction of these light gases are used for combustion.

A direct comparison of the gas cleanup technologies required that the tar reforming cleanup process in the NREL model be replaced with the Therminator process model discussed in the previous section. The process model developed by NREL [1] was completely reproduced at RTI (feed prep to ethanol production and separation) using a newer version of AspenPlus® (V7.1). The RTI process model was validated by comparing the outputs with the results from the NREL model. A comparison of key process streams published in the NREL report and calculated with RTI's updated model is shown in Table 17. The stream compositions and flow conditions from the RTI model match very closely with the NREL results.

The mixed alcohols synthesis block in the NREL model is a highly integrated scheme designed to maximize ethanol production by maximizing syngas conversion. As mentioned before, some of the light gases are consumed to supply process heat and methanol is recycled to the reformer section to produce syngas. The various process heat streams are also tightly balanced so as to make the overall process close to energy-neutral (almost no net heat/ electricity input or output). This extensive recycle scheme in the

syngas cleanup and fuel synthesis operations were very difficult to reproduce when the tar reformer block was replaced with the Therminator block for syngas cleanup. Therefore, for the simplicity, the RTI process model was configured without any recycle and modified as a single pass fuel synthesis process. The byproduct streams - lights gases and the higher alcohols - are converted to electricity based on their heating values. Therefore, when comparing the tar reformer and the Therminator, the amount of liquid product from the single pass fuel synthesis and the net electricity generated from the byproducts and unconverted syngas are used in the process assessment.

Table 18 shows a comparison of the clean syngas outputs from the single pass mixed alcohols production scheme with both the tar reforming and Therminator cleanup processes for the same biomass feed. The table also shows the biomass feed and raw syngas output from the gasifier. As seen from the table, the Therminator process is designed to have better contaminant (tars, NH_3 and H_2S) removal compared to the tar reforming cleanup process. Further, as the RTI catalyst was assumed to have no reforming activity, the light hydrocarbon concentrations were unchanged in the Therminator process, whereas in the tar reforming process, benzene and lower hydrocarbons are also reformed along with the tars and hence, there is a significant drop in CH_4, C_2H_4, etc., accompanied by an increase in the H_2 flow rate. The difference in the CO_2 flow rates in the output streams is due to the acid gas removal section in the NREL model (designed to remove CO_2 and H_2S), which was not included in the Therminator process.

Two different scenarios were analyzed for each syngas cleanup process (tar reforming and tar cracking with the Therminator):

Case # 1: Partial CO conversion – current state of technology single pass conversion of CO to mixed alcohols, based on chemical reactions and selectivities from the alcohol synthesis reactor in the NREL model.

Case # 2: Full CO conversion - A hypothetical case for complete CO conversion assuming product selectivities similar to Case #1 to complete recycle of unconverted reactants.

Table 19 shows the product yields, electricity outputs and total income comparisons for four different cases, two each for tar reforming and tar cracking with the Therminator. The table also shows the results for the base case (fully integrated mixed alcohols production scheme from the NREL Design Report). The ethanol yield for the single pass cases is lower compared to the base case, but after accounting for the electricity credit, the total income estimated for the single pass cases are comparable to the total income calculated for the base case in the NREL Design Report. The NREL base case produced 48,726 lb/hr of ethanol product and 11.5 MW of electricity. With a fuel price of $2.005/gal and an electricity price of $0.1155/kWh, the total income for the NREL base case is $16,082/hr.

In both the partial (#1) and full (#2) CO conversions cases, the tar cracking method produces more ethanol than the Therminator. This is due to the higher yields of CO and H_2 in the Tar reforming process (Table 18), which is caused due to the reforming of benzene and lower hydrocarbons in the Tar reformer. As discussed before, in Therminator tars are decomposed, but lower hydrocarbons are assumed to be unaffected. Therefore, due to the higher concentrations of lower hydrocarbons in Therminator syngas, the corresponding light gas byproduct streams have a higher heating value. Thus, more electricity can be produced by using the Therminator process. The product yields for Case #1 with tar reforming are 21,668 lb/hr of ethanol and 71.7 MW of electricity which nets a total income of $14,839/hr. The product yields for Case #1 with tar cracking in the Therminator are 14,396 lb/hr of ethanol with 91.1 MW of electricity that generates a total income of $14,872/hr. Thus, these two cleanup technologies have similar total incomes despite the disparity in ethanol produced. When conditions were changed to complete conversion of CO, more alcohol was produced and the electricity output was reduced as seen in Therminator Case # 2 and Tar reforming Case # 2. However, the total incomes for these cases are also similar.

Synthetic Gasoline production via DME

The performance of tar cracking with the Therminator was also compared with the tar reforming process for production of synthetic fuel via DME process. The feed prep, gasification and syngas cleanup

blocks (tar cracking with the Therminator and tar reforming) were identical to the mixed alcohols production process. An Aspen Plus® process block for the synthetic gasoline catalytic fuel synthesis process was developed at RTI. The synthetic gasoline process combines clean syngas conversion to a mixture of methanol and DME with a second stage dehydration over a zeolite catalyst to convert methanol and DME to gasoline range hydrocarbons.

The clean syngas from the Therminator and the tar reformer blocks (Table 18) was fed to the DME process block. The syngas entering this block is first compressed to 63 bar (915 psia) and then heated to 240°C (464°F, preferred operating temperature of the downstream fuel synthesis reactor) in a heater block. The syngas to gasoline conversion process consists of two reactors. The first reactor converts CO and hydrogen to methanol and DME by the following reactions. The water gas shift reaction is assumed to be at equilibrium in this reactor.

$$CO + 2\ H_2 \rightarrow CH_3OH$$

$$2\ CH_3OH \rightarrow CH_3OCH_3 + H_2O$$

$$CO + H_2O \rightarrow H_2 + CO_2$$

This reactor is operated isothermally at 240°C (464°F) and 62.9 bar (912 psia). A 60% CO conversion is assumed based on some preliminary laboratory experiments conducted at RTI. 95% of the methanol produced is further converted to DME. The overall process is exothermic and the heat released is used to produce steam for electricity generation. The second reactor converts all the methanol and DME to various hydrocarbon components.

$$2CH_3OH \rightarrow C_2H_4 + 2H_2O$$

$$CH_3OCH_3 \rightarrow C_2H_4 + H_2O$$

$$C_2H_4 \rightarrow 2(\text{-}CH_4\text{-})$$

The temperature and pressure of the second reactor are set at 425°C (797°F) and 62.7 bar (910 psia), respectively. This process is slightly endothermic and the heat required is added by a heater block. The yields of various product hydrocarbons are based on the following product distribution observed in the Mobil's methanol-to-gasoline (MTG) [23] process:

Light Gas	1.4%	Highly branched alkanes	53%
Propane	5.5%	Highly branched alkenes	12%
Propene	0.2%	Naphthenes (cycloalkanes)	7%
Isobutane	8.6%	Aromatics	28%
n-Butane	3.3%		
Butenes	1.1%		
C_5^+ Gasoline	79.9%		

The resulting product stream is cooled and distilled to produce gasoline (C5+ compounds) and light gases. The light gases are combusted to produce electricity. Two different cases for each of the Therminator and Tar reforming processes are considered, similar to that in the mixed alcohols process:

Case # 1: 60% CO conversion (RTI internal experiments and industry state-of-the-art)

Case # 2: 100% CO conversion with similar product selectivities as case#1

The results for the four cases are shown in Table 20. Similar to the mixed alcohols process, synfuel yield is higher in Tar reformer cases compared to the corresponding Therminator cases, but the total income (including the electricity credit) is slightly higher for the Therminator cases. Therefore, if coproduction of synfuel and electricity is desired the Therminator process can provide some cost benefit compared to the tar reforming process.

Conclusions

Catalysts tested for tar cracking activity include spent FCC, olivine, Zeolites (USY, etc.), and nickel-based materials. Tar cracking experiments at RTI were performed in a fluidized-bed reactor system. Tar cracking reactions were operated at 600-700°C to match the gasifier outlet temperature and maximize the thermal efficiency of the syngas clean-up process. Although a reaction temperature of 600°C is more appropriate, reactions were also operated at 700 °C to understand the effect of temperature on catalyst performance. The feed to the reactor consisted of 60 mol% gas, either N_2 or syngas based on the experiment, 40 mol% water and 35 g/Nm^3 of tar to simulate syngas produced during atmospheric pressure indirect steam gasification of biomass.

Initially, catalyst screening experiments were conducted in a simulated syngas mixture containing H_2, CO, and CO_2. The high concentration of these components made it difficult to quantitatively measure the amount of tar cracking products. Consequently, catalysts were tested under an inert atmosphere to probe the tar cracking reaction pathways.

Olivine has good reforming activity at temperatures above 800 °C. However, at 600-700 °C it is not very active as the tar conversion ranged from 20-39 % respectively. From the four zeolite materials tested for tar cracking activity, tar conversion was highest when using the commercial FCC catalyst as the bed material at both 600 (74% conversion) and 700 °C (81% conversion). Compared to the commercial FCC catalyst, which uses zeolite USY, spray dried USY showed significantly lower conversion (33% and 52%, respectively) at 600 and 700 °C. The Ni catalysts tested performed the best demonstrating almost complete tar conversion even at 600°C.

In a separate task, process models were developed to evaluate the relative thermodynamic efficiencies and net product costs for biofuel production processes as a function of the integrated gas cleanup technology. Conceptual designs of an integrated biomass gasification process incorporating a tar cracking (RTI) or tar reforming (NREL) gas cleanup unit operation for commercial-scale biofuels production were considered.

The relative thermodynamic efficiencies and costs were evaluated for the two syngas cleanup options with two fuel synthesis options, mixed alcohols or methanol-to-gasoline. The mixed alcohol synthesis was used to validate the RTI model by comparing it with the state-of-the-art in the literature. The methanol-to-gasoline fuel synthesis process was chosen as an alternative because it has a higher single pass conversion efficiency and greater liquid product yield.

The Therminator process has the potential to be more effective for removing contaminants (tars and sulfur gases) than the tar reformer based cleanup process; however, the overall syngas yields are lower because the light hydrocarbons are reformed to CO and hydrogen.

Overall, the total income from the Therminator cases is comparable to the corresponding Tar reforming cases. Tar reforming is a better syngas cleanup process options if the objective is to maximize biofuel production because syngas yields are higher due to the light gas (predominantly methane) reforming to CO and hydrogen. However, the tar cracking syngas cleanup option has advantages if cogeneration (fuel + electricity production) is the objective. The Therminator process can offer significant benefits in terms of simplicity of operation and lower capital costs, as multiple contaminants (tars, sulfur, and ammonia) can be remediated in a single process unit operation and has the potential for higher total incomes.

References

1. Phillips, S.D., *Technoeconomic analysis of a lignocellulosic biomass indirect gasification process to make ethanol via mixed alcohols synthesis.* Industrial & Engineering Chemistry Research, 2007. **46**(26): p. 8887-8897.
2. Herman, R.G., *Advances in catalytic synthesis and utilization of higher alcohols.* Catalysis Today, 2000. **55**(3): p. 233-245.
3. Wender, I., *Reactions of synthesis gas.* Fuel Processing Technology, 1996. **48**(3): p. 189-297.
4. Fierro, J.L.G., *Catalysis in C1 chemistry: future and prospect.* Catalysis Letters, 1993. **22**(1-2): p. 67-91.
5. Iglesia, E., et al., *BIFUNCTIONAL REACTIONS OF ALKANES ON TUNGSTEN CARBIDES MODIFIED BY CHEMISORBED OXYGEN.* Journal of Catalysis, 1991. **131**(2): p. 523-544.
6. Ribeiro, F.H., et al., *PREPARATION AND SURFACE-COMPOSITION OF TUNGSTEN CARBIDE POWDERS WITH HIGH SPECIFIC SURFACE-AREA.* Chemistry of Materials, 1991. **3**(5): p. 805-812.
7. Keller, V., et al., *THE EFFECT OF SURFACE-COMPOSITION ON THE ACTIVITY AND SELECTIVITY IN SKELETAL REARRANGEMENT OF HYDROCARBONS ON BULK AND MODEL TUNGSTEN CARBIDES.* Catalysis Today, 1993. **17**(3): p. 493-504.
8. Ranhotra, G.S., A.T. Bell, and J.A. Reimer, *CATALYSIS OVER MOLYBDENUM CARBIDES AND NITRIDES .2. STUDIES OF CO HYDROGENATION AND C2H6 HYDROGENOLYSIS.* Journal of Catalysis, 1987. **108**(1): p. 40-49.
9. Ranhotra, G.S., et al., *CATALYSIS OVER MOLYBDENUM CARBIDES AND NITRIDES .1. CATALYST CHARACTERIZATION.* Journal of Catalysis, 1987. **108**(1): p. 24-39.
10. Kuba, S., et al., *Reaction pathways in n-pentane conversion catalyzed by tungstated zirconia: effects of platinum in the catalyst and hydrogen in the feed.* Journal of Catalysis, 2003. **219**(2): p. 376-388.
11. Lemaitre, J., B. Vidick, and B. Delmon, *CONTROL OF THE CATALYTIC ACTIVITY OF TUNGSTEN CARBIDES .1. PREPARATION OF HIGHLY DISPERSED TUNGSTEN CARBIDES.* Journal of Catalysis, 1986. **99**(2): p. 415-427.
12. Vidick, B., J. Lemaitre, and B. Delmon, *PREPARATION OF HIGH SURFACE-AREA TUNGSTEN CARBIDE.* Acta Chimica Academiae Scientarium Hungaricae, 1982. **111**(4): p. 449-463.
13. Vidick, B., J. Lemaitre, and B. Delmon, *CONTROL OF THE CATALYTIC ACTIVITY OF TUNGSTEN CARBIDES .2. PHYSICOCHEMICAL CHARACTERIZATIONS OF TUNGSTEN CARBIDES.* Journal of Catalysis, 1986. **99**(2): p. 428-438.
14. Vidick, B., J. Lemaitre, and L. Leclercq, *CONTROL OF THE CATALYTIC ACTIVITY OF TUNGSTEN CARBIDES .3. ACTIVITY FOR ETHYLENE HYDROGENATION AND CYCLOHEXANE DEHYDROGENATION.* Journal of Catalysis, 1986. **99**(2): p. 439-448.
15. Friedlander, A.G., R. Courty, and R.E. Montarnal, *AMMONIA DECOMPOSITION IN PRESENCE OF WATER-VAPOR .1. NICKEL, RUTHENIUM AND PALLADIUM CATALYSTS.* Journal of Catalysis, 1977. **48**(1-3): p. 312-321.
16. Friedlander, A.G., R. Courty, and R.E. Montarnal, *AMMONIA DECOMPOSITION IN PRESENCE OF WATER-VAPOR .2. KINETICS OF REACTION ON NICKEL-CATALYST.* Journal of Catalysis, 1977. **48**(1-3): p. 322-332.
17. Yoshida, K. and G.A. Somorjai, *CHEMISORPTION OF CO, CO2, C2H2, C2H4, H-2 AND NH3 ON CLEAN FE(100) AND (111) CRYSTAL-SURFACES.* Surface Science, 1978. **75**(1): p. 46-60.

18. Choudhary, T.V., C. Sivadinarayana, and D.W. Goodman, *Catalytic ammonia decomposition: COx-free hydrogen production for fuel cell applications.* Catalysis Letters, 2001. **72**(3-4): p. 197-201.
19. Katrib, A., et al., *THE MULTISTRUCTURE OF OXIDIZED REDUCED TUNGSTEN CARBIDE SURFACE(S).* Catalysis Letters, 1994. **29**(3-4): p. 397-408.
20. Craig, J.D., *Development of a Small Scale Biomass-Fueled Integrated-Gasifier Gas Turbine Power Plant: Phase 1." Final Report* 1996, Western Regional Biomass Energy Program.
21. Faaij, A., et al., *Gasification of biomass wastes and residues for electricity production.* Biomass & Bioenergy, 1997. **12**(6): p. 387-407.
22. Rupar, K. and M. Sanati, *The release of organic compounds during biomass drying depends upon the feedstock and/or altering drying heating medium.* Biomass & Bioenergy, 2003. **25**(6): p. 615-622.
23. Kam, A.Y., M. Schreiner, and S. Yurchak, *Chapter 2-3: Mobil Methanol-to-Gasoline (MTG) Process*, in *Handbook of Synfuels Technology*, R.A. Meyers, Editor. 1984, McGraw-Hill Book Company: New Tork.
24. Topp-Jorgensen, J., *The Topsoe Integrated Gasoline Synthesis.* Petrole et Techniques, 1987. **333**: p. 11-17.
25. Topp-Jorgensen, J., *Topsoe Integrated Gasoline Synthesis - The TIGAS Process*, in *Methane conversion : proceedings of a symposium on the production of fuels and chemicals from natural gas, Auckland, April 27-30, 1987*, D.M. Bibby, Editor. 1988, Elsevier: Amsterdam ; New York. p. 293-305.

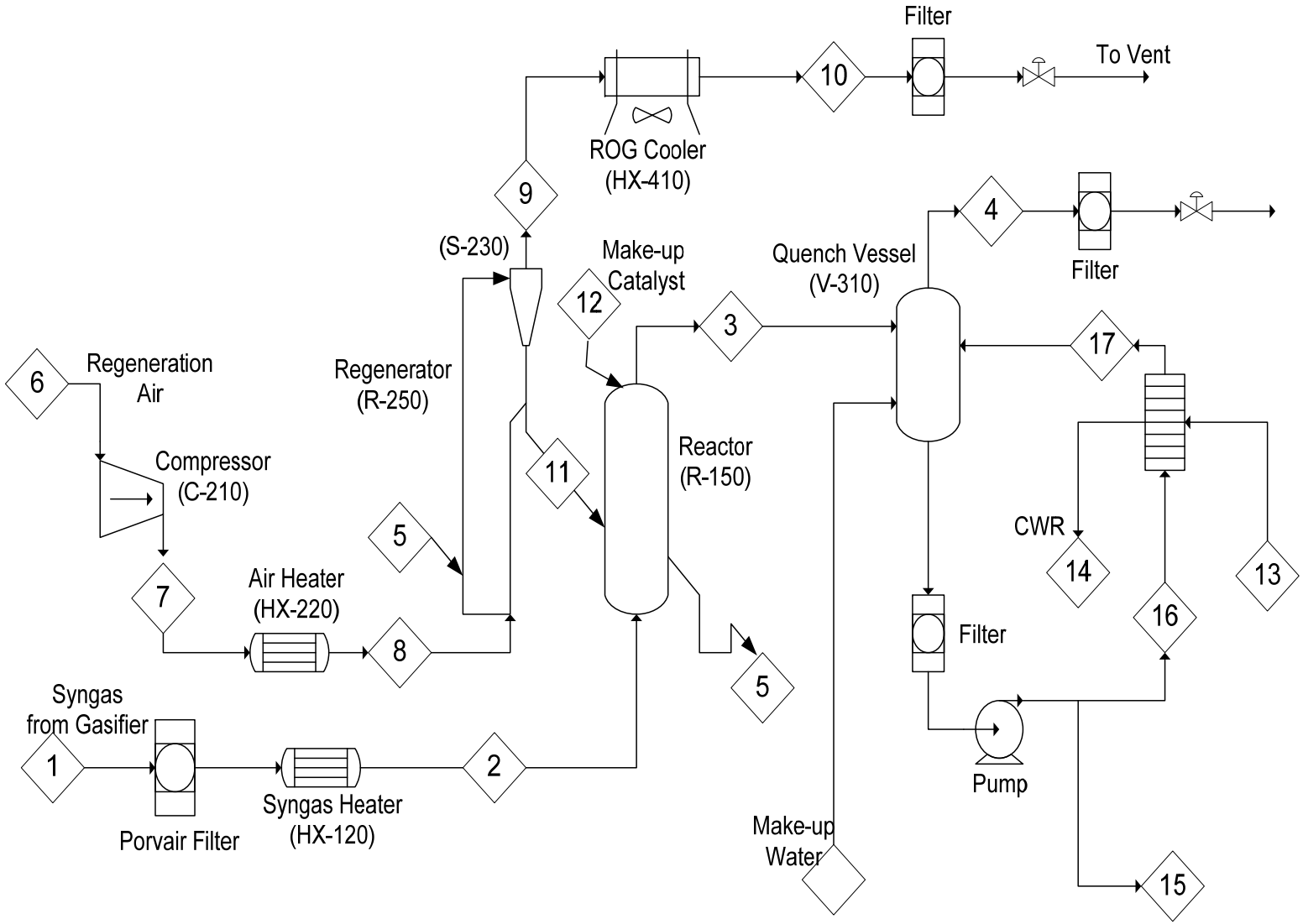

Figure 46: PFD of Biomass Syngas Cleanup Using Therminator

Table 16: Stream Table – Biomass Syngas Cleanup Using Therminator

Therminator Mtrls. & Energy Balance	UNITS	1	2	3	4	5	6	7	8	9	10	11	13	14	15	16	17
Temperature	°F	801	1112	1112	120	1112	68	264	264	1368	250	1368	80	100	120	120	100
Temperature	°C	427.0	600.0	600.0	48.9	600.0	20.0	128.8	128.8	742.2	121.1	742.2	26.7	37.9	48.9	48.9	37.8
Pressure	psia	32.5	32.5	29.5	27.5	29.5	12.5	32.5	32.5	32.5	32.5	32.5	47.5	42.5	27.5	37.5	32.5
Pressure	bar	2.24	2.24	2.03	1.90	2.03	0.86	2.24	2.24	2.24	2.24	2.24	3.27	2.93	1.90	2.59	2.24
Total Mass Flow	lb/hr	143	143	139	79	454	62	62	62	65	65	450	4,840	4,840	61	4,840	4,840
Total Act. Vol. Flow	ACFM	2	2	2	1	8	1	1	1	1	1	8	81	81	1	81	81
Total Std. Vol. Flow	SCFM	2	2	2	2	8	1	2	2	1	2	8	255	220	2	187	168
Enthalpy Flow	MMBtu/hr	-0.5	-0.5	-0.5	-0.2	-3.0	0.0	< 0.001	< 0.001	0.0	-0.1	-2.9	-33.0	-32.9	-0.4	-32.3	-32.4
Component Mass Flow																	
H_2	lb/hr	5.11	5.11	5.45	5.45										trace	trace	trace
CO	lb/hr	35.49	35.49	35.49	35.44										0.05	3.97	3.97
N_2	lb/hr			0.46	0.46		46.42	46.42	46.42	46.42	46.42				0.00	0.05	0.05
O_2	lb/hr						14.22	14.22	14.22	4.62	4.62						
Ar	lb/hr						0.79	0.79	0.79	0.79	0.79						
CO_2	lb/hr	28.32	28.32	28.32	27.44		0.03	0.03	0.03	13.23	13.23				0.88	70.09	70.12
H_2O	lb/hr	64.68	64.68	64.68	5.75		0.38	0.38	0.38	0.38	0.38		4840.10	4840.10	58.92	4712.75	4712.77
H_2S	lb/hr	0.03	0.03	0.03	0.03										0.00	0.12	0.12
SO_2	lb/hr									0.01	0.01						
NH_3	lb/hr	0.57	0.57	0.00	trace										trace	trace	trace
CH_4	lb/hr	3.89	3.89	3.89	3.83										0.06	4.90	4.90
Aromatics(C_6H_6)	lb/hr	0.72	0.72	0.72	0.16										0.56	44.37	44.37
Tar ($C_{10}H_8$)	lb/hr	3.88	3.88	0.04	< 0.001										0.04	3.10	3.10
C	lb/hr					4.49						0.89					
$ZnTiO_3$	lb/hr					0.21						0.22					
ZnS	lb/hr					0.01											
TiO_2	lb/hr					0.01											
Catalyst (Zeolite)	lb/hr					449.10						449.10					
Fluid Phase Mole Fraction																	
H_2		0.303	0.303	0.319	0.523										6 PPB	6 PPB	6 PPB
CO		0.152	0.152	0.150	0.245										536 PPM	536 PPM	536 PPM
N_2				0.002	0.003		0.773	0.773	0.773	0.773	0.773				6 PPM	6 PPM	6 PPM
O_2							0.207	0.207	0.207	0.067	0.067						
Ar							0.009	0.009	0.009	0.009	0.009						
CO_2		0.077	0.077	0.076	0.121		300 PPM	300 PPM	300 PPM	0.140	0.140				0.006	0.006	0.006
H_2O		0.430	0.430	0.424	0.062		0.010	0.010	0.010	0.010	0.010		1.000	1.000	0.990	0.990	0.990
H_2S		110 PPM	110 PPM	99 PPM	155 PPM										13 PPM	13 PPM	13 PPM
SO_2										34 PPM	34 PPM						
NH_3		0.004	0.004	24 PPM	trace										trace	trace	trace
CH_4		0.029	0.029	0.029	0.046										0.001	0.001	0.001
Aromatics(C_6H_6)		0.001	0.001	0.001	398 PPM										0.002	0.002	0.002
Tar ($C_{10}H_8$)		0.004	0.004	36 PPM	107 PPB										92 PPM	92 PPM	92 PPM

Table 17: Validation of RTI's process model (red) with the NREL results (black)

Stream #		105		202		210		224		362		592C	
Stream Description		Gasifier Inlet		Gasifier Outlet		Char Combustor Outlet		Syngas to Conditioning		Syngas from Conditioning		Ethanol Product	
Total Flow	lb/hr	193,387	193,388	5,217,952	5,217,933	5,416,086	5,416,068	232,824	232,709	279,885	279,649	48,726	48,760
Temperature	°F	220	220	1,633	1,633	1,823	1,823	1,633	1,633	110	110	110	110
Pressure	psia	25	25	23	23	21.4	21.4	21.4	21.4	415	415	35	35
Vapor Fraction		0	0	1	1	1	1	1	1	1	1	0	0
Hydrogen	lb/hr			3,465	3,459			3,465	3,459	15,501	15,485		
Water	lb/hr	9,669	9,669	82,789	82,787	25,664	25,543	82,790	82,787	843	838		
Carbon Monoxide	lb/hr			80,309	80,234			80,309	80,234	215,478	215,279		
Nitrogen	lb/hr					318,734	318,651			4,168	4,168		
Oxygen	lb/hr					16,278	16,271						
Argon	lb/hr					5,436	5,435						
Carbon Dioxide	lb/hr			37,488	37,468	96,318	96,512	37,488	37,468	37,234	37,220		
Hydrogen Sulfide	lb/hr			161	161			161	161	28	28		
SO_2	lb/hr					27	27						
Ammonia	lb/hr			355	355			355	355	25	28		
Methane	lb/hr			16,577	16,565			16,577	16,565	3,954	3,950		
Ethane	lb/hr			474	475			474	475	7	7		
Ethylene	lb/hr			7,971	7,970			7,971	7,970	636	635		
Acetylene	lb/hr			753	752			753	752	60	60		
Propane	lb/hr									1,598	1,597		
n-Butane	lb/hr									293	293		
Pentane +	lb/hr									55	55		
Benzene	lb/hr			607	608			607	608	4	4		
Methanol	lb/hr											244	245
Ethanol	lb/hr											48408	48442
Propanol	lb/hr											71	71
Tar ($C_{10}H_8$)	lb/hr			1,822	1,823			1,821	1,823	1	1	3	3
Olivine (Solid)	lb/hr			4,951,355	4,951,355	4,951,850	4,951,850	50	50				
Ash	lb/hr	0	0	0	0	1,779	1,779	0	0				
Char	lb/hr	0	0	33,826	33,922	0	0	3	3				
Wood	lb/hr	183,718	183,718	0	0			0	0				
Enthalpy	MMBtu/hr	-481	-481	1,337	1,337	1,937	1,937	-615	-614	-520	-519	-127	-127

Table 18: Clean syngas outputs from Tar reforming and Therminator processes

		Biomass Feed	Raw Syngas (Gasifier Outlet)	Clean Syngas	
	UNITS			Tar reforming	Therminator
Temperature	°F	60	1633	464	464
Temperature	°C	16	889	240	240
Pressure	psia	14.7	21.4	910.0	910.0
Pressure	bara	1.0	1.5	62.7	62.7
Total Mass Flow	lb/hr	367,437	232,771	131,086	157,500
Total Mole Flow	lbmol/hr	183,718	11,443	9,536	7,462
Enthalpy Flow	MMBtu/hr	-1699.4	-615.4	-253.2	1.9
Component Mass Flow					
H_2	lb/hr		3465.0	11049.87	4709.75
CO	lb/hr		80309.0	91782.79	65434.71
N_2	lb/hr			226.57	291.33
O_2	lb/hr				
Ar	lb/hr				
CO_2	lb/hr		37488.0	24094.70	60203.68
H_2O	lb/hr	183718.3	82790.0	250.25	972.98
H_2S	lb/hr		161.0	27.23	11.08
SO_2	lb/hr				
NH_3	lb/hr		355.0	30.55	<0.01
CH_4	lb/hr		16577.0	2860.67	16494.09
C_2H_6	lb/hr		474.0	4.10	467.91
C_2H_4	lb/hr		7971.0	688.00	7889.80
C_2H_2	lb/hr		753.0	64.95	745.18
C_3-C_4	lb/hr				
C_5+	lb/hr				
Aromatics (C_6H_6)	lb/hr		607.0	5.24	290.90
Napthenes	lb/hr				
Durene	lb/hr				
Tar ($C_{10}H_8$)	lb/hr		1821.0	1.57	0.11
Biomass	lb/hr	183718.3			
Char	lb/hr		3.4		

Table 19: Product outputs and total income comparisons for Tar reforming and Therminator cases (Mixed alcohols process)

Ethanol Production via Mixed Alcohols		No Recycle (Single Pass)				Base case (with Recycle from NREL Report)
	Units	Tar Reforming # 1	Tar Reforming # 2	Therminator # 1	Therminator # 2	
Light Product Gas	lb/hr	108,169.1	94,235.9	138,753.2	125,457.8	0.0
Ethanol Product	lb/hr	21,667.6	34,073.2	14,395.6	25,545.7	48,726.0
Heavy Alcohol Product	lb/hr	3,928.1	6,314.9	2,643.0	4,791.1	8,790.0
Electricity from Light Gases	MW_e	67.6	44.2	81.9	62.2	0.0
Electricity from Heavy Alcohols	MW_e	5.1	8.3	3.5	6.3	11.5
Electricity Generated (Misc.)	MW_e	5.4	6.5	12.0	8.2	8.1
Total Electricity Consumed	MW_e	6.4	6.7	6.3	6.3	8.1
Net Electricity Generated	MW_e	71.7	52.3	91.1	70.3	11.5
Fuel Price ($2.005/gal)[$]	$/hr	$ 6,558	$ 10,312	$ 4,353	$ 7,727	$ 14,747
Electricity Price ($0.1155/kWh)[#]	$/hr	$ 8,281	$ 6,036	$ 10,519	$ 8,123	$ 1,324
Total Income	$/hr	$ 14,839	$ 16,348	$ 14,872	$ 15,850	$ 16,071

Notes:

[$] **EIA's Annual Energy Outlook 2010 (2009 price from Table 1 of Reference Case).**

[#] **EIA's Short Term Energy Outlook Report 2009 average price.**

Table 20: Product outputs and total income comparisons for Tar reforming and Therminator cases (DME process)

Biofuel production via DME		No Recycle (Single Pass)			
	UNITS	Tar Reforming # 1	Tar Reforming # 2	Therminator # 1	Therminator # 2
Light Product Gas	lb/hr	116,676.3	107,283.6	146,636.4	139,587.6
Synfuel (C5+)	lb/hr	14,408.7	23,801.4	10,864.1	17,912.9
Electricity from Light Gases	Mwe	70.2	46.0	82.2	64.1
Electricity Produced (Misc.)	Mwe	37.3	46.2	35.0	41.7
Total Electricity Consumed	Mwe	30.2	30.2	22.5	22.5
Net Electricity Produced	MWe	77.3	62.0	94.8	83.3
Fuel Price ($2.005/gal)[$]	$/hr	$ 5,845	$ 9,655	$ 4,384	$ 7,243
Electricity Pirce ($0.1155/kWhr)[#]	$/hr	$ 8,932	$ 7,162	$ 10,945	$ 9,621
Total Income	$/hr	$ 14,777	$ 16,817	$ 15,329	$ 16,864

Notes:

[$] **EIA's Annual Energy Outlook 2010 (2009 price from Table 1 of Reference Case).**

[#] **EIA's Short Term Energy Outlook Report 2009 average price.**